Theses and Dissertations

12-2012

Performance and Cost Analysis of a Structured Concrete Thermocline Thermal Energy Storage System

Matt Nicholas Strasser
University of Arkansas, Fayetteville

www.manaraa.com

PERFORMANCE AND COST ANALYSIS OF A STRUCTURED CONCRETE
THERMOCLINE THERMAL ENERGY STORAGE SYSTEM

PERFORMANCE AND COST ANALYSIS OF A STRUCTURED CONCRETE THERMOCLINE THERMAL ENERGY STORAGE SYSTEM

A thesis submitted in partial fulfillment
of the requirements for the degree of
Master of Science in Civil Engineering

By

Matthew N. Strasser
Harding University
Bachelor of Science in Mechanical Engineering, 2011

December 2012
University of Arkansas

ABSTRACT

Increasing global energy demands and diminishing fossil fuel resources have raised increased interest in harvesting renewable energy resources. Solar energy is a promising candidate, as sufficient irradiance is incident to the Earth to supply the energy demands of all of its inhabitants. At the utility scale, concentrating solar power (CSP) plants provide the most cost-efficient method of harnessing solar energy for conversion to electrical energy. A major roadblock to the large-scale implementation of CSP plants is the lack of thermal energy storage (TES) that would allow the continued production of electricity during the absence of constant irradiance. Sensible heat TES has been suggested as the most viable form of TES for CSP plants. Two-tank fluid TES systems have been incorporated at several CSP plants, significantly enhancing the performance of the plants. A single-tank thermocline TES system, requiring a reduced liquid media volume, has been suggested as a cost-reducing alternative. Unfortunately, the packed-aggregate bed of such TES system introduces the issue of thermal ratcheting and rupture of the tank's walls. To address this issue, it has been suggested that structured concrete be used in place of the aggregate bed. Potential concrete mix designs have been developed and tested for this application. Finite-difference-based numeric models are used to study the performance of packed-bed and structured concrete thermocline TES systems. Optimized models are developed for both thermocline configurations. The packed-bed thermocline model is used to determine whether or not assuming constant fluid properties over a temperature range is an acceptable assumption. A procedure is developed by which the cost of two-tank and single-tank thermocline TES systems in the capacity range of 100-3000 MWh$_e$ can be calculated. System Advisory Model is used to perform life-cycle cost and performance analysis of a central receiver plant incorporating four TES scenarios: no TES, two-tank TES, packed-bed thermocline

TES, and structured concrete thermocline TES. Conclusions are drawn as to which form of TES provides the most viable option. Finally, concrete specimens cast from the aforementioned mix designs are tested in the presence of molten solar salt, and their applicability as structured filler material is assessed.

This thesis is approved for recommendation
to the Graduate Council.

Thesis Director:

_____

Dr. R. Panneer Selvam

Thesis Committee:

_____

Dr. Micah Hale

_____

Dr. Ernest Heymsfield

THESIS DUPLICATION RELEASE

I hereby authorize the University of Arkansas Libraries to duplicate this thesis when needed for research and/or scholarship.

Agreed   _____
             Matthew N. Strasser

Refused   _____
             Matthew N. Strasser

ACKNOWLEDGMENTS

I must first and foremost thank God for granting me the desire and capability to do this work; without him, nothing is possible (Proverbs 25:2, Philippians 4:13).

I would like to express the deepest gratitude for my advisor Dr. Panneer Selvam. He has been an excellent mentor, helping to educate me, not only in my area of research, but about the research process as a whole. Our many talks about areas of life ranging from religion to politics and the economy have definitely expanded my diversity of thought. Our work within this thesis has been a definite success, and I look forward to our success in the upcoming years.

I would like to thank Dr. Micah Hale and Dr. Ernest Heymsfield for serving on my committee and providing valuable suggestions and criticism.

I am most grateful for my colleagues that worked on this project before me: Marco Castro, Joel Skinner, Brad Brown, and Emerson John. Their work provided a solid foundation from which I could build.

I would like to thank technicians Mark Kuss and David Peachee for their help in operating, trouble-shooting, and repairing the testing equipment used in this work.

Lastly, I would like to acknowledge and thank the Department of Energy for funding and supporting my research efforts.

DEDICATION

I would like to dedicate this thesis to my parents, Fred and Rebecca Strasser. They have been very supportive of me and encouraged me to pursue my interests and strive for excellence in what I do. Thank you for providing me with the opportunity to excel.

TABLE OF CONTENTS

LIST OF FIGURES

LIST OF TABLES

NOMENCLATURE

Variables

A_c = Cross sectional area of tank (m^2)

$A_{s,shape}$ = Surface area of shape being considered (m^2)

$A_{s,sphere}$ = Surface area of sphere with equivalent volume to shape being considered (m^2)

α = Surface area shape factor (dimensionless)

α_M = Thermal diffusivity of concrete (m^2/s)

C_p = Specific heat capacity (J/kg.K)

$C_{pF,avg}$ = Average fluid specific heat (J/kg.K)

D = Sphere diameter (m)

ε = Void fraction of bed (dimensionless)

h = Convection coefficient (W/m^2.K)

h_v = Interstitial heat transfer coefficient (W/m^3.K)

k = Thermal conductivity (W/m.K)

$k_{F,avg}$ = Average fluid thermal conductivity (W/m.K)

m = Mass (kg)

$\dot{m}$ = Mass flow rate (kg/s)

$N_{u,sphere}$ = Nusselt number for flow over a sphere (dimensionless)

P = Perimeter of fluid flow channel (m)

P_r = Prandlt number (dimensionless)

ρ = Density (kg/m^3)

ρ_f = Average of fluid densities at surface and free stream temperatures (kg/m^3)

Q = Stored energy (J)

r_{sphere} = Radius of sphere with equivalent volume to shape under consideration (m)

R_e = Reynolds number (dimensionless)

S = Cross sectional area of fluid flow channel (m^2)

t = time (s)

T = Temperature (K or ˚C)

T_B = Temperature of bed material (˚C)

T_M = Temperature of concrete material (˚C)

T_F = Temperature of heat transfer fluid (˚C)

ΔT = Temperature change (K or ˚C)

μ = Viscosity (kg/m.s)

μ_{avg} = Average of fluid viscosity at surface and free stream temperatures (kg/m.s)

μ_∞ = Viscosity at free stream temperature (kg/m.s)

μ_s = Viscosity at surface temperature (kg/m.s)

v_{avg} = Average fluid velocity (m/s)

V = Fluid flow velocity (m/s)

V_B = Solid material volume in bed region of tank (m^3)

V_F = Fluid material volume in bed region of tank (m^3)

Numeric Model Variables

$A_1 = (\rho C_p)_F$

$A_2 = (\dot{m} C_p)_F$

$A_3 = (\rho C_p)_B$

$C_1 = \varepsilon A_1$

$C_2 = A_2/A_c$

$C_3 = (1-\varepsilon)A_3$

Subscript 't' = Corresponds to current time step

Subscript 't+1' = Corresponds to upcoming time step

Superscript 'J' = Corresponds to element whose temperature is being solved for

Superscript 'J-1' = Corresponds to element preceding the element currently being solved

Δt = Time step (s)

Δy = Node spacing (m)

LIST OF ACRONYMS

CSP = Concentrating Solar Power

DOE = Department of Energy

EIA = Energy Information Administration

EPRI = Electric Power Research Institute

HTF = Heat Transfer Fluid

HPC = High Performance Concretes

IEA = International Energy Agency

LCOE = Levelized Cost of Electricity

LHS = Latent Heat Storage

NREL = National Renewable Energy Laboratories

NSTTF = National Solar Thermal Test Facility

PBTC = Packed Bed Thermocline

PCM = Phase Change Material

SAM = System Advisory Model

SCTC = Structured Concrete Thermocline

SNL = Sandia National Laboratories

TES = Thermal Energy Storage

TRNSYS = Transient System Simulation Tool

CHAPTER 1: INTRODUCTION AND THESIS OBJECTIVES

1.1 Introduction

The population of the world is increasing at a rapid rate; increasing with the population is the global energy demand. According the Energy Information Administration (EIA), the amount of energy consumed by the average United States citizen increased by 44% between 1949 and 2009 (from 214-308 million Btu or 226-336 TJ) (Energy Perspectives, 2009). The vast majority of this energy is supplied by fossil fuels (EIA, Energy Perspectives, 2009). As the United States' population continues to increase, it can be assumed that the general energy consumption trend, pictured in Figure 1, will continue.
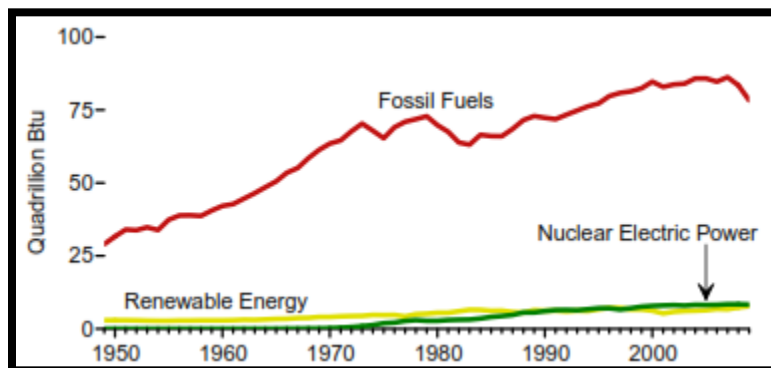
Figure 1: Yearly United States Energy Consumption by Sources (EIA, Energy Perspectives, 2009)

A nation's energy supply is a matter of national security and stability; without a reliable power grid, the operation of critical facilities such as hospitals and military installations can be put in jeopardy. Unfortunately, the United States has not been energy self-sufficient since the 1950's, importing more than 60% of the oil it consumes (SNL, 2011). To attain increased national security and a stable energy supply to drive national growth in the future, it is imperative that the United States diversify its energy supply to include alternative, renewable energy sources. Table 1 provides a comparison of the cost of producing electricity using various

1

technologies, using both renewable and nonrenewable resources, and the associated capacity factors of these technologies.

Table 1: Cost of Electricity and Capacity Factor for Various Technologies (EIA, 2012)

Source of Power for Production of Electricity	Cost Prediction (2010 $) for 2017	
	Average LCOE (¢/kWht)	Capacity Factor (%)
Coal		
Conventional	9.96 ¢	85.00%
Advanced	20.39 ¢	85.00%
Natural Gas		
Conventional Combined Cycle	6.18 ¢	87.00%
Advanced Combined Cycle	5.89 ¢	87.00%
Conventional Combustion Turbine	9.46 ¢	30.00%
Advanced Combustion Turbine	8.04 ¢	30.00%
Wind		
Inshore	9.68 ¢	34.00%
Offshore	33.06 ¢	27.00%
Solar		
Photovoltaic	15.69 ¢	25.00%
Thermal	**25.1 ¢**	**20.00%**
Nuclear	11.27 ¢	90.00%
Geothermal	9.96 ¢	92.00%
Biomass	12.02 ¢	83.00%
Hydro	8.99 ¢	53.00%

Solar energy is a promising potential alternative energy source. The earth's atmosphere continuously receives a mean irradiance of about 1.35 kW/m^2, leading to a net energy reception rate of $1.7(10)^{17}$ W; however, much of this energy is absorbed or scattered in the atmosphere (Goswami, Kreith, & Kreider, 2000). The mean irradiance of the Earth is much smaller, reportedly varying from 150-300 W/m^2 (Goswami et al., 2000). If less than 1% of the Earth's irradiance could be harvested and converted at 10% efficiency, sufficient energy would be produced to exceed the needs of the world's population (Goswami et al., 2000).

Solar radiation is harvested in one of two ways: it is collected by photovoltaic cells and directly converted to electricity using semiconductors or it is concentrated and captured and used

to drive a steam power cycle. Photovoltaic systems currently available on the market generally range in efficiency between 12-20% (EIA, 2009). Conversion efficiencies of up to 43.5% have been achieved in lab-scale testing (Wesoff, 2011); however, such photovoltaic systems are not cost competitive for large-scale power production at this time. Concentrating solar power (CSP) plants have been recognized as a possible supplier of the large quantities of needed electrical energy (Xu, Wang, He, Li, & Bai, 2012).

One problem plaguing the large-scale implementation of CSP plants is the intermittent nature of irradiance at any given location on the Earth (Brown, Strasser, & Selvam, 2012). The Earth's irradiance varies due to factors such as the position of the sun, cloud cover and density, etc. and is absent at night. For CSP plants to be implemented on a large scale, their capacity factors will have to be improved by finding a way to guarantee a steady heat source to the plant amid unsteady irradiance. The key to operation with fluctuating irradiance is to incorporate thermal energy storage (TES) into the power plants. TES can function as a capacitor, increasing the temperature of the liquid media when solar irradiance is not intense enough to heat it to desired levels, or act as a battery, allowing the power plant to continue producing power well after the sun has set (Adinberg, Zvegilsky, & Epstein, 2010).

A reasonable question, regarding the necessity of TES, is why not increase the capacity of the plant and store the excess electrical power produced for use when solar irradiance is not available. The answer to this question is that storing electrical energy is considerably more expensive than storing energy in alternative forms and generating the electric power as needed. A comparison of energy storage technologies is provided in Table 2.

Table 2: Energy Storage Cost Comparison of Various Technologies (Schoenung, 2011)

Technology	$/kWh	Efficiency
SLA Battery	$330.00	80.00%
LI Battery	$600.00	85.00%
Super Capacitor	$10,000.00	95.00%
HS Flywheel	$1,600.00	95.00%
Pumped Hydro	$75.00	85.00%
Sensible Heat	$31.00	93.00%

TES systems considered for application in a CSP plant fall under one of three categories: sensible heat storage, phase change storage, or chemical storage (Tahat, Babus'Haq, & O'Callaghan, 1993). Sensible heat storage systems have been suggested as the most practical method of energy thermal energy storage (Herrmann & Kearney, 2002); currently, all power plants incorporating TES employ sensible heat storage.

Sensible heat is defined as the amount of energy released from a material as its temperature is increased or decreased (Gil, et al., 2010). Most sensible heat TES systems operate by elevating the temperature of a volume of liquid media and storing it for later use. These systems can be classified into one of the following two categories: two-tank, in which hot and cold liquid media are stored in separate tanks, and single-tank, thermocline systems, in which both hot and cold liquid media are stored in the same tank. In either system, one of the most costly components is the liquid media inventory [(Herrmann & Kearney, 2002) and (Pacheco, Showalter, & Kolb, 2002)]. Filler materials are currently being investigated to reduce the necessary volume of liquid media, thereby decreasing the cost of sensible heat TES. Concrete has been suggested as a potential TES media, providing storage at the cost of $1/kWh_t (Herrmann & Kearney, 2002).

Some level of testing of concrete as TES media has been conducted. One concept involved casting a steel heat exchanger in a concrete block and circulating thermal oil through

4

the heat exchanger in the temperature range of 300°C-400°C (Laing, Lehmann, FiB, & Bahl, 2009). A similar concept involved casting a steel heat exchanger in concrete prisms and circulating molten salt through the heat exchanger in the elevated temperature range of 450°-500°C (Skinner, Brown, & Selvam, 2011). However, due to the high cost of stainless steel heat exchangers necessary to avoid deterioration from the corrosive salt, this concept is not cost effective (Skinner et al., 2011). A proposed, cost-decreasing alternative is a single-tank thermocline TES, using molten salt as the liquid media and geometrically-optimized, structured concrete filler material (Brown et al., 2012).

It is ideal for TES systems to operate at the maximum possible temperature, as this increases the energy storage density of the system and the efficiency of the Rankine power cycle executed by power plants (Kearney, et al., 2002). Unfortunately, concrete is susceptible to spall or explode at temperatures exceeding 300˚C. (John, Hale, & Selvam, 2011). High performance concretes (HPCs) have been designed and reported to sustain thermal cycling at temperatures of up to 600°C, demonstrating their potential as filler material in a sensible heat TES application (John et al., 2011). Significant modeling work has been conducted to optimize the geometry of the filler concrete using a 2D heat transfer model developed based upon the work of Schmidt and Willmott (1981) and is reported by Brown [(Brown et al., 2012) and (Brown, 2012)].

This work focuses on the optimization as well as cost and performance evaluation of a single-tank thermocline TES system incorporating a binary molten salt (60% KNO_3 40% NaO_3) as liquid media and structured HPC as a filler material. Previous work reports a maximum TES system efficiency of 65.59% (Brown, 2012); this value falls significantly short of the DOE's goal of 93% for the year 2020. Modeling is re-investigated with the goal of optimizing a TES system to attain efficiency at or exceeding the DOE's goal.

System Advisory Model (SAM), a product of NREL, is used to simulate the life-cycle performance of a CSP plant incorporating the optimized structured concrete thermocline TES system. The thermocline modeling function in SAM is adapted from Transient System Simulation Tool (TRNSYS). This thermocline model is developed based on the 1D Schumann equation and valid for modeling packed bed thermocline systems composed of small particles. In this work, a packed bed thermocline model based upon this 1D model is developed and its results are compared with those of the 2D structured concrete thermocline model. A procedure is discussed by which the input data of the packed bed model can be modified to attain similar performance to that predicted by the 2D structured concrete thermocline model. This allows the simulation of a structured concrete thermocline using SAM's 1D thermocline function. A study is conducted in which the accuracy of assuming constant versus variable fluid properties is assessed.

To attain a comparison of the performance of this TES configuration with other sensible heat configurations, three other configurations are considered: no TES, packed-bed thermocline TES, and two-tank liquid TES. To allow the simulation of these TES scenarios, a procedure is developed to determine a unit capacity cost for thermocline and two-tank TES systems in the range of 100-3000 MWh$_t$. Conclusions are drawn as to whether a structured concrete thermocline is a viable TES option.

John (2012) suggested concrete mix designs as possible candidates for filler material in a structured concrete thermocline TES system. Beams are cast from each of these mix designs and subjected to testing in circulating molten salt; the performance of these beams is assessed based upon deterioration. Conclusions are drawn as to whether the concrete mix designs are ready for testing in an actual thermocline system.

1.2 Thesis Objectives

Following the introductory chapter of this thesis, a comprehensive literature review is provided in Chapter 2. The literature review discusses the three categories of TES with a concentration on sensible heat thermal energy storage. Within the field of sensible heat TES emphasis is placed on thermocline TES systems. A review and discussion of TES systems incorporated at CSP plants, both presently and in the past, is also presented. Following this literature review, the primary objectives of the thesis, as presented below, are addressed.

Objective 1: *Evaluate previous studies conducted to optimize the geometry of structured filler material in a concrete thermocline TES system. If possible, optimize the geometry further to attain improved TES system efficiency.*

- In the work of Brown (2012), the geometry of structured concrete filler material was optimized to attain a TES system efficiency of 65.59%; this is well short of the DOE's goal of 93% for the year 2020. If higher efficiencies cannot be attained, this TES concept is not viable. The optimization work conducted by Brown will be investigated and new modeling will be conducted to determine if increased system efficiency is attainable.

Objective 2: *Perform a comparative cost and performance analysis of a CSP plant incorporating a structured concrete thermocline TES system.*

- SAM, a product of NREL, allows the simulation of a power plant incorporating various forms of TES; the software performs lifecycle cost and performance analysis. SAM will be attained from NREL and used to study the impact of various TES configurations on the cost and performance of a central receiver CSP plant.

- SAM's thermocline model is a 1D two-phase simulation, using the Schumann equation to describe heat transfer between solid and fluid material. The model developed to study

the structured concrete thermocline is a 2D two-phase model. The 2D model considers radial heat transfer; therefore, it can be inferred that the temperature distributions predicted by the two models may not be the same. However, if SAM is to be used to study a CSP plant with a structured concrete thermocline TES system, it must be possible to analyze the structured concrete thermocline with the 1D model and attain similar results as predicted by the 2D model.

- o A 1D thermocline model will be developed, using the Schumann equation to describe interstitial heat transfer, so that the temperature distributions calculated by the thermocline model used in SAM may be compared with the results of the 2D model used to study the structured concrete thermocline.

- o If temperature profiles and TES system efficiencies predicted by the 1D and 2D models vary significantly, a process will be developed to attain similar temperature distributions from the 1D model as produced by the 2D model.

- SAM does not calculate the cost of the TES system. When using SAM, the user specifies a plant capacity and the desired number of hours of operation on stored energy; based upon these inputs, SAM determines the required storage capacity in MWh_t for the plant. From this storage capacity, it is necessary to determine the capacity cost, or cost per kilowatt-hour of TES. Therefore, it is necessary to establish a means of calculating the TES capacity cost for both two-tank and single-tank thermocline TES systems.

Objective 3: *Determine if assuming constant fluid properties is an acceptable assumption.*

- In this work, molten solar salt is the liquid media considered; its properties, such as viscosity, density, and specific heat at constant pressure vary widely with temperature. In most works found in literature, it is assumed that using the properties based upon the

8

www.manaraa.com

middle temperature of the operating range (300˚C-400˚C) provides sufficient accuracy. However, as the temperature range is increased, such as that considered in this work (300˚C-585˚C), the variation of the properties from those at the median temperature increases. The amount of error attained by assuming constant properties will be investigated graphically using the 1D thermocline model.

Objective 4: *Conduct performance evaluations of concrete mix designs developed for application in a structured concrete thermocline TES system.*

- Based on the work of John (2012), concrete mixture designs have been specified as potential candidates for application in a structured concrete thermocline. Small cube specimens were tested by John in constant temperature and thermal cycling in the presence of both molten salt and air. This testing involved heating the specimens in an oven where the whole specimen was heated at a uniform rate; therefore, it is not known how concrete specimens made from these mix designs will respond to stresses induced by thermal gradients. A laboratory test system has been designed and constructed; concrete beam specimens will be cast from two of John's proposed four mix designs and subjected to thermal cycling in this test system. The performance of the members will be evaluated to determine if the concrete mix designs are still probable candidates for TES media in a structured thermocline.

9

CHAPTER 2: LITERATURE REVIEW

2.1 Introduction

The purpose of this literature review is to identify and discuss the methods in which solar energy is collected and stored; an emphasis is placed on sensible heat thermal energy storage (TES). The review begins by discussing the three major methods of collecting and concentrating solar radiation. Examples of power plants incorporating each method of energy collection are discussed as well. Following the discussion of energy collection methods, the three major categories of TES are discussed. Examples of existing TES systems are presented as their type is discussed. The focus of this work is sensible heat storage; therefore, this is the major area of discussion. Existing sensible heat storage systems are presented and discussed, along with heat transfer fluids (HTFs) and solid media used in these systems.

2.2 Concentrating Solar Power: Methods of Collection

Thermal energy collection for fueling electricity production can be classified into one of three major categories: Dish, Linear Concentrator, or Central Receiver (Brosseau et al., 2005).

2.2.1 Dish

Dish systems use a curved, reflective dish to track the sun and focus its radiation on a receiver located above the dish. This receiver uses the heat energy to produce electricity by executing a Stirling cycle. This method of energy concentration leads to operational temperatures of up to 800°C (DOE, 2008). Partially due to this high operating temperature, dish systems are the most efficient electricity-producing CSP technology, reportedly providing a solar-to-electrical conversion efficiency of up to 25-30% (IEA, 2010). The current small size of typical dish systems, most producing in the range of 3-25 kW, makes their near-term application for primarily niche markets (DOE, 2008). Pictured in Figure 2 depicts a pilot scale dish power

plant at the National Solar Thermal Test Facility (NSTTF) operated through Sandia National Labs.

Figure 2: Prototype 150 kW Dish Plant at National Solar Thermal Test Facility (Fraser, 2005)

Individual dish systems produce relatively small quantities of energy; therefore, the only way to effectively use them for large-scale power production is to install numerous dishes at a sight. Dish systems are currently the most expensive form of CSP collection; however, it is forecasted that mass production of the units will lead to them becoming cost-competitive with other CSP technologies (IEA, 2010). To date, no large scale dish CSP power plants have been installed. However, plans are in place to install a 500 MW power plant dish CSP plant by the year 2025. This installment, made by Stirling Engine Systems and Southern California Edison, will consist of 20,000 dishes spread over 4,500 acres in the Mojave Desert (DOE, 2008). A smaller 300 MW plant is also being constructed by Stirling Engine Systems and San Diego Gas & Electric located in California's Imperial Valley (DOE, 2008).

2.2.2 Linear Concentrators

Linear concentration is carried out by one of two collector types: parabolic trough or linear Fresnel receivers.

11

2.2.2.1 Parabolic Trough

Parabolic trough collectors are composed of rows, of curved mirrors with a fixed stainless steel tube suspended at the mirror's focal point. Collection troughs sizes vary up to 100 m in length and five to six meters across (IEA, 2010). As the troughs track the sun, HTF is circulated through the tubes and heated by the concentrated solar radiation. The tubes are coated with materials to increase degree to which they absorb the radiation; additionally, they are incased in evacuated glass tubes to decrease radiation losses (IEA, 2010). Troughs are capable of heating the HTF to temperatures of up to 390°C. Parabolic troughs are a well-developed and mature technology, as they have been in use for over twenty years (EPRI, 2010). Reported thermal-to-electrical efficiencies for parabolic trough systems reach 15% (IEA, 2010). The majority of CSP plants in use today employ parabolic trough receivers (DOE, 2008). Figure 3 depicts the trough array at Solana in Gila Bend, AZ.

Figure 3: Parabolic Troughs from the 280 MW Power Plant Solana under Construction in Gila Bend, AZ (Siemens, 2009).

Currently, 11 CSP plants are in operation in the United States, falling under the size range of 1-80 MW (NREL, 2011). Numerous CSP trough power plants are currently under

construction in the United States. Examples include the Solana Plant (Figure 3) and the Palen Solar Power Project. The Solana plant, scheduled to come online in 2013, spans 1,920 acres and is projected to supply 70,000 households with energy; when completed, it will be the largest parabolic trough CSP plant in operation in the world (Abengoa, 2012). The prominence of Solana amongst parabolic trough plants will be short lived, however, because the 500 MW Palen Solar Power Project located near Desert Center, California is scheduled to come online in 2014 (NREL, 2010). When completed, the Palen Project will replace Solana as the largest parabolic trough power plant in operation.

2.2.2.2 Linear Fresnel

Linear Fresnel collection systems consist of rows of flat or curved mirrors that track the sun and focus its radiation on a fixed receiver. This type of CSP receiver system offers the lowest start-up cost due to its simple design and components (IEA, 2010). However, CSP plants incorporating linear Fresnel receivers have the lowest solar-to-electrical efficiency, falling in the range of 8-10% (IEA, 2010). Linear Fresnel CSP systems have received limited interest to date, as parabolic trough systems, offering higher efficiencies, have been the area of focus in linear CSP collection. Figure 4 depicts the linear Fresnel array a Puerto Errado 2 in Calasparra, Spain.

13

Figure 4: Linear Fresnel Array at the 30 MW Puerto Errado 2 CSP Plant in Calasparra, Spain (PE2, 2010)

Puerto Errado 2 (PE2) has been in operation since March 2012; it is currently the largest linear Fresnel CSP plant in operation (CleanEnergy, 2012). PE2 occupies almost 173 acres (NREL, 2011), and the solar collection field contains over 302,000 m^2 of aperture area (NovatecSolar, 2012). PE2 is projected to supply 15,000 households with energy (NovatecSolar, 2012). Efforts are currently underway to reduce the production cost of the Fresnel lenses used in Linear Fresnel CSP plants to make this technology more viable.

2.2.3 Central Receiver

Central receiver (power tower) collection systems consist of a field of flat mirror panels, known as heliostats, which track the sun and focus solar radiation on an elevated central receiving tower. Heliostats range in size, up to an area of 125 m^2; receiver towers also vary in size, up to the height of 165 m (Abengoa, PS20, the Largest Solar Power Tower Worldwide, 2012). Central receiver units typically collect heat at temperatures of up to 565°C (DOE, 2008); however, potential operating temperatures in the 1000°C-1300°C range have been reported (Romero, Buck, & Pacheco, 2002). Due to these high operating temperatures, the solar-to-

14

electrical efficiency of central receiver CSP plants is reportedly in the range of 20-35% (IEA, 2010). The large range in efficiency variation is due to the difference in the typical operating temperature of $565^{\circ}C$ and the potential range of $1000^{\circ}C$-$1300^{\circ}C$. Figure 5 depicts the tower and heliostat array of PS20 in Seville, Spain.

Figure 5: Central Receiver and Heliostats at the 20 MW PS20 Plant in Seville, Spain (Molina, 2009)

PS20 has been operational since 2009; it is currently the largest central receiver CSP power plant in operation. Its solar collection field spans 210 acres and is composed of 1255 120 m^2 heliostats; the central receiver, stands at a height of 165 m (Abengoa, 2012). PS20 reportedly provides sufficient energy for 10,000 households (Abengoa, 2012).

2.3 Primary Methods of TES

A major problem faced by solar power plants today is the intermittent nature of the solar energy supply. Fluctuations in the supply of heat from the collectors to the power blocks in the power plants lead to non-constant power production. Additionally, CSP plants that have not been constructed as hybrids, with backup fossil fuel supplies, are forced to go offline during nighttime hours. Integrating TES into CSP plants solves the aforementioned problems. The

15

ability to incorporate reasonably cheap TES into CSP plants gives them a significant advantage over renewable technologies such as photovoltaic or wind turbines; it is much cheaper to store heat energy and generate electricity as it is needed than it is to generate the electricity and store it until it is needed (Herrmann & Kearney, 2002).

Stored thermal energy allows the continued operation of the plant's power block after the sun sets. Due to cloud cover, contamination in the air, etc., the supply of heat from the collector field fluctuates. Stored thermal energy can increase the plant's efficiency by maintaining the temperature of the HTF flow from the collector field at the desired operating temperature for the power block (Laing et al., 2009). Reducing the variation in the temperature of the HTF input to the power block also extends the life expectancy of the block's components by reducing the thermal cycling they experience (Laing et al., 2009). Aside from increasing the life expectancy of the block, maintain a constant energy generation rate increases the ease of incorporating the plants into the power block, by eliminating fluctuations in the energy supply that must be smoothed out using power generated by fossil fuel back-ups (Laing et al., 2006). TES systems are classified into one of three categories based upon the mechanism through which they store energy: chemical storage, latent heat storage, or sensible heat storage.

2.3.1 Chemical TES

Chemical TES systems store energy by using thermal energy from the collector field to drive a reversible endothermic reaction in the storage media; for a material to be applicable for chemical energy storage (CES) application, the reaction that it undergoes during energy storage must be completely reversible (Herrmann & Kearney, 2002). The energy stored in the material is later released during discharge in an exothermic reaction. In most cases, a catalyst is necessary to trigger the exothermic reaction (Herrmann & Kearney, 2002). CES systems provide

a high energy storage density, reportedly up to an order of magnitude greater than that of phase change storage (PCS) (Tahat et al., 1993). CES allows large quantities of energy to be stored at low temperatures, eliminating the need for costly, insulated containment vessels (Gil, et al., 2010). However, during the exothermic discharge process, the energy is made available at very high temperatures. Table 3 provides a list of some of the most investigated chemical reactions for CES applications.

Table 3: Potential CES Materials and Reaction Information (Gil, et al., 2010)

CES technology is relatively new and currently undergoing significant research and development; however, there are no CES applications in operation at this time. Though the potential benefits make this technology very appealing, there are numerous drawbacks associated with CES. Though the chemistry is understood, incorporating it into a TES system is complex compared with system designs in other forms of TES. Additionally, the materials used in CES must be considered: they are cited as having high costs, being flammable, and being toxic (Herrmann & Kearney, 2002). Nevertheless, as new materials and reactions are studied, along with methods of conducting and harvesting energy from the reactions, this TES technology offers a promising approach to TES in the future.

2.3.2 Latent Heat TES

Latent heat, also known as phase change, TES systems (LHS TES systems) store energy in the form of heat absorbed when a material undergoes a change in physical state. LHS is

www.manaraa.com

considered for TES storage in the 270 ˚C -410˚C temperature range, but has been investigated at temperatures of up to 547˚C (Tahat et al., 1993). LHS is attractive for several reasons. It allows the storage of large quantities of energy in a small volume: 5-14 times the storage density offered by sensible heat TES materials such as water, rock, or masonry (Sharma, Tyagi, Chen, & Buddhi, 2009). Additionally, it allows the energy to be stored and retrieved at constant temperatures, the temperatures at which phase change occurs. Finally, LHS is a theoretically isothermal process, meaning that storage efficiency should approach 100% (Adinberg, Zvegilsky, & Epstein, 2010).

Energy is absorbed during any of the following phase changes: solid-to-gas, solid-to-liquid, or liquid-to-gas; it is released when the phase change process is reversed. Solid-to-gas phase changes release the greatest quantity of heat; however, these phase changes also result in the greatest change in phase change material (PCM) volume (Sharma et al., 2009). This significant volume change results in containment problems and increased complexity of LHS system design. Solid-to-liquid phase changes release significantly less heat, but result in much less PCM volume change, reportedly in the range of 10% (Sharma et al., 2009). The solid-to-liquid phase change is the most widely used in LHS at the present.

There are numerous characteristics that must be taken into account when selecting a PCM for a LHS system. The material should change phase in the desired temperature range and have a large latent heat. It is desirable that the PCM also have high thermal diffusivity. To increase energy storage density, it is desired that the PCM have a significant density. To simplify design of the containment system and heat exchangers, the PCM should exhibit a minimal change in volume during phase change and have a low vapor pressure. LHS systems store energy when the PCM undergoes a phase change; therefore, it is necessary that the PCM not exhibit supercooling.

18

Supercooling of even a few degrees Centigrade decreases the efficiency of the LHS; and five to ten degrees Centigrade can completely stop the function of a LHS system (Sharma et al., 2009). To increase the life of the system, it is desirable that the PCM be capable of undergoing many cycles without breaking down and that it not be chemically reactive with containment vessels. For safety purposes, the toxicity and flammability of the PCM should be minimal. Finally, to reduce the cost of the system, it is desirable that the PCM be cheap and abundant.

2.3.2.1 Classes of Phase Change Materials

PCMs capable of operation at any practical temperature range are available in each of the three major classes: organics, inorganics, and eutectics. A detailed summary and description of materials in each of the discussed classes can be found in the work of Sharma et al. (2009).

- **Organics** compose the largest class of LHS materials. Organics can further be classified as paraffins, which are n-alkanes (CH_3-CH_2-CH_3), or non-paraffins, which are esters, alcohols, and glycols. Non-paraffins offer up to twice the energy storage density; however, they are less chemically stable at high temperatures and more toxic then are paraffins
  - **Pros** noncorrosive and chemically stable
  - **Cons** low thermal conductivity, low latent heat, and flammability

- **Inorganics** provided nearly twice the energy storage density offered by organic LHS materials. Inorganics can be further classified as hydrates, which are alloys of salts and water, or metallics. Hydrates are considered to be the most applicable group of PCM's for LHS storage (Adinberg et al., 2010). Unfortunately, the salts tend to precipitate from the hydrate over a series of cycles. Metallics offer large thermal conductivity and energy

19

storage density; however, their significant weight has detracted from interest in their application.

- o **Pros** moderate latent heat, minimal volume change with phase change, low toxicity, and low corrosion
- o **Cons** precipitation of salt from hydrate and significant weight of metallics

- **Eutectics** are a new class of phase change materials for which little research has been reported. During the endothermic, energy-storing phase, two or more substances crystallize together at the same temperature. They provide significant energy storage density with minimal segregation of any individual substance.
  - o **Pros** high chemical stability and moderate storage density
  - o **Cons** no significant work has been reported

2.3.2.2 Improving Heat Transfer in Latent Heat TES Systems

The major problem associated with PCM heat transfer systems is developing an efficient method of transferring heat to and from the system. During discharging of the TES system, the PCM usually solidifies after discharging its energy; the solidified material coats the heat exchangers and inhibits heat transfer from the system. Numerous configurations of PCM and heat exchangers have been identified and experimented with; this discussion will concern the two primary configurations: shell-and-tube and encapsulated.

2.3.2.2.1 Shell and Tube Configuration

The shell-and-tube PCM is the most widely used PCM configuration in LHS TES investigation today (Agyenim et al., 2010). The configuration of a single exchanger is provided in Figure 6 along with the HTF flow direction during charging and discharging.

20
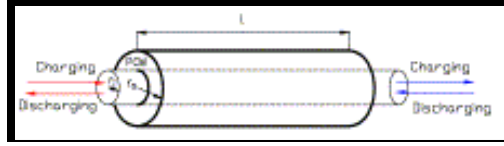
Figure 6: Shell and Tube PCM Configuration (Aggenim et al., 2010)

Attaching fins to the heat exchanger has been suggested as the most economic means of enhancing heat transfer; however, the effectiveness of this solution is limited, as the PCM solidifies on the fins as it does on the tube of the heat exchanger (Adinberg et al., 2010). Other suggested approaches taken to increasing the heat transfer rate are to insert a graphite or metal framework into the PCM (Agyenim et al., 2010) or disperse conductive particles, such as graphite and carbon fiber, into the PCM (Zalba et al., 2003).

2.3.2.2.2 Encapsulated Configuration

An alternative PCM arrangement to the shell-and-tube design is to encapsulate the PCM in spherical capsules. This offers a significant improvement in heat transfer, as the numerous small capsules expose much surface area for heat transfer. During charge and discharge, a fluid is circulated through the bed of capsules to transport energy. Unfortunately, this PCM arrangement seems to be prohibitively expensive for large-scale TES at this time.

2.3.3 Sensible Heat TES

Sensible heat TES systems store heat by elevating the temperature of the energy storage media. This form of TES is the area of focus in this work because it is currently considered the most feasable and to date, all CSP power plants incorporating TES store the energy as sensible heat. The quantity of energy stored in a given system during charging is defined by EQ. 2.1.

$$Q = mC_p\Delta T \hspace{4cm} EQ.\, 2.1$$

Q = Stored Energy (J)

m = Media Mass (kg)

21

C_p = Media Specific Heat (J/kg.K))

ΔT = Temperature Change (K)

Advantages commonly associated with sensible heat storage are low media costs, simple system design, and high thermal conductivity in the media (Tahat et al., 1993). It is desirable to minimize the cost of the energy storage as much as possible to reduce power production costs. When selecting energy storage media, desirable thermal properties include high specific heat capacity, high thermal conductivity, and compatibility with high temperatures. Significant heat capacity and compatibility with high teperature ranges are desirable because they increase the storage density of the TES system and the efficiency of Rankine power cycle executed by the power plant. Significant thermal conductivity is desired because it allows a more rapid rate of heat transfer in the TES system during charging and discharging. Additional material considerations include the longterm chemical stability of the media and corrosive properties of the media.

Sensible heat TES systems are typically constructed in one of three formats: passive systems, two-tank liquid systems, or single tank thermocline systems. Passive systems consist of a mass of solid TES media, which is charged and discharged by a liquid media being circulated through heat exchangers at its surface or imbedded within it. Two-tank liquid systems are charged by storing a quantity of heated liquid media at the upper opperating temperature limit of the CSP plant. After this thermal energy is discharged, the liquid media is stored in a cold tank, at the lower opperating limit of the plant, until it is withdrawn to be charged again. In thermocline systems, both hot and cold TES media are contained within the same tank. Due to the natural buoyant forces of the fluid, hot liquid media is contained in the uppper portion of the tank and cold liquid media is contained in the lower of the tank; a thermal gradiant, or

22

thermocline, exists between the two temperature regions.   Each form of sensible heat TES is discussed in detail later in Chapter 2.

2.3.3.1 Liquid Materials in Sensible Heat TES

Liquid materials play important roles in all types of sensible heat TES systems, serving as heat transfer fluids (HTFs) which transport concentrated heat from the solar collector, heat storage media, and as HTF transporting heat from storage to the power plant's power block. When selecting liquid media for a TES system, numerous considerations must be made.   It is desirable that the fluid have a low vapor pressure, so that costly pressure vessels are not needed for containing the fluid.   Additionally, a low viscosity is desirable, as this reduces the required pumping power for the system.

An addition consideration in selecting liquid media is that it must be capable of operating within the power plants specified temperature range.   When designing the collector field and power block, a design operating temperature range is specified.   The liquid media should be selected so that it is chemically stable at the upper temperature limit of the system and still in a liquid state at the lower temperature limit.   Numerous fluids have been considered for application as liquid media in sensible heat TES systems including water, air, mineral oils, synthetic oils, and sodium (Gil, et al., 2010).   Table 4 provides a listing of some of the most commonly-used liquid TES media and their properties.

Table 4: Commonly-Used Liquid TES Media and Properties (Herrmann & Kearney, 2002)

Liquid Media	Operating Temperature (^{o}C)		Average Density (kg/m^3)	Average Heat Capacity (kJ/kg.K)	Volume Specific Heat Capacity (kWh$_t$/m^3)	Media Cost (US$/kg)	Media Cost (US$/kWh$_t$)
	Low	High					
Mineral Oil	200	300	770	2.6	55	0.30	4.2
Synthetic Oil	250	350	900	2.3	57	3.00	43.0
Silicone Oil	300	400	900	2.1	52	5.00	80.0
Nitrite Salts	250	450	1,825	1.5	152	1.00	12.0
Nitrate Salts	265	565	1,870	1.6	250	0.50	3.7
Carbonate Salts	450	850	2,100	1.8	430	2.40	11.0
Liquid Sodium	270	530	850	1.3	80	2.00	21.0

2.3.3.2 Nitrate Salts as Liquids in Sensible Heat TES

In recent years, nitrate salts have emerged as the most promising liquid storage media option due to their relatively low cost, low vapor pressure, and compatibility with operation at the high temperatures. Additionally, these salts are non-flammable and non-toxic (Herrmann & Kearney, 2002). Table 5 provides the results of a parametric study carried out to demonstrate the cost reduction in a TES system when the fluid media in changed from Therminal VP-1, a synthetic oil, to a ternary salt. In the 'Case ID' line, '2T' corresponds to a two-tank fluid system and 'TC' corresponds to a single-tank thermocline system.

Table 5: Reduction in TES Costs through Incorporation of Salt as Liquid Media (Kearney, et al., 2002)

Case ID	VP-1 No Sto	VP-1 66bar 2T	VP-1 66bar TC	Salt 450°C 2T	Salt 450°C TC	Salt 500°C 2T	Salt 500°C TC
Solar Field Size [m²]	270,320	427,280	427,280	425,100	425,100	425,100	425,100
Investment Cost [M$]	110,291	175,251	169,546	171,405	159,556	164,583	156,158
Thermal Storage Cost [M$]	0	21,330	15,897	19,674	8,390	14,141	6,117
Annual O&M cost [k$/yr]	3,583	4,088	4,088	4,282	4,282	4,282	4,282
Net Electric [GWh]	107.5	169.2	169.1	183.9	182.9	185.7	184.4
Mean Solar to electric efficieny	14.64%	14.58%	14.57%	15.92%	15.84%	16.08%	15.97%
LEC [USD/MWh]	**139.7**	**131.5**	**128.1**	**119.9**	**113.9**	**115.1**	**111.0**
LEC Reduction	-	5.9%	8.3%	14.2%	18.5%	17.6%	20.6%
Thermal Storage Cost $/kWh el	0.0	64.6	48.2	59.6	25.4	42.9	18.5
Thermal Storage Cost $/kWh th	0.0	23.7	17.7	23.6	10.1	17.4	7.5

The only significant drawbacks to incorporating nitrate salts as TES media are their high freezing temperatures and corrosive properties. Their high freezing temperatures require that special precautions have to be taken in system design to prevent salt solidification in pipe lines. Because of the salts' corrosive properties, all piping and containment vessels need be constructed from stainless steel; the corrosive properties also require that expensive specialized valves be used to regulate the flow. Research to lower the freezing point of these salts is ongoing. Table 6 presents the chemical composition of the three commonly used nitrate salts and their associated pricing (Energy storage costs are based on 200°C temperature increase).

Table 6: Composition, Melting Point, and Cost of Three Commonly-Used Nitrate Salts (Kearney, et al., 2002)

Property Composition (%)	Solar Salt	Hitec	Hitec XL
$NaNO_3$	60	7	7
KNO_3	40	53	45
$NaNO_2$	---	40	---
$Ca(NO_3)_2$	---	---	48
Melting Point (°C)	220	142	120
Cost per kg (US$/kg)	0.93	0.49	1.19
Energy Storage Cost (US$/kWh$_t$)	5.8	10.7	15.2

This work is largely concerned with reducing the cost of TES; therefore, Solar Salt, described in the first column of Table 6, is considered. Though it has a significantly higher melting point than the other options, its much-lower cost makes it the most attractive option. The thermo-physical properties of Solar Salt vary widely with temperature; they are expressed in equation form in EQ.2.2-EQ.2.5 (Xu et al., 2012).

- Density, ρ (kg/m^3)

$$\rho = 2090 - 0.636(T_{°C})$$ EQ.2.2

- Specific Heat, C_p (J/kg.K)

$$C_p = 1443 - 0.172(T_{°C})$$ EQ.2.3

- Thermal Conductivity, k (W/m.K)

$$k = 0.443 + 1.9(10)^{-4}(T_{°C})$$ EQ.2.4

- Viscosity, μ (kg/m.s)

$$\mu = [22.714 - 0.12(T_{°C}) + 2.281(10)^{-4}(T_{°C})^2 - 1.474(10)^{-7}(T_{°C})](10)^{-3}$$ EQ.2.5

From EQ.2.2-EQ.2.5, it can be seen that the thermo-physical properties vary widely over Solar Salt's operational range. This variation should at least be considered in modeling the performance of TES systems; much of the modeling conducted to date is based upon average fluid thermo-physical properties. For most TES system work conducted to date, the operational temperature range considered is about 100°C; in this limited range, using average fluid thermo-physical properties might not have serious impact on the model's accuracy. However, when Solar Salt is considered as the liquid media, operation ranges of over 300°C are possible. Over this wide range, significant variation of thermo-physical properties occurs and should at least be considered. A comparative study is conducted to evaluate the error induced by assuming

26

average thermo-physical properties instead of using actual thermo-physical properties; this study is presented in Section 3.1.4.

2.3.3.3 Solid Materials in Sensible Heat TES

Though molten salts can store energy much more cheaply than thermal oils, it is desired to find cheaper energy storage media. Numerous solid materials have been investigated for application in sensible heat TES systems. Desirable solid media characteristics include but are not limited to low cost, readily available, high heat capacity, low void fraction, compatibility with liquid media, and non-hazardous (Pacheco et al., 2002). A wide variety of solid materials have been investigated for this application; some promising solid media options and their thermo-physical properties are presented in Table 7.

Table 7: Thermo-Physical Properties and Cost of Some Investigated Filler Materials (Herrmann & Kearney, 2002)

Solid Media	Operating Temperature (^{o}C)		Average Density (kg/m^3)	Average Heat Capacity (kJ/kg.K)	Volume Specific Heat Capacity (kWh$_t$/m^3)	Media Cost (US$/kg)	Media Cost (US$/kWh$_t$)
	Low	High					
Sand-Rock-Mineral Oil	200	300	1,700	1.30	60	0.15	4.2
Reinforced Concrete	200	400	2,200	0.85	100	0.05	1.0
NaCl Solid	200	500	2,160	0.85	150	0.15	1.5
Cast Iron	200	400	7,200	0.56	160	1.00	32.0
Cast Steel	200	700	7,800	0.60	450	5.00	60.0
Silica Fire Brick	200	700	1,820	1.00	150	1.00	7.0
Magnesia Fire Brick	200	1,200	3,000	1.15	600	2.00	6.0

In addition to the materials identified above, limestone and quartzite course aggregate and sand have been identified as promising solid media candidates [(Brosseau, Kelton, Ray,

Edgar, Chisman, & Emms, 2005) and (Pacheco et al., 2002)].   Testing determined that both materials are chemically compatible with molten Solar Salt and capable of operating at the high upper temperature limits of Solar Salt.   Based upon the solid media presented in Table 7, concrete provides the cheapest energy storage media.   Laing suggests a combination of concrete and thermal oils for sensible heat TES (Laing et al., 2009).   The replacement of thermal oil with Solar Salt provides a cheaper means of TES.   A problem with incorporating concrete and Solar Salt in a TES system is that typical structural concrete loses strength at high temperature. Additional concerns are that the corrosive salt may degrade the aggregate and cementitious materials composing the concrete.   The development of concrete capable of retaining its structural and chemical stability in the elevated operating temperature ranges that Solar Salt is capable of operating in could significantly reduce the cost of TES.

2.4 Sensible Heat TES System Classification

Sensible heat TES systems are classified in numerous ways.   They are classified as either passive or active based upon the movement and configuration of the energy storage media.   They are classified as direct or indirect based upon the circulation of the HTF and liquid media. Lastly, they are classified as single or dual media systems based upon the type of media in which thermal energy is stored.

2.4.1 Passive Sensible Heat TES

In passive storage TES systems, HTF only enters the TES media during charging and discharging cycles (Gil, et al., 2010).   This type of TES system earns its name because the TES media, a solid, never moves; the heat is transported to and from it by a liquid transfer fluid.   To date, concrete and cartable ceramics are the primary solid media considered in this application (Tamme, Laing, & Steinmann, 2004).

28

Laing reports that the ceramic is based on Al_2O_3 binder and contains iron oxides as aggregates; these oxides are a byproduct from steel production (Laing, Steinmann, Tamme, & Richter, 2006). The concrete contains blast furnace cement as binder, and a combination of iron oxides and flue ash compose the aggregate (Laing et al., 2006). A comparison of the thermo-physical properties of these two materials is presented in Table 8. Though the ceramic has better thermal properties, concrete provides the better option because of its lower cost and higher strength.

Table 8: Thermal Properties of Castable Ceramics and High Temperature Concrete (T=350°C) (Laing et al., 2006)

Material	Castable Ceramic	High Temperature Concrete
Density (kg/m^3)	3500	2750
Specific Heat (J/kg.K)	866	916
Thermal Conductivity (W/m.K)	1.35	1.0
Thermal Strain Rate (10^{-6}/K)	11.8	9.3
Material Strength	Low	Medium
Crack Initiation	Few Cracks	Several Cracks

Passive sensible heat TES systems tested to date consist of heat exchangers embedded in concrete and ceramic specimens. Energy is transferred to and from the media by HTF which is circulated through the heat exchangers. Laing et al successfully demonstrated TES using thermal oil as HTF and a 20 m^3 concrete block with an imbedded array of 132 tube exchangers as storage media (Laing et al., 2009). This system operated in the temperature range of 350-400°C. The un-insulated block-and-tube unit tested by Laing et al is pictured in Figure 7. A study indicated that to provide a storage capacity of 1100 MWh$_{th}$ would require 50,000 m^3 of special concrete designed for high temperature applications (Laing et al., 2009).

Figure 7: Un-insulated 20 m³ Concrete Block-and-Tube TES Unit tested by Laing at DLR-German Aerospace Center (Laing et al., 2006)

To increase the energy storage density of a passive concrete TES system John et al developed ultra-high performance concrete (UHPC) that maintains structural integrity at temperatures of up to 600°C (John et al., 2011). Selvam and Castro investigated the effects of different heat exchanger configurations, such as plain-tube and finned-tube, and optimized the heat exchangers to provide the optimum rate of heat exchange to cost ratio (Selvam & Castro, 2010). Castro found that the optimum balance of performance and cost in the heat exchanger was provided by the heat exchanger fin configuration of a helicoidal auger (Selvam & Castro, 2010). Skinner combined the work of John and Selvam and Castro, testing concrete blocks with a single imbedded heat exchanger in the elevated temperature range of 400 °C -500°C (Skinner et al., 2011). During testing, Skinner noted significant cracking in the concrete due to dissimilar thermal strain rates of concrete and the stainless steel heat exchangers (Figure 8). The cracking was successfully mitigated by applying soft interface material at the interface of the concrete and heat exchanger (Skinner et al. 2011).

Figure 8: Cracking in Concrete Block with No Soft Material at Interface of Concrete and Stainless Steel Heat Exchanger (Skinner et al., 2011)

Skinner concluded that at this time, the block-and-tube system is prohibitively expensive due to the high cost of the stainless steel heat exchangers; however, they are required if molten salt is used as the HTF because of the salt's corrosive properties (Skinner et al., 2011). Gil et al reached the same conclusion, adding that the rate of heat transfer from the HTF to the concrete is relatively slow (Gil, et al., 2010). Additionally, the temperature of the heat transfer media exiting the system is not constant during charge, decreasing the efficiency of the power block's Rankin cycle (Skinner, 2011). Currently, no CSP plants incorporate passive storage.

2.4.2 Active Sensible Heat TES

Active TES systems are distinguished by forced convection heat transfer into the storage media. In active TES systems, heat energy is collected from the receiver and stored in tanks; two primary systems are used: two-tank fluid system and single-tank thermocline system. The active TES system can be further classified as direct or indirect based upon the manner in which the HTF is circulated.

2.4.2.1 Primary Tank Systems in Active Sensible Heat TES

2.4.2.1.1 Two-Tank Fluid TES

The two-tank fluid tank system is the most common configuration used in active sensible heat TES to date (Laing et al., 2009). The operation of two-tank TES systems is illustrated in Figure 9; in the first step, liquid media from the cold tank is heated in the solar collector and stored in the hot storage tank. When stored energy is needed, hot liquid media is drawn from the

31

hot storage tank and sent to the power plants power block. From the power block, the now cold fluid is returned to the cold storage tank.
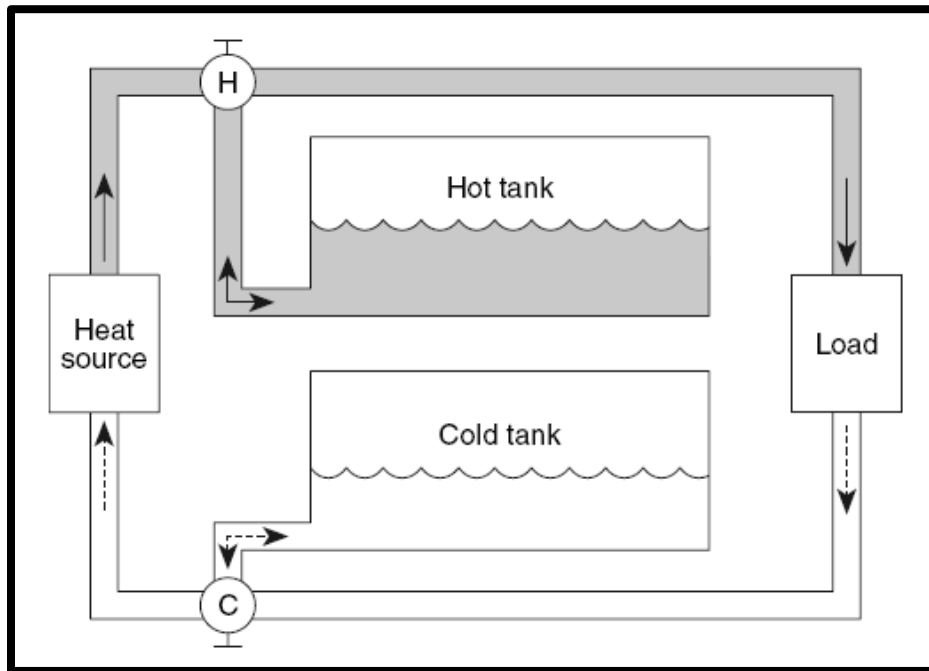
Figure 9: Illustration of Two-Tank Liquid Media TES System (Hammerschlag, Pratt, Schaber, & Widergren, 2006)

The two-tank fluid TES system is relatively simple in that the hot and cold liquid media are stored separate from each other, preventing any mixing. Another benefit of these systems is that about 85% of the hot tank volume is usable for TES (Pacheco et al., 2002). High cost is the major drawback to the two-tank fluid TES system. Compared to the one-tank thermocline TES system, the two-tank fluid TES system has a significantly larger liquid media inventory and an additional tank. Liquid media is known to be the most significant contributor to TES system costs. Pacheco states that the named contributors result in the two-tank liquid system costing about 35% more than the single tank thermocline system (Pacheco et al., 2002).

2.4.2.1.2 Single-Tank Thermocline TES

The single-tank thermocline TES concept has gained significant interest as efforts continue to reduce the cost of TES. The operation of a single-tank thermocline TES system is

illustrated in Figure 10. During the charging or energy storage cycle, cold liquid media is drawn from the base of the tank, heated in the solar collector, and added back to the top of the tank. During the discharging or energy retrieval cycle, hot liquid media is drawn from the top of the tank, sent to the power block of the power plant, and returned to the base of the tank.
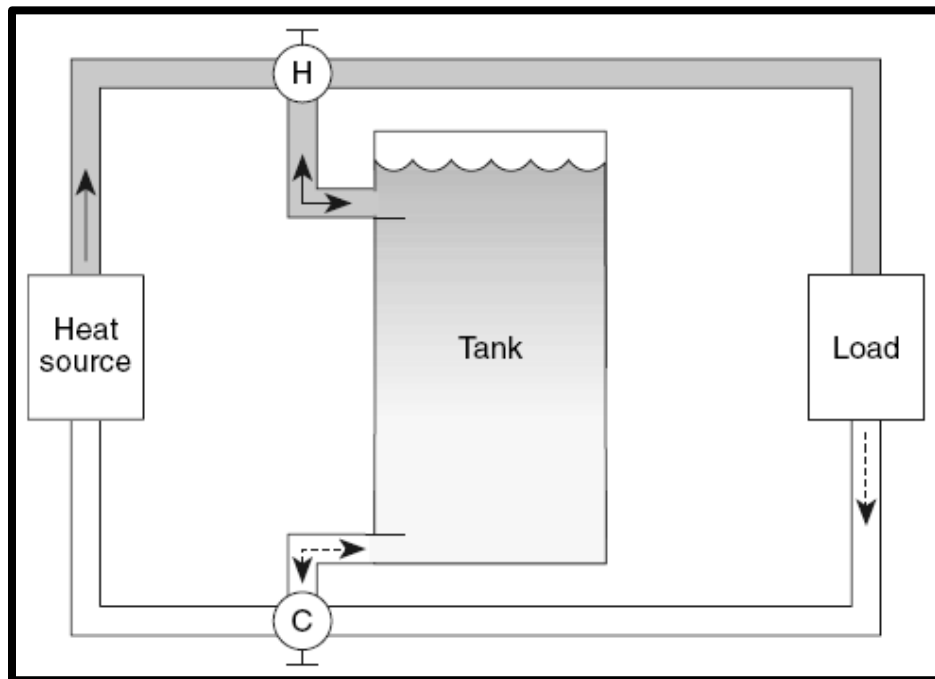
Figure 10: Illustration of Single Tank Thermocline TES (Hammerschlag et al., 2006)

The key to operating a single-tank thermocline TES system is that thermal stratification must exist at all times within the tank. This means that three unique temperature regions should be present at all times: a cold region at the base of the time, an intermediate thermal gradient, and a hot region at the top of the tank. During charging cycles, the hot region of the tank expands as more energy is stored; during discharging cycles, the cold region of the tank expands as energy is retrieved from the tank. Ideally, the region of the tank occupied by the thermocline, or thermal gradient, should not expand during charging or discharging. Figure 11 illustrates the movement of the temperature profile in a typical single-tank thermocline during a discharge cycle.
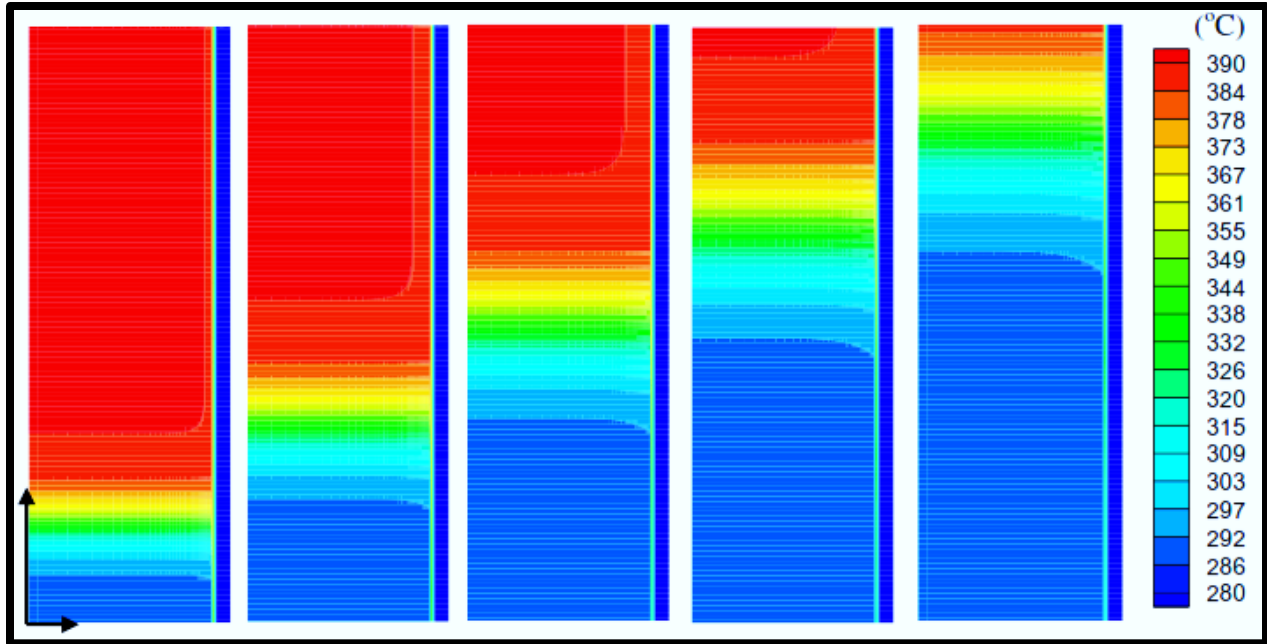
Figure 11: Temperature Profile in Single-Tank Thermocline TES System during Discharging (Left to Right with Time) (Xu et al., 2012)

2.4.3 Indirect and Direct Sensible Heat TES

Sensible heat TES systems are classified as indirect or direct based upon the flow of HTF and liquid media exhibited by the system.

2.4.3.1 Indirect TES

In indirect TES systems, the HTF and liquid storage media are separate fluids; the HTF circulates through the solar collector then passes through a heat exchanger where it passes the heat to the liquid storage media (Gil, et al., 2010). Figure 12 provides a schematic of a parabolic trough CSP power plant incorporating active indirect storage in a two-tank fluid TES system. Typically, thermal oil or other fluid with a low freezing temperature is used as the HTF to collect heat and transport it to the heat exchanger. A benefit of this configuration is that there is no concern of molten salt solidifying in the lines of the collection field. The downside to indirect sensible heat TES systems is that the oil-to-salt heat exchanger they require adds significant cost to the system.

34
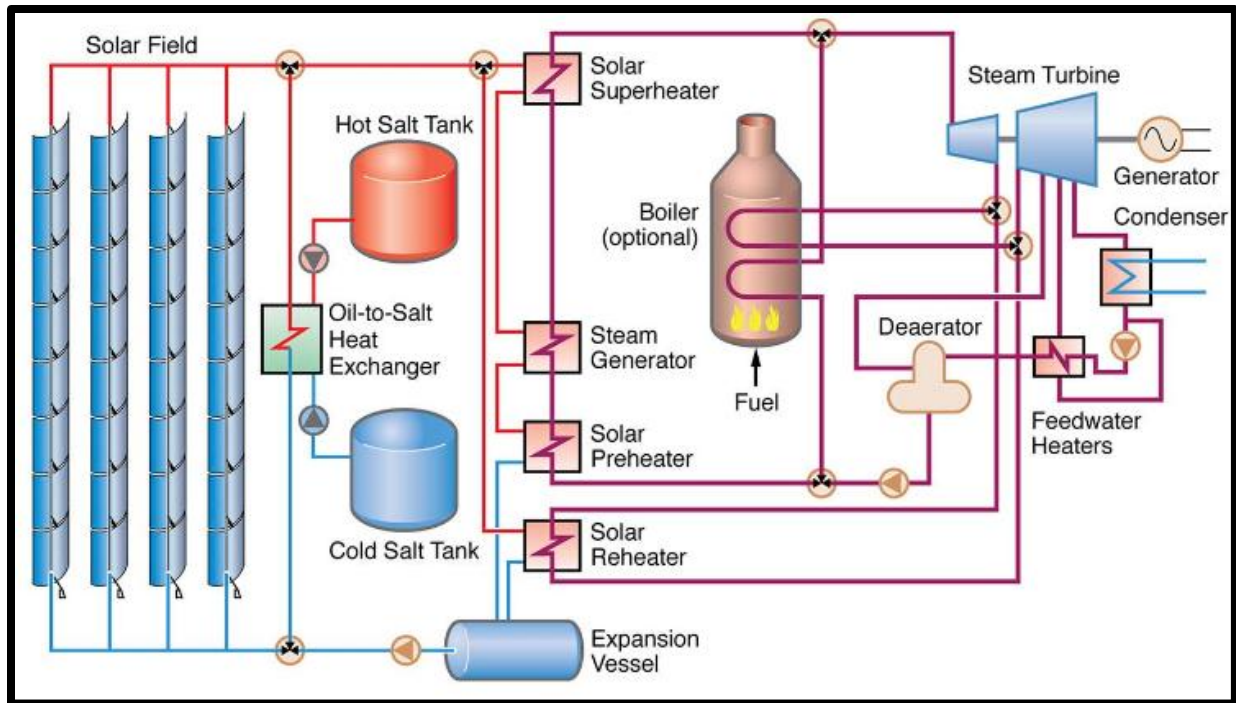
Figure 12: Parabolic Trough CSP Power Plant Incorporating Two-Tank AIS (EPRI, 2010)

2.4.3.2 Direct TES

In direct TES systems, the same fluid serves as both HTF and liquid storage media. Figure 13 provides a schematic of a central receiver CSP power plant incorporating two-tank active direct storage in a two-tank fluid system. Direct TES systems are cheaper than indirect TES systems because they do not require a HTF-to-liquid media heat exchanger.
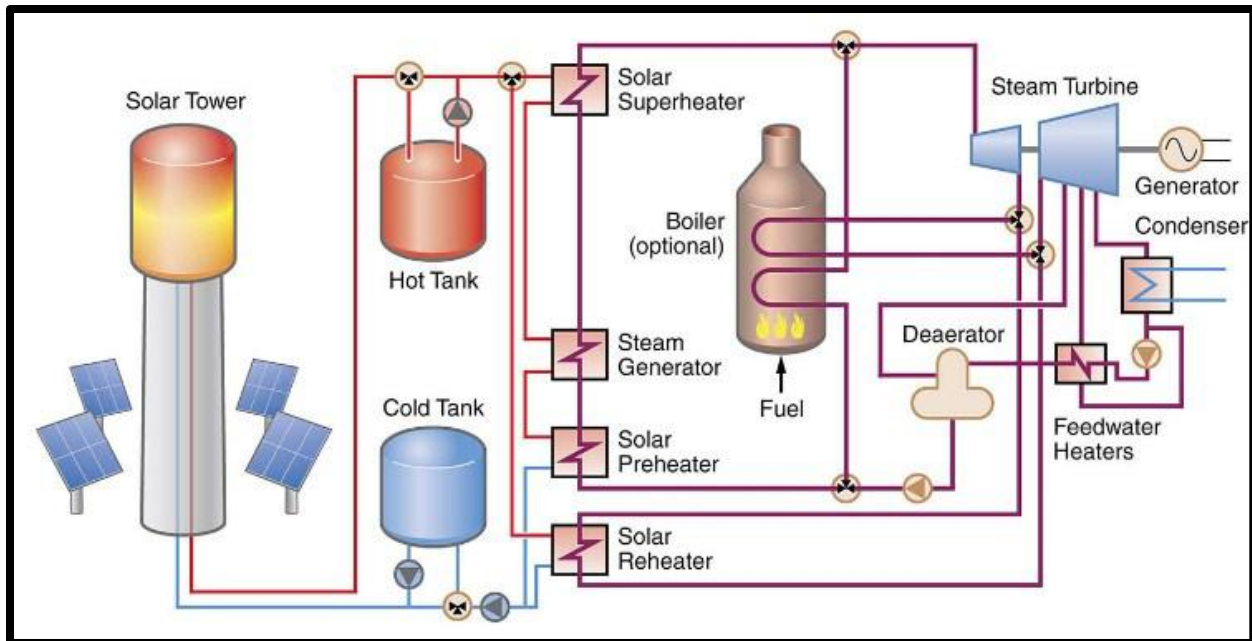
Figure 13: Central Receiver CSP Power Plant Incorporating Two-Tank ADS (EPRI, 2010)

As molten salts continue to rise in popularity, the direct TES system offers the most cost effective configuration. However, the use of molten salts in TES requires that precautions be taken to insure that they do not solidify in the system's piping. Countermeasures taken to make sure the salt does not solidify in the piping include placing heat traces along the pipes and circulating heated fluid from storage through the solar collection field lines during nighttime hours.

2.4.4 Single and Dual Media TES Systems

2.4.4.1 Single Media TES

A single media TES system is a system in which thermal energy is stored in only one media. Examples of single media TES systems include single-tank fluid thermocline and two-tank fluid systems. The major problem with single media fluid TES systems is the high cost and large inventory of the liquid media that they require. Most TES systems installed to date incorporate single media TES systems.

2.4.4.2 Dual Media TES

Dual media systems are TES systems in which both solid and liquid media are used in tandem to store heat. By definition, they are systems in which the capacitance of the solid and liquid are significant enough to not be neglected (Gil, et al., 2010). Dual media systems have gained significant interest because they allow a significant volume of expensive liquid storage media to be replaced with cheaper filler material. Reference Table 7 for a list of some solid media considered for application in dual media TES. Dual media TES is employed in single-tank thermocline systems; these systems can be further classified as packed bed or structured.

2.4.4.2.1 Packed Bed Thermocline TES

Packed bed systems are the most widely used configuration of thermocline TES systems. In packed bed TES systems, a significant volume of solid, porous filler material pieces is contained within a tank. Liquid media is circulated through the bed to transfer energy to and retrieve energy from the media. A schematic of a packed bed thermocline is provided in Figure 14 along with the charge/discharge fluid flow directions.
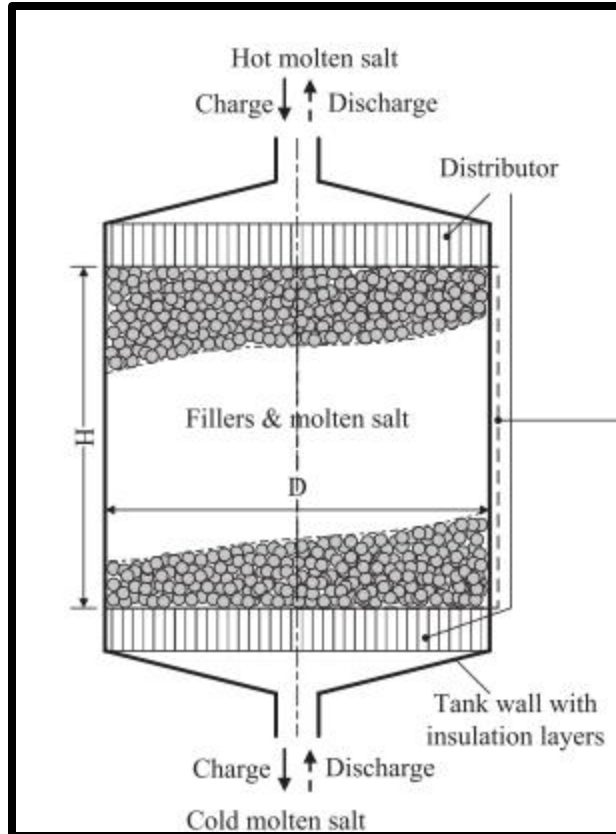
Figure 14: Schematic of Packed Bed Thermocline with Fluid Flow Directions Labeled (Xu et al., 2012)

Low media porosity is desired, as this decreases the necessary liquid media volume for the system. Typical reported bed porosities range from 0.22-0.25 [(Pacheco et al., 2002), (Brosseau et al., 2005), and (Flueckiger, Yang, & Garimella, 2011)]. In thermocline-type sensible heat TES systems (to be discussed later), the filler material is noted for enhancing thermal stratification in the storage tank compared with stratification of a fluid only tank (Brown, 2012).

One significant problem associated with packed bed TES systems is known as thermal ratcheting. During a charge cycle, the temperature of the tank is increased, as hot HTF flows into the tank. Typical storage tanks are constructed from stainless steel which has a significantly higher thermal strain rate than any investigated filler materials. As the tank walls heat up and expand, filler material settles from above, occupying this new volume. During the discharge

38

cycle, the tank's temperature decreases and the walls contract; however, the settled filler material volume prevents the walls from returning to their initial location. This induces a residual stress in the walls and over repeated thermal cycles can lead to catastrophic rupture of the tank (Flueckiger et al., 2011).

The issue of thermal ratcheting can be addressed in two ways. The first approach is to place reinforcement around the tank to resist its outward expansion. The second approach is to develop a structured filler material to place inside the tank in place of the packed bed (Brown et al., 2012).

<u>2.4.4.2.2 Structured Thermocline TES</u>

The concept of developing structured filler material for a single-tank thermocline TES is a relatively new concept, developed in the work of Brown (Brown et al., 2012). The benefits provided by structured filler material are threefold. First, a significant volume of liquid media is displaced by a much cheaper concrete. Second, the issue of thermal ratcheting of the tank walls, a plaguing problem in packed bed thermocline TES is avoided. Finally, the geometry of the concrete filler can be optimized to enhance heat transfer and TES system response time, or the rate at which energy can be stored in and retrieved from storage. Though the structured concrete thermocline has not yet left the testing stage, it provides a promising option for TES in the future.

2.5 CSP Power Plants Incorporating TES

This section presents and discusses examples of CSP plants employing TES that are in operation now or that were in operation in the past. TES systems are classified as either direct or indirect, and then classified further within these subsections.

2.5.1 Direct TES CSP Power Plants

2.5.1.1 Active Direct Storage: Steam Storage

Active direct storage (ADS) CSP power plants incorporating direct steam generation use water as HTF and generate steam in the solar collection field. It is not economical to store steam directly; therefore, steam accumulators are used to store sensible heat in pressurized, saturated liquid water (Medrano, Gil, Martorell, Potau, & Cabeza, 2010). An example of this concept is the 10 MW PS10 solar plant in Seville, Spain. PS10 has been in operation since 1999; it is a central receiver plant that produces steam at 250°C and 40 bar (Medrano et al., 2010). The plants ADS system consists of 4 tanks and can store about 12 MWh$_{th}$, sufficient thermal energy to operate for 50 minutes. The plant's solar-to-electrical efficiency is about 17.5% with storage efficiency of about 92.4%. Figure 15 depicts one of the four TES tanks at the PS10 solar plant.

Figure 15: Energy Storage Tank at 10 MW Central Receiver ADS Plant in Seville, Spain (Medrano et al., 2010)

2.4.1.2 Active Direct Storage: Two-Tank Oil Storage

The SEGS I plant in California is a parabolic trough CSP plant employing two-tank fluid TES; thermal oil is used as the HTF and liquid storage media. SEGS operates in the temperature range of 240-307°C and has capability to store sufficient energy for up to three hours of

40

operation (Medrano et al., 2010). The synthetic oil used as HTF comprised 42% of the TES system cost, rendering it cost-ineffective (Medrano et al., 2010). Since the SEGS I experiment, the two-tank oil ADS concept has not been repeated. The SEGS I power plant and parabolic trough field are pictured in Figure 16.

Figure 16: 10 MW SEGS I Power Plant and Trough Array in California (NREL, Parabolic Trough Power Plant System Techology, 2010)

2.4.1.3 Active Direct Storage: Two-Tank Molten Salt Storage

Solar Two, located in California, incorporated a two-tank molten salt storage system; this plant operated between the temperature limits of 290-565°C and was capable of storing 105 MWh$_t$ (Medrano et al., 2010). The cold HTF storage tank contained three 25 kW$_e$ heaters to prevent the fluid temperature from falling below 290°C and the hot HTF storage tank contained four 25 kW$_e$ heaters to prevent the fluid temperature from falling below 565°C (Medrano et al., 2010). The Solar Two plant achieved a solar-to-electric efficiency of 19% with a round-trip storage efficiency of 97% (Medrano et al., 2010). Solar Two only was operational for 4 years, from 1995-1999, before it was decommissioned. Figure 17 depicts the central receiver and hot and cold storage tanks at Solar Two.

Figure 17: Central Receiver and Hot and Cold HTF Tanks at Solar Two in California (NASS, 2012)

Gemasolar is a 19.9 MW plant located near Seville Spain that began operation in 2011; it incorporates a two-tank molten salt ADS system providing up to 15 hours of TES (NREL, 2011). Gemasolar operates between the temperature limits of 290-565°C. The plant was initially commissioned under the name Solar Tres as a 15 MW plant. Storage allows the plant to produce electricity for 6500 of the 8760 hours of the year, which is significantly more than other CSP plants (Medrano et al., 2010). Solar-to-electric efficiency and TES roundtrip efficiency values are not available at this time. Figure 18 depicts the central receiver of the Gemasolar plant; the hot and cold storage tanks may be seen to the left and right of the receiver.

Figure 18: Central Receiver and Energy Storage Tanks at 19.9 MW Gemasolar Plant in Seville, Spain (Harrington, 2012)

2.4.1.4 Active Direct Storage: Single-Tank Molten Salt Thermocline Storage

To date, only one thermocline ADS has been demonstrated; this plant, Solar One, was constructed in Daggett, CA and operated from 1982-1988. It was designed as a 10 MW central receiver plant incorporating a packed bed thermocline TES; aggregate and sand were used as solid media and oil was used as the HTF (Medrano et al., 2010). This plant was never very successful, struggling to operate for eight hours a day; it provided a solar-to-electric efficiency of 16% (Medrano et al., 2010). In 1995, Solar One was converted into Solar Two (See Section 2.4.1.3). Figure 19 depicts the Solar One central receiver and thermocline TES tank.

Figure 19: Central Receiver and Thermocline Tank at 10 MW Solar One in Daggett, CA (Morris, 2011)

2.5.2 Indirect TES CSP Power Plants

To date, only a single CSP power plant employing active indirect TES has been constructed. This plant, Andasol I located in Grenada, Spain is a 50 MW parabolic trough CSP plant incorporating a two-tank molten salt TES system. It has been operational since 2008, supplying about 200,000 households with electricity (NREL, 2011). Andasol operates between the temperature limits of 293 ^{o}C -393°C; it incorporates Diphenyl/Biphenyl oxide as HTF and molten salt as liquid storage media. Energy storage permits Andasol I to operate for up to 7.5 hours on stored heat (Medrano et al., 2010). Because of the relatively low operating temperature range, Andasol has a somewhat low solar-to-electric energy conversion efficiency average of 14.7% (Medrano et al., 2010). Figure 20 depicts the trough array and hot and cold energy storage tanks at the Andasol plant, which are reportedly 14 m in height and 36 m in diameter (NREL, Concentrating Solar Power Projects: Andasol-1, 2011).

Figure 20: Two-Tank TES and Trough Array at 50 MW Andasol I in Grenada, Spain (Craig, 2011)

2.6 TES System Cost Estimation

Before deciding on the type of TES system to install at a CSP plant, it is crucial to complete an economic analysis to determine the cost-minimizing option. Attaining estimates for the two TES configurations considered today, two-tank liquid and single-tank thermocline is a significant challenge, as system costs are dependent on numerous contributors. The complexity in cost estimation largely lies in understanding the costs of the components in each system; because not much work has been completed in this area, the only way to attain thorough estimates would be to go through the design on a piecewise basis and price all components. Additionally, estimating the construction and management costs associated with a project of this magnitude and complexity would require a significant background in project design and management.

In 2010, the Electric Power Research Institute (EPRI) released a report detailing the design and cost of both single-tank thermocline and two-tank TES systems (EPRI, 2010). The TES systems reported by EPRI range in size between 100 MWh_t and 3500 MWh_t and are

designed as both indirect and direct systems. Additional design considerations include incorporation in parabolic trough CSP plants (Operating temperature limit of 400°C) and incorporation in central receiver CSP plants (Operating temperature limit of 560°C). For this work, only systems incorporating central receiver systems and direct TES are of interest. EPRI's cost estimates for two-tank and thermocline TES systems are summarized in Table 9 and Table 10 respectively.

Studying the values presented in these tables provides a good benchmark and comparison of direct, two-tank and thermocline TES systems. Additionally, it provides valuable insight into the significant cost contributors, both direct and indirect, that should be considered in estimating the cost of a TES system. The values presented below are reasonably accurate, reportedly within 20-30% of the actual component costs (EPRI, 2010).

Table 9: EPRI Cost Estimation of Two-Tank TES Systems Based on Capacity (EPRI, 2010)

Complete TES System Cost Estimate				
Capacity (MWh$_t$)	**100**	**500**	**1000**	**3000**
Direct Costs				
Foundation	$369,000	$1,280,000	$2,270,000	$12,000,000
Platform and Steel	$1,252,000	$1,182,000	$2,112,000	$1,640,000
Storage Tanks	$2,555,000	$8,576,000	$13,434,000	$37,026,000
Insulation	$65,000	$148,000	$219,000	$440,000
Filler Preheating Equip.	$0	$0	$0	$0
Surge Tanks	$0	$0	$0	$0
Pumps and PCE	$1,410,000	$2,830,000	$4,250,000	$9,450,000
Salt Melting System	$1,480,000	$2,020,000	$2,700,000	$3,380,000
Piping and Valves	$463,000	$1,016,000	$1,383,000	$2,750,000
Electrical	$179,000	$241,000	$298,000	$732,000
Instrumentation/Controls	$293,000	$293,000	$293,000	$343,000
Quartzite ($12.95/ton)	$0	$0	$0	$0
Salt ($0.53/lb)	$1,210,000	$6,060,000	$12,100,000	$36,400,000
Energy Cost Melting Salt	$8,000	$37,000	$80,000	$120,000
Direct Subtotal	**$9,284,000**	**$23,683,000**	**$39,139,000**	**$104,281,000**
Indirect Costs				
Contingency (15% Direct)	$1,392,600	$3,552,450	$5,870,850	$15,642,150
Material Sales Tax (8.75% Direct)	$812,350	$2,072,263	$3,424,663	$9,124,588
Engineering (3% Direct)	$278,520	$710,490	$1,174,170	$3,128,430
Construction Indirect Costs	$3,870,000	$6,400,000	$7,975,000	$12,700,000
Construction Management	$1,500,000	$1,500,000	$1,500,000	$1,500,000
Indirect Subtotal	**$7,853,470**	**$14,235,203**	**$19,944,683**	**$42,095,168**
TES System Cost Summary				
Total	**$17,137,470**	**$37,918,203**	**$59,083,683**	**$146,376,168**
Capacity Cost ($/kWh$_t$)	**$171.37**	**$75.84**	**$59.08**	**$48.79**

Table 10: EPRI Cost Estimation of Thermocline TES Systems Based on Capacity (EPRI, 2010)

Complete TES System Cost Estimate				
Capacity (MWh$_t$)	100	500	1000	3000
Direct Costs				
Foundation	$342,000	$1,240,000	$2,280,000	$6,560,000
Platform and Steel	$1,095,000	$1,145,000	$1,182,000	$1,641,000
Storage Tank	$1,715,000	$7,900,000	$11,700,000	$31,130,000
Insulation	$253,000	$606,000	$944,000	$1,148,000
Filler Preheating Equip.	$215,000	$636,000	$1,100,000	$2,360,000
Surge Tanks	$32,000	$95,000	$240,000	$450,000
Pumps and PCE	$1,170,000	$2,590,000	$3,890,000	$8,670,000
Salt Melting System	$1,420,000	$1,680,000	$1,990,000	$3,320,000
Piping and Valves	$464,000	$1,020,000	$1,380,000	$2,750,000
Electrical	$179,000	$242,000	$298,000	$732,000
Instrumentation/Controls	$293,000	$293,000	$293,000	$343,000
Quartzite ($12.95/ton)	$622,000	$709,000	$819,000	$1,260,000
Salt ($0.53/lb)	$586,000	$2,930,000	$5,780,000	$17,300,000
Energy Cost Melting Salt	$4,000	$18,000	$36,000	$110,000
Direct Subtotal	**$8,390,000**	**$21,104,000**	**$31,932,000**	**$77,774,000**
Indirect Costs				
Contingency (15% Direct)	$1,258,500	$3,165,600	$4,789,800	$11,666,100
Material Sales Tax (8.75% Direct)	$734,125	$1,846,600	$2,794,050	$6,805,225
Engineering (3% Direct)	$251,700	$633,120	$957,960	$2,333,220
Construction Indirect Costs	$839,000	$2,100,000	$3,195,000	$7,750,000
Construction Management	$1,500,000	$1,500,000	$1,500,000	$3,000,000
Indirect Subtotal	**$4,583,325**	**$9,245,320**	**$13,236,810**	**$31,554,545**
TES System Cost Summary				
Total	**$12,973,325**	**$30,349,320**	**$45,168,810**	**$109,328,545**
Capacity Cost ($/kWh$_t$)	**$129.73**	**$60.70**	**$45.17**	**$36.44**

2.7 Conclusions from Literature Review and Motivation for Thesis

TES is needed for CSP power plants to become primary suppliers of electricity. Aside from the fact that TES increases power plant efficiency by providing heat to the power block at a constant rate, it also allows electricity to be produced at night when the sun's irradiance is not present but demand for electricity still is. Though plants could be upsized so as to produce

48

excess electricity during daylight hours and store it for nighttime use, it is much cheaper to store energy as heat than as electricity.

Molten salts are identified as a very promising liquid media because they allow high operating temperatures and have low costs relative to other liquid media used in TES. TES system costs can be reduced by containing the molten salt in a single-tank thermocline TES system. A further reduction in cost can be recognized by displacing a significant volume of the molten salt inventory with a solid media. To avoid the issue of thermal ratcheting of the tank's walls associated with loose filler material, structured concrete has been suggested as filler material (Brown et al., 2012).

Concrete mix designs have been developed and preliminary testing has demonstrated their compatibility with molten salt up to a temperature of $600^{\circ}C$ (John, 2012). Testing consisted of both isothermal tests and thermal cycling tests in which cube specimens were heated in an oven in the presence of both air and molten salt (John, 2012). The results of this testing identify four concrete mix designs as candidates for application in a structured concrete and molten salt TES system. However, further testing of the mix designs is necessary before they are tested in a thermocline system. During the reported specimen testing, the specimens were heated at a uniform, slow rate preventing the establishment of thermal gradients within the specimens. Structured concrete filler material, if the units of filler material are of any significant size, within a thermocline system will most certainly be subject to thermal gradients. Therefore, the effects of possible resulting thermal shock on the specimens must be evaluated through further testing.

TES systems are expensive to construct and operate; therefore, it is expedient to understand the operational parameters that allow optimum system performance. One approach to gaining this insight is to experiment; however, even at the test scale, TES systems are very

49

costly. An alternative approach is to conduct numeric simulations to optimize system parameters before testing. Optimized geometries for structured concrete filler material are reported in the work of Brown (Brown, 2012). This work employs a 2D finite difference based model developed by Selvam (Selvam, 2011). One approach to demonstrate the performance and economic viability of a structured concrete TES system, is to simulate the overall performance of a CSP power plant incorporating a single-tank thermocline TES system compare the results to the performance of CSP power plants incorporating other types of TES.

The National Renewable Energy Lab (NREL) has developed a software package known as System Advisory Model (SAM) that allows the simulation of CSP power plants with various forms of TES, including the packed-bed single-tank thermocline TES system. Unfortunately, there is no structured single-tank thermocline TES system option.

The thermocline function of SAM employs a 1D heat transfer model based on the Schumann equation, widely used and accepted for modeling heat transfer for fluid flow through packed beds. To simulate the effects of structured filler material using SAM, it is necessary to first understand the interworking of the thermocline model based on the Schumann equation. After this understanding is attained, parameters of the Schumann Model can be varied to attain similar results to those of the 2D Model. These adjusted parameters of the Schumann Model then can be input to SAM, effectively simulating a CSP power plant with a single-tank structured concrete TES system.

CHAPTER 3: MODELING OF THERMOCLINE TES SYSTEMS

TES systems are very expensive to construct and operate; therefore, it is expedient to understand the operational parameters that will allow optimum system performance. One approach to gaining this insight is to experiment; however, even at the test scale, TES systems are very costly. An alternative approach is to conduct numeric simulations to optimize thermocline system operations.

The majority of thermocline TES simulations to date have been based upon the two-phase Schumann Model (Singh, Saini, & Saini, 2009). The 1D Schumann Model provides a good, relatively-simple means of describing heat transfer in a packed-bed thermocline TES system. However, it makes many simplifying assumptions, which are discussed in Section 3.1. In previous work, a 2D Model was developed and used to describe heat transfer in a structured concrete thermocline TES system (Brown, 2012).

One of the goals of this thesis is to perform a life cycle cost and performance analysis of a power plant with a structured thermocline TES system. Significant work has been put into optimizing the geometry of the structured media using a 2D heat transfer model and can be found in the work of Brown (2012). System Advisory Model (SAM), a CSP plant modeling software made available through NREL, is capable of simulating a CSP plant with thermocline TES over a life cycle. It has been decided that this software should be used to model the cost and performance of a structured thermocline system for comparison with other configurations of sensible heat TES systems, such as the two-tank fluid-only system and the packed-bed thermocline system.

The thermocline TES module was recently added to SAM by incorporating the model originally written for Transient System Simulation Tool (TRNSYS) (NREL, 2012). The

TRNSYS thermocline model uses the 1D Schumann equation to describe interstitial heat transfer. To accurately simulate a structured concrete thermocline in SAM, the 1D and 2D models must be used, for the specified parameters, to simulate the performance of the given thermocline. If the temperature profiles and system efficiencies are similar, it is acceptable to treat the structured concrete thermocline as a packed bed thermocline when modeling it. However, if the system efficiency and temperature profiles are significantly different, it is necessary to modify the input parameters so as to attain similar performance from the 1D model as the 2D model.

The 1D packed-bed thermocline (PBTC) model, its fundamental assumptions, and numerical development are discussed in section 3.1. Convergence and optimization studies are presented and discussed. A study is presented in which the impact of assuming constant fluid properties is conducted and conclusions about the validity of this assumption are drawn. Finally, optimized models considering a packed bed of quartzite and a packed bed of limestone aggregate are presented.

The 2D structured concrete thermocline (SCTC) model and its fundamental assumptions are discussed in Section 3.2. The model optimized previously in the work of Brown (2012) is presented and discussed. A study is conducted to further optimize the STC model; a final optimized model is presented.

SAM is discussed in Section 3.3. Some previous works incorporating SAM are briefly discussed, along with basic operation and input data information. Discussion then moves to cover the type of CSP plant being used and the specifics of the plant. Finally, a procedure for calculating the necessary TES unit capacity cost values for each TES system being considered is presented.

52

3.1 1D Packed-Bed Thermocline Model (PBTC)

The Schumann equation was developed to describe heat transfer between a fluid and porous media as the fluid flows through it (Schumann, 1929). It is classified as a two-phase model because the solution of the Schumann equation allows for both the solid and fluid temperatures to be known at each location along the thermocline tank. This 1D model assumes that there is a uniform temperature across every cross sectional location of the tank, meaning no heat transfer occurs in the radial direction.

3.1.1 Schumann Equation and Assumptions

3.1.1.1 Schumann Equation

EQ.3.1 and EQ.3.2 are the governing equations for expressing the respective fluid and solid temperatures along the height of the thermocline tank as expressed by Pacheco (Pacheco et al., 2002). The subscripts 'F' and 'B' correspond to fluid and bed respectively.

$$\left(\rho C_p\right)_F \varepsilon \frac{\partial T_F}{\partial t} = -\frac{\left(\dot{m}C_p\right)_F}{A_c}\frac{\partial T_F}{\partial y} - h_v(T_F - T_B) \qquad \text{EQ. 3.1}$$

$$\left(\rho C_p\right)_B (1-\varepsilon)\frac{\partial T_B}{\partial t} = -h_v(T_B - T_F) \qquad \text{EQ. 3.2}$$

T_F = Fluid temperature (℃)

T_B = Bed temperature (℃)

t = Time (s)

ρ = Density (kg/m³)

C_p = Specific heat capacity (J/kg. K)

h_v = Interstitial heat transfer coefficient (W/m³. K)

A_c = Tank cross section (m²)

ε = Bed void fraction

$\dot{m}$ = Fluid mass flow rate (kg/s)

The bed void fraction (EQ.3.3) is the ratio of fluid volume contained within the bed to the combined fluid and solid volume contained within the bed. It is important to note that the fluid volume reference refers to only the bed region of the thermocline tank, as the upper and lower 10% of thermocline tanks is usually occupied by fluid alone; the fluid volume in these regions does not factor into the calculation of the bed's void fraction. A void fraction of 0.0 corresponds to a completely solid bed and void fraction of 1.0 corresponds to a completely fluid bed. Larger aggregate sizes result in larger void fractions, while smaller aggregate sizes and aggregate and sand combinations yield smaller void fractions. Void fractions used in previous models include 0.42 (Mawire, McPherson, van den Heetkamp, & Mlatho, 2009), 0.24 (Pacheco et al., 2002), 0.23 [(Adeyanj, 2009) and (McMahan, 2006)], and 0.22 (Xu et al., 2012).

$$\varepsilon = \frac{V_F}{V_F + V_B} \qquad\qquad\qquad\qquad EQ.\ 3.3$$

V_F = fluid volume in bed region of thermocline tank (m^3)

V_B = solid bed material volume within bed region of thermocline tank (m^3)

Developing the interstitial heat transfer coefficient between the fluid and packed bed is perhaps the most challenging aspect of using the Schumann equation. This discussion concerns flow around spheres and through beds of spherical particles, as the PBTC model being developed assumes spherical bed material. Significant quantities of research in the area of convection heat transfer for fluid flowing around spheres has led to the development of an expression for the Nusselt number, as seen in EQ.3.4 (Çengel, 2007). This expression is that it is known to bear up to 30% error (Çengel, 2007). Presented with the expression are limitations on the Prandtl and Reynolds numbers.

54

$$N_{u,sphere} = 2 + \left[0.4R_e^{\frac{1}{2}} + 0.06R_e^{\frac{2}{3}}\right] P_r^{\frac{2}{5}} \left(\frac{\mu_\infty}{\mu_s}\right)^{\frac{1}{4}} \qquad \text{EQ. 3.4}$$

$3.5 \leq R_e \leq 80,000$

$0.7 \leq P_r \leq 380$

R_e = Reynolds number

P_r = Prandtl number

μ_∞ = Fluid viscosity at free stream temperature (kg.m/s)

μ_s = Fluid viscosity at sphere surface temperature (kg.m/s)

To calculate the Nusselt number presented in EQ.3.4, it is necessary to first calculate the Reynolds and Prandtl numbers. Both values are computed using material properties that correspond to the average of the solid surface and fluid stream temperatures. EQ.3.5 and EQ.3.6 are expressions for the Reynolds and Prandtl Numbers respectively (Çengel, 2007).

$$R_e = \frac{\rho_{F,avg} D_{sphere} v_{avg}}{\mu_{avg}} \qquad \text{EQ. 3.5}$$

ρ_F = Average fluid density (kg/m^3)

D_{sphere} = Sphere diameter (m)

v_{avg} = Average fluid velocity (m/s)

μ_{avg} = Average fluid viscisity (kg.m/s)

$$P_r = \frac{C_{pF,avg} \mu_{avg}}{k_{F,avg}} \qquad \text{EQ. 3.6}$$

$C_{pF,avg}$ = Average fluid specific heat (J/kg.K)

μ_{avg} = Average fluid viscisity (kg.m/s)

$k_{F,avg}$ = Average fluid thermal conductivity (W/m.K)

After calculating the Reynolds and Prandtl numbers, the Nusselt number is calculated using EQ.3.4. After attaining the Nusselt number, the convection coefficient, "h", is calculated using EQ.3.7.

$$h = \frac{N_{u_{sphere}} k_{F,avg}}{D}$$
EQ. 3.7

In most applications, namely heat exchangers, where forced convection is the primary mode of heat transfer, the fluid flow is over a uniform surface, making it convenient to leave the convection coefficient in terms of surface area. However, in the packed bed application, it is convenient to express this coefficient as a function of volume, accounting for the surface area of the spherical particles composing each division of the thermocline storage tank. The expression for the volumetric interstitial convection coefficient, "h_v", as provided by Pacheco is presented in EQ.3.8 (Pacheco et al., 2002).

$$h_v = \frac{6h(1 - \varepsilon)\alpha}{D}$$
EQ. 3.8

h = Convection coefficient (W/m^2.K)

ε = Bed void fraction

α = Surface area shape factor

D = Bed particle diameter

The surface area shape factor accounts for the shape of the filler material composing the packed bed. It is defined as the ratio of the surface area of a sphere having the same volume as the shape being considered to the surface area of the shape. This definition is expressed by EQ.3.9.

$$\alpha = \frac{A_{s,sphere}}{A_{s,shape}} = \frac{4\pi r_{sphere}^2}{A_{s,shape}}$$
EQ. 3.9

56

$A_{s,sphere}$ = Surface area of sphere with equivalent volume (m²)

$A_{s,shape}$ = Surface area of shape being considered (m²)

r_{sphere} = Radius of sphere with equivalent volume to shape (m)

In this work, it is assumed that the shape of the material composing the packed bed is spherical; therefore the shape factor has a value of 1.

Numerous works provide alternative approaches to calculating the volumetric heat transfer coefficient aside from the procedure outlined in EQ.3.4-EQ.3.9. Xu et al. (2012) provides a literature review in which five different expressions for the volumetric heat transfer coefficient are presented and compared. Comparing the result from EQ 3.8 with results using Xu's expressions, it was found that the results predicted by four of the five expressions agreed within 30%.

3.1.1.2 PBTC Model Assumptions

The PBTC model provides a simplified means of attaining a transient temperature profile for a porous media with fluid passing through it. These assumptions, as recorded by Schumann, are presented below (Schumann, 1929).

- Individual particles composing the packed bed have high enough thermal diffusivity or are small enough to prevent thermal gradients from forming within them. This means that a particle may be assumed to be at a given temperature throughout its volume.

- Convection is the dominate mode of heat transfer in the system; therefore, heat transfer between particles in the bed or through the fluid by conduction can be neglected.

- At any given point, the rate of heat transfer from fluid to solid is proportional to the temperature difference between fluid and solid at that point.

- Thermo physical properties are constant.

- No heat is lost to the environment.

3.1.2 Numeric Formulation of PBTC Model

Derivations of the partial differential equations governing the PBTC Model can be found in literature [(McMahan, 2006) and (Schumann, 1929)]; because the validity of this model has been demonstrated in numerous works and is not questioned, there is no need to go through the mathematical exercise. The numeric model is developed using EQ.3.1 and EQ.3.2 to describe heat transfer within the system.

The first step in developing the numeric model is to determine the solution type: explicit or implicit. An explicit solution involves writing a series of equations that can be solved directly, in this case for the fluid and bed temperatures at each location along the tank's height in the present time step. The explicit solution is advantageous in that it requires no numeric solver; the major drawback to this solution is that a time step limitation exists. If a time step greater than the limit is used, the solution diverges. The implicit solution is advantageous because it is valid for any time step length. In larger, more computation intensive models, the implementation of a numeric solver might bear more significant concerns of increased run time. However, for this relatively simple model, the number of computations executed by the solver has little impact on the simulation's runtime. For this reason, an implicit solution type was selected for the model basis. The computational domain, or thermocline tank, considered in this model is pictured in Figure 21.
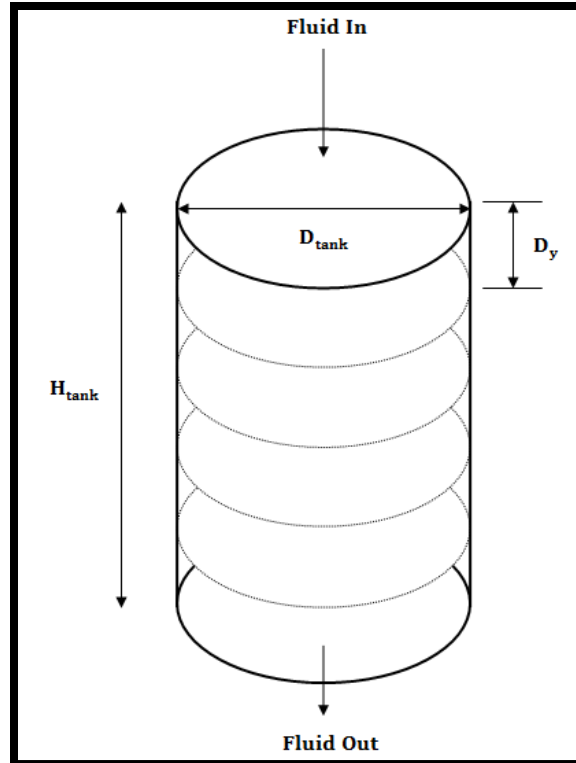
Figure 21: Computational Domain of Packed Bed Thermocline

Figure 21 depicts the computational domain for a packed bed thermocline undergoing a charge cycle; this is made evident by the fluid being added to the top of the tank. Also labeled in the figure are the tank height, the thickness of each differential element considered, and the tank diameter. The numeric models for the charge and discharge cycles are almost identical except for two differences. The differences are as follow:

- Backward difference is used in modeling the charging cycle while forward difference is used in modeling the discharge cycle.

- The temperature of the top element is fixed at the maximum operating temperature during the charge cycle while the temperature of the bottom element is fixed at the minimum operating temperature during the discharge cycle.

Backward difference is used in modeling the charging cycle because the solution process moves from the first node to the last with the temperature of the first element always being

known. It is necessary to use forward difference in the discharge cycle because the solution process moves from the last node to the first, with the temperature of the last slice always being known. The temperature of the first node is fixed during the charge cycle because it is assumed that hot heat transfer fluid is being added to the system at a constant temperature and exiting at a decreased temperature. The temperature of the last element is fixed during the discharge cycle because it is assumed that cold fluid is fed into the base of the tank to retrieve heat from the solid media and exits at an elevated temperature. Because the models of the charge and discharge cycles are so similar, only the charge cycle is developed in detail.

To begin the explicit solution procedure, it is necessary to assume an initial temperature distribution throughout the computational domain. This includes setting the temperature of the first node to the maximum fluid inlet temperature. After assuming this temperature distribution, a series of equations is developed to describe the temperature of the solid and fluid in each element in the upcoming time step. The fluid and solid temperatures of an element in the upcoming time step are functions of the elements fluid and solid temperatures in the current time step and the fluid and solid temperatures of the element located before it in the upcoming time step. This is illustrated in Figure 22.
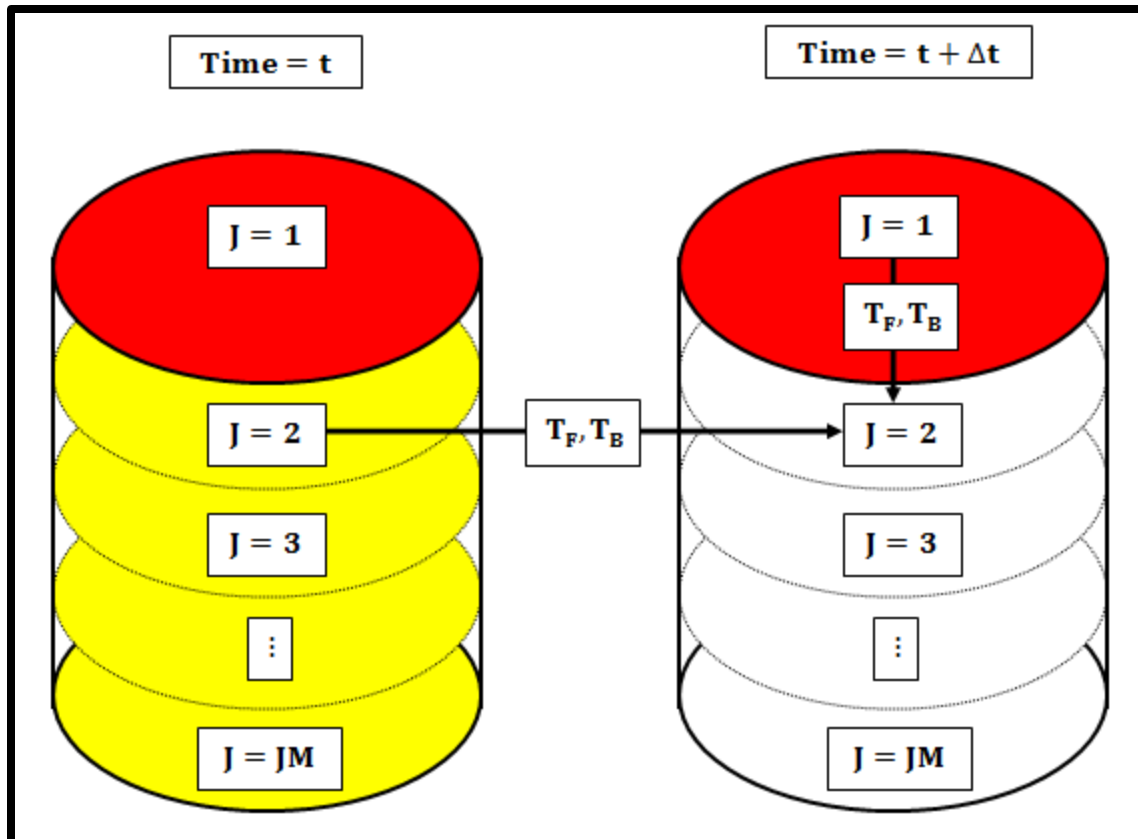
Figure 22: Fluid and Solid Temperatures Used in Computing Element 2's Temperature during Charge Cycle (Colored Elements Indicate Known Solid and Fluid Temperatures)

In Figure 22, the figure on the left is a representation of the computational domain at the current time. Each element, corresponding to a 'J', is colored, as the fluid and solid temperature at each location is known. The color red indicates the constant maximum fluid inlet temperature while the color yellow simply indicates the temperature is already known. The goal is to calculate the temperature distribution in the domain to the right, representing the upcoming time step. Because this discussion concerns a charge cycle, the temperature of the first element is fixed (therefore colored). When solving for the fluid and solid temperatures of the second element, 'J=2', the fluid and solid temperatures the fluid and solid temperatures from element 'J=2' at time 't' and the fluid and solid temperatures from element 'J=1' at time 't+Δt' are used, as indicated by the arrows.

The numeric formulation of the explicit solution discussed above is presented below. EQ.3.1 and EQ.3.2 are taken as the starting points for the development of the numeric descriptions of the temperature distribution of the fluid and solid phases respectively.

- Fluid Phase Finite Difference Formulation

$$\left(\rho C_p\right)_F \varepsilon \left[\frac{\partial T_F}{\partial_t}\right] + \frac{\left(\dot{m}C_p\right)_F}{A_c}\left[\frac{\partial T_f}{\partial_y}\right] - h_v[T_B - T_F] = 0 \qquad \text{EQ.3.10}$$

ρ = Fluid density (kg/m^3)

C_p = Fuid specific heat (J/kg. K)

ε = Bed void fraction

$\dot{m}$ = Fluid flow rate (kg/s)

A_c = Tank cross sectional area (m^2)

y = Position along tank (m)

h_v = Interstitial heat transfer coefficient (W/m^3. K)

t = Time (s)

T_B = Bed temperature (℃)

T_F = Fluid Temperature (℃)

Now make the following substitutions: $A_1 = \left(\rho C_p\right)_F$ $A_2 = \left(\dot{m}C_p\right)_F$

$$C_1 = \varepsilon A_1 \qquad C_2 = A_2/A_c$$

$$C_1\left[\frac{\partial T_F}{\partial_t}\right] + C_2\left[\frac{\partial T_F}{\partial_y}\right] - h_v[T_B - T_F] = 0 \qquad \text{EQ.3.11}$$

Now construct the numeric model with respect to time and space.

$$C_1\left[\frac{T_{F_{t+\Delta t}} - T_{F_t}}{\Delta t}\right]^J + C_2\left[\frac{T_F^J - T_F^{J-1}}{\Delta y}\right]_{t+\Delta t} + h_v[T_B - T_F] = 0 \qquad \text{EQ.3.12}$$

Superscript (J) = Corresponds to element being solved

62

Superscript ($J - 1$) = Corresponds to element before element being solved

Subscript (t) = Corresponds to current time step

Subscript ($t + \Delta t$) = Corresponds to upcoming time step

Δt = Time step length (s)

Δy = Node spacing (m)

Now factor the expression and group terms.

$$[T_F]_{t+\Delta t}^J \left(\frac{C_1}{\Delta t} + \frac{C_2}{\Delta y} + h_v \right) - [T_F]_{t+\Delta t}^{J-1} \left(\frac{C_2}{\Delta y} \right) - [T_F]_t^J \left(\frac{C_1}{\Delta t} \right) - [T_B]_{t+\Delta t}^J (h_v) = 0 \qquad \text{EQ. 3.13}$$

From EQ.3.13, the expression is placed in a form that that is compatible with a successive over-relaxation (SOR) solver. The SOR solver is a variation of the Gauss-Seidel approach to solving series of linear equations that leads to faster solution convergence. Using the SOR solver, the fluid temperature distribution within the tank is found. After obtaining the fluid temperature distribution in the upcoming time step, the temperature distribution of the bed material is solved for explicitly.

- Solid Phase Finite Difference Formulation

$$\left(\rho C_p \right)_B (1 - \varepsilon) \frac{\partial T_B}{\partial t} = -h_v (T_B - T_F) \qquad \text{EQ. 3.2}$$

Now make the following substitutions: $A_3 = \left(\rho C_p \right)_B \qquad C_3 = (1 - \varepsilon) A_3$

$$C_3 \left[\frac{\partial T_b}{\partial t} \right] = -h_v [T_B - T_F] \qquad \text{EQ. 3.14}$$

Now construct the numeric model with respect to time and space.

$$C_3 \left[\frac{T_{B_{t+\Delta t}} - T_{B_t}}{\Delta t} \right]^J = h_v [T_F - T_B]_{t+\Delta t}^J \qquad \text{EQ. 3.15}$$

Now factor the expression and group terms.

63

$$[T_B]^J_{t+\Delta t}\left(\frac{C_3}{\Delta t}+h_v\right)-[T_B]^J_t\left(\frac{C_3}{\Delta t}\right)-[T_F]^J_{t+\Delta t}(h_v)=0 \qquad \text{EQ. 3.16}$$

The local bed temperature is solved for directly from EQ.3.16. To increase the accuracy of this solution procedure, the solution of the fluid temperature and bed temperature profiles is repeated using the temperature values calculated in the previous iteration as the initial temperature distributions. The number of times the solution procedure is repeated in each time step is optimized by studying the convergence of the temperature profiles with respect to the number of times the solution procedure is repeated.

3.1.3 PBTC Model Validation and System Convergence Study

The numeric model, when executed, determines the temperature distribution in both the fluid and solid material contained within the thermocline tank. In the preliminary stages of working with the model, it is necessary to optimize its operation to achieve the maximum possible accuracy and minimum runtime. Additionally, it is necessary to evaluate the results of the model, making sure that the results are comparable to those reported in literature.

The model operates by reading the necessary input data, such as coefficients, runtime, time step length, etc., from an input data file, executing the program, and writing the resulting temperature distribution to an output file. A sample input file developed using sample values presented by McMahan (2006) is presented in Figure 23 with the first row of numbers corresponding to the first five elements in the column of descriptions and the second row corresponding to the remaining seven elements in the column of descriptions.

Figure 23: Sample Input File for PBTC Model

3.1.3.1 Comparison of PBTC Model and Pacheco Model

Holding the remaining input data constant, the run time was varied between 30 minutes and 3 hours and the temperature profile of the solid media was tracked at each 30 minute interval. A similar exercise was performed by Pacheco et al using slightly different material properties and tank dimensions but a similar operating temperature range (Pacheco et al., 2002). Figure 24 depicts a comparison of the results of the charge cycle temperature profiles attained by Pacheco et al (Left) with the results predicted by the PBTC model (Right).
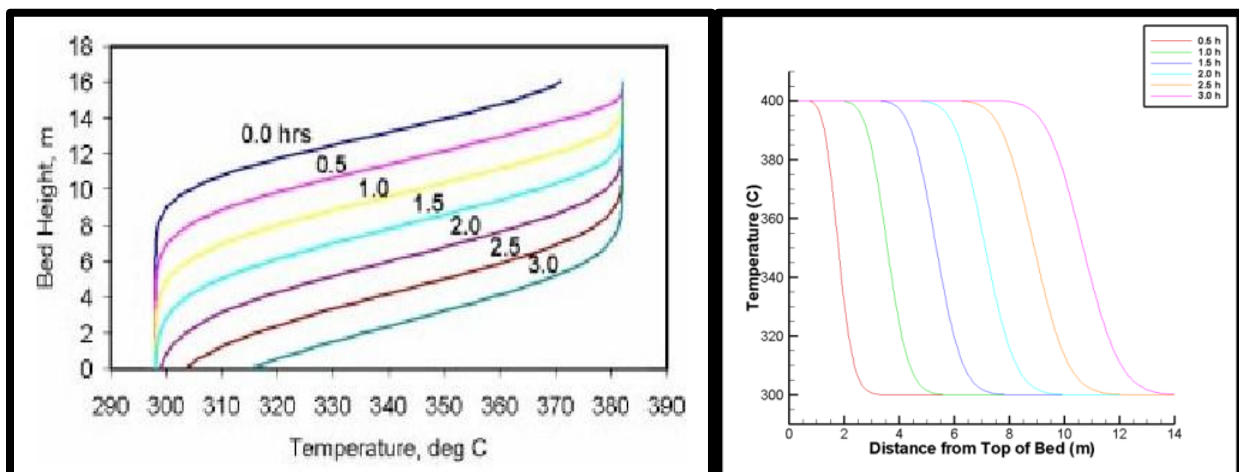
Figure 24: Comparison of Charge Cycle Temperature Profiles from Literature (Left) and from the PBTC Model (Right) (Pacheco et al., 2002)

65

From the comparison presented in Figure 24, it can be seen that both cases predict the expected 'S' shaped temperature profiles. In both cases, the fully charged portion of the bed, the portion at the maximum operating temperature, increases steadily throughout the charging process. Small differences in the temperature profiles predicted by the two models can be due to the use of different filler material properties and other system parameters. From this qualitative comparison, it can be concluded that the PBTC model correctly employs the Schumann equations in calculating heat transfer within the thermocline TES system.

An additional comparison that can be made is to track the outlet fluid temperature during the charge cycle. Initially, this fluid outlet temperature should be nearly equal to the minimum operating temperature, as the high-temperature fluid transfers its energy to the solid media. However, as time passes and more of the media is heated, the fluid outlet temperature should begin to climb, as all of its energy is not passed to the solid media. A graphical representation of the fluid inlet and outlet temperatures during a charge cycle, as reported by Pacheco et al, is presented in Figure 25 (Left). For comparison purposes, the same fluid temperature profiles, attained from the PBTC model, are also provided in Figure 25 (Right).
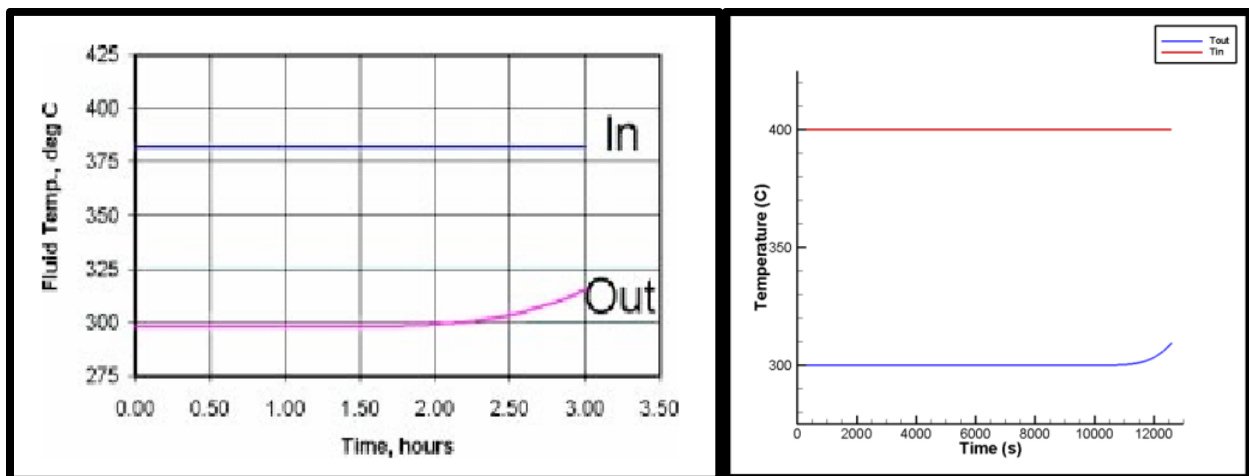
Figure 25: Inlet and Outlet Fluid Temperatures during 3.5 Hour Charge Cycle from Literature (Left) and from the PBTC Model (Right) (Pacheco et al., 2002)

From Figure 25, it can be seen that the fluid inlet temperature is held constant throughout the charge cycle. For the charge cycles predicted by Pacheco's model and by the PBTC model, it can be seen that the fluid outlet temperature remains constant through most of the charge cycle. Nearing the end of the cycle, most of the solid media has been heated above the lower temperature limit; therefore, all energy is not transferred from the fluid to the solid media. This results in the increase of the outlet fluid temperature that is predicted by both models.

Based upon the comparisons of charge cycle temperature profiles (Figure 24) and the fluid outlet temperatures during the charge cycle (Figure 25), it can be concluded that the PBTC model performs similarly to the Pacheco packed-bed thermocline model. For this reason, it is concluded that the PBTC model accurately models heat transfer for fluid flowing through a packed aggregate bed. Having validated the PBTC model by comparing it with published and accepted work, the next step is to optimize the model's parameters.

3.1.3.2 Convergence Study of PBTC Model Parameters

Having established that the PBTC thermocline model is reasonably accurate through comparison with works in literature, the next undertaking is to study the effects of various system parameters on the convergence of the solution. In this section, three parameters are studied: time step length, spacing between differential elements, and the number of times the system's temperature distribution is solved for at each time step (Reference Section 3.1.2 for the initial discussion of the third model parameter mentioned). It should be noted that aside from the parameter being studied in each case, all other parameters are held constant to the initial values presented in the input file presented in Figure 23.

In any numeric model, it is important to determine the ideal time step length. The solution type implemented in this work is implicit; therefore, there is no constraint on the

maximum time step as there is for an explicit solution type. However, using too large of a time step can lead to a decrease in the model's accuracy. Conversely, using too small of a time step can lead to an increased model run time with minimal gained accuracy. In this model, the number of calculations made, even at small time steps is not significant enough to slow the model too much. However, because some larger models can reportedly take days and even months to execute, it is good programming practice to determine the time step which allows for an optimum balance between accuracy and minimized model runtime. Results from a convergence study of the effects of varying the time step on the bed's temperature profile are presented in Figure 26.
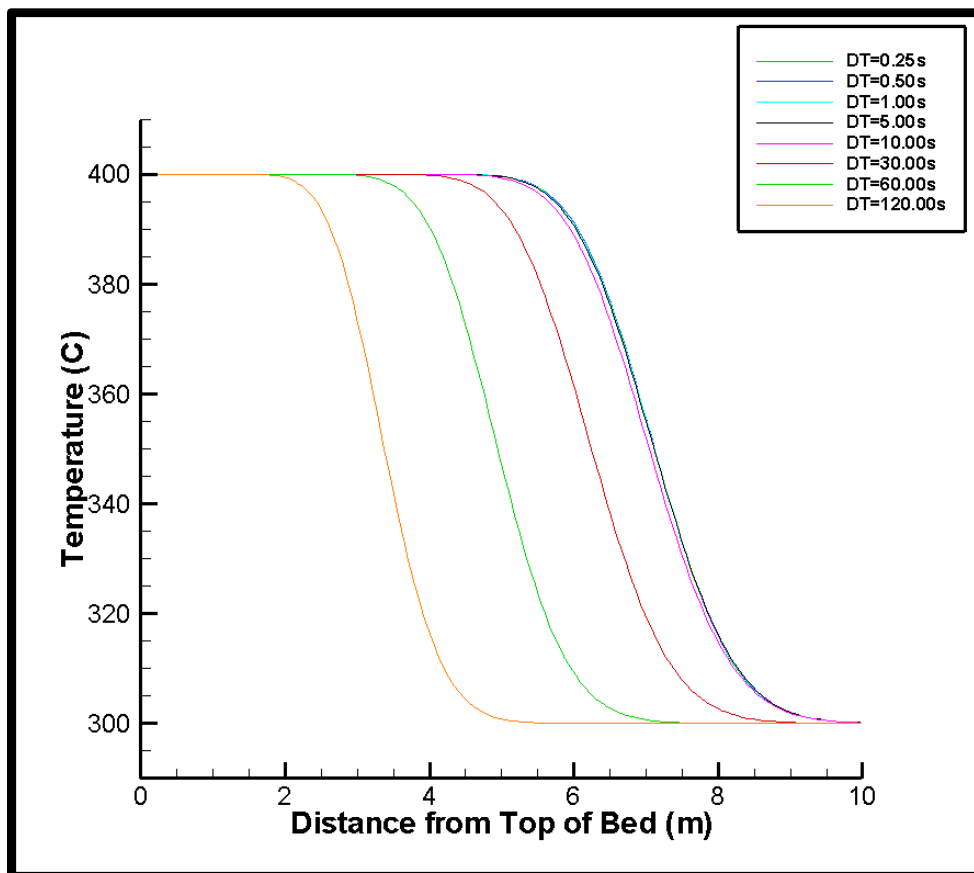
Figure 26: Impact of Time Step on Temperature Profile

In this study, all parameters were held constant except for the time step, which was varied between 0.25s and 120.0s. From Figure 26, the profiles obtained using a time step of up to 5.0s

68

are indistinguishable; though the profile corresponding to the 10s time step demonstrates some drift from the group, it is still considered a converged solution. As the time step is increased to 30.0s and beyond, significant drift is present in the solution. From these results, it can be concluded that the time step of 5.0s provides the best combination of minimized time step and computational accuracy.

The second parameter to be investigated is the number of differential elements necessary to obtain a converged solution. As is the case with decreasing the time step, increasing the number of differential elements increases the number of necessary computations, thereby increasing the model's runtime. The results of a convergence study in which the number of nodes used in calculating the temperature profile was varied are presented in Figure 27.
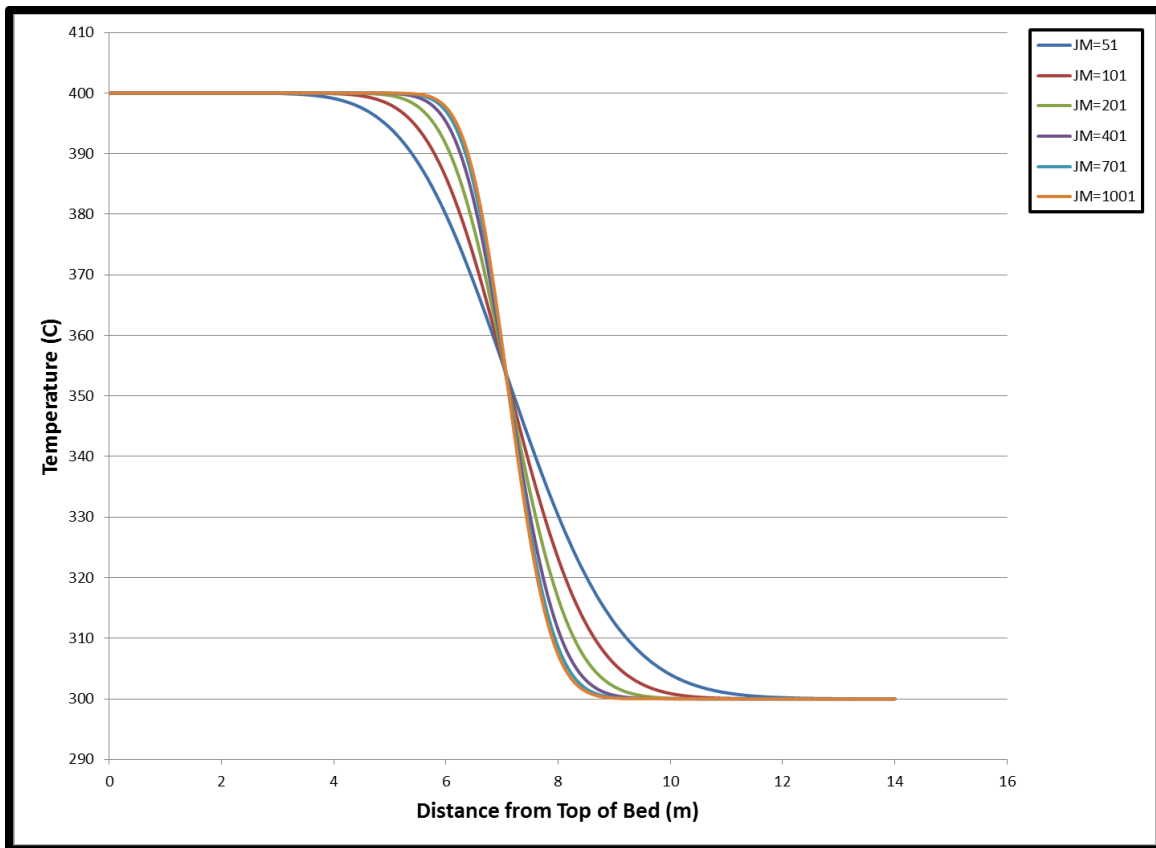
Figure 27: Convergence of Temperature Profile with Increased Number of Nodes

From Figure 27, it can be seen that the number of differential elements used does not affect the model's results as significantly as the time step length does. As the number of elements decreases, the sharpness of this profile gradually begins to diminish. Based upon the temperature profiles, using 401-1001 nodes produces indistinguishable temperature profiles; as the number of differential elements used decreases below 201, the sharpness of thermocline region begins to diminish significantly. It can be concluded that 201 nodes provides the optimum balance between model accuracy and computational time. It should be recognized that this number of nodes has been determined as optimum for the tank height used in this case. If the tank height is increased or decreased, the necessary optimum number of nodes can be expected to increase and decrease respectively. For any study involving a taller solid material bed, this optimization study should be repeated.

The final parameter optimized to be optimized is the number of times that the fluid and bed temperature profiles are solved for at each time step. As a reminder, the fluid temperature profile is solved for implicitly at each time step; following the implicit solution of the fluid temperature profile, the temperature profile of the solid bed is solved for explicitly. To increase the accuracy of this solution procedure, the complete fluid and solid temperature profiles are computed multiple times at each time step. The temperature profiles computed in the previous iteration are assumed as initial temperature profiles in each subsequent solution. To minimize the number of computations, a study is conducted to evaluate the effect of increasing the number of solution repetitions at each time step on the final bed temperature profile. Temperature profiles generated for varying numbers of calculation repetition are presented in Figure 28.
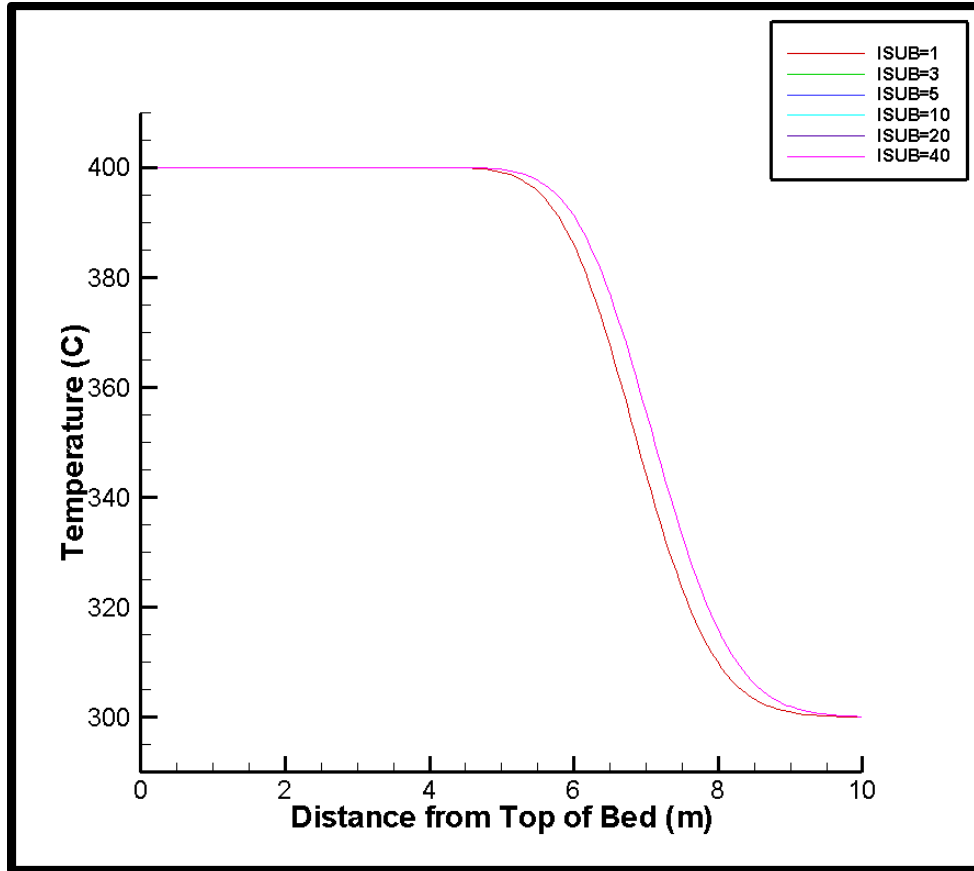
Figure 28: Impact of Number of Repetitions of Calculating Fluid and Bed Temperatures

From Figure 28, it can be seen that temperature profiles generated using one to three to forty calculations repetitions are indistinguishable. However, if the profile is only calculated once, it can be seen that the profile is calculated with less accuracy. Therefore, it is concluded that executing 3 successive calculations at each time step renders the optimum balance between computational speed and accuracy.

3.1.4 Impact of Temperature-Dependent Fluid Properties on PBTC Model

In his initial work, one of Schumann's assumptions was that thermo-physical properties of the fluid flowing through the porous media were constant (Schumann, 1929). At the time of his work, this assumption was necessary, as only the analytical solution approach was possible. However, with the aid of computers and numeric solution processes, it is possible to model a

71

packed bed thermocline considering temperature-dependent fluid properties, and compare the results with those obtained assuming constant fluid properties.

Research to reduce sensible heat TES system costs is heavily concentrated around reducing the cost of liquid media and increasing the operational temperature range of this liquid media. Molten salts have demonstrated much promise as liquid media, as they are significantly cheaper than thermal oils and allow a much higher operating temperature range. As the temperature range over which TES systems store energy increases, so does the error in assuming constant liquid properties. The molten salts considered in this work allow operation in temperature ranges exceeding 300°C; therefore, it is necessary to assess the error that is accrued using the constant liquid property assumption.

Two temperature ranges are evaluated: 290°C-390°C, as used in most thermal oil CSP plants and the two-tank molten salt Andasol CSP plant, and 290°C-565°C, as considered in this work. For each temperature range, mass flow rates of 900 kg/s and 1500 kg/s are considered, corresponding to charge cycle durations of 6 h and 4 h respectively. Temperature profiles considering constant and variable fluid properties are provided and conclusions are drawn regarding the accuracy of the constant versus the variable property model. System parameters and bed material and properties held constant through all models are presented in Table 11.

Table 11: Properties Held Constant for All Models

Bed Properties	
Density (kg/m^3)	2500.0
Specific Heat (J/kg.K)	830.0
Average Particle Diameter (m)	0.0137
Porosity	0.22
System Parameters	
Tank Height (m)	14.0
Tank Diameter (m)	37.0
Time Step (s)	1.0
Nodes Used	201

3.1.4.1 Case I: Mass Flow Rate of 900 kg/s

The mass flow rate of 900 kg/s was selected because it corresponds to a charge time of about six hours for the specified system. Fluid properties for the temperature range of 290°C-390°C are based on the median temperature of 340°C and properties for the temperature range of 290°C-565°C are based on the median temperature of 428°C. Table 12 provides fluid properties and the convection coefficient used in the constant property models. Fluid properties for the variable properties models are calculated at each time step using the equations presented in Chapter 2.

Table 12: Constant Properties for Case I: Mass Flow Rate of 900 kg/s

Properties	340°C	428°C
Specific Heat (J/kg.K)	1381.52	1366.38
Density (kg/m^3)	1873.76	1817.79
Viscosity (kg.m/s)	0.0249	0.0158
Thermal Conductivity (W/m.K)	0.5076	0.5240
Convection Coefficient (W/m^2.K)	220.363	233.415

The initial postulation is that increasing the temperature range over which the TES system operates will increase the difference in the charge cycle temperature profiles of the constant and variable property models. Temperature profiles generated for six-hour charge cycles over the 290°C-390°C and 290°C-565°C temperature ranges are presented in Figure 29.

73
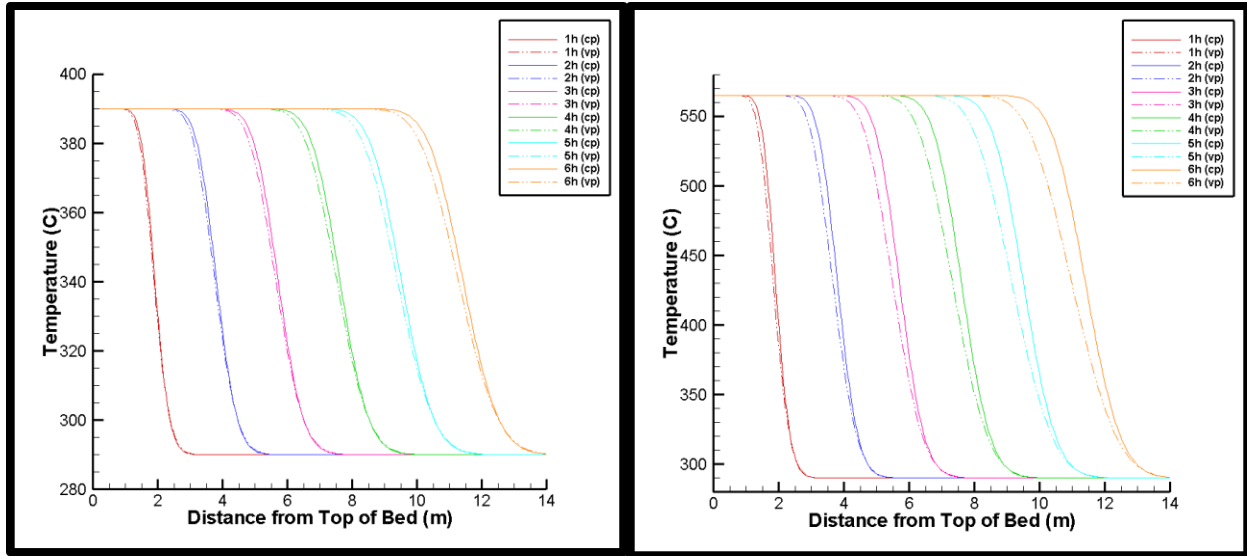
Figure 29: Temperature Profiles Generated Using Constant (Solid Line) and Variable (Dashed Line) Fluid Properties during Six-Hour Charge Cycle: 290°C-390°C (Left) and 290°C-565°C (Right)

Based upon the temperature profiles generated in Figure 29, it can be concluded that increasing the temperature range does increase the error accrued when assuming constant liquid material properties. However, the overall error in assuming constant material properties, represented by the area between the solid and dashed-line profiles is relatively small. The results of this trial case indicate that assuming constant material properties over-predicts the amount of energy stored; however, the error is miniscule, therefore acceptable for the modeling applications in this work.

3.1.4.2 Case II: Mass flow Rate of 1500 kg/s

A second study is conducted to determine if the duration of the charge cycle plays significantly impacts the accrued error. For this case, the mass flow rate of the fluid is increased to 1500 kg/s, effectively decreasing the charge time to approximately four hours. Average fluid properties and convection coefficients used in Case II are presented in Table 13. Fluid properties for the variable fluid property models are calculated at each time step using the equations presented in Chapter 2.

74

Table 13: Constant Properties for Case II: Mass Flow Rate of 1500 kg/s

Properties	340°C	428°C
Specific Heat (J/kg.K)	1381.52	1366.38
Density (kg/m³)	1873.76	1817.79
Viscosity (kg.m/s)	0.0249	0.0158
Thermal Conductivity (W/m.K)	0.5076	0.5240
Convection Coefficient (W/m².K)	263.537	279.958

There is no initial postulation as to whether increasing the mass flow rate and decreasing the duration of the charge cycle will increase or decrease the accrued error in the amount of energy stored in the system. Temperature profiles for the four-hour charge cycle of TES systems assuming a temperature ranges of 290°C-390°C and 290°C-565°C are presented in Figure 30.
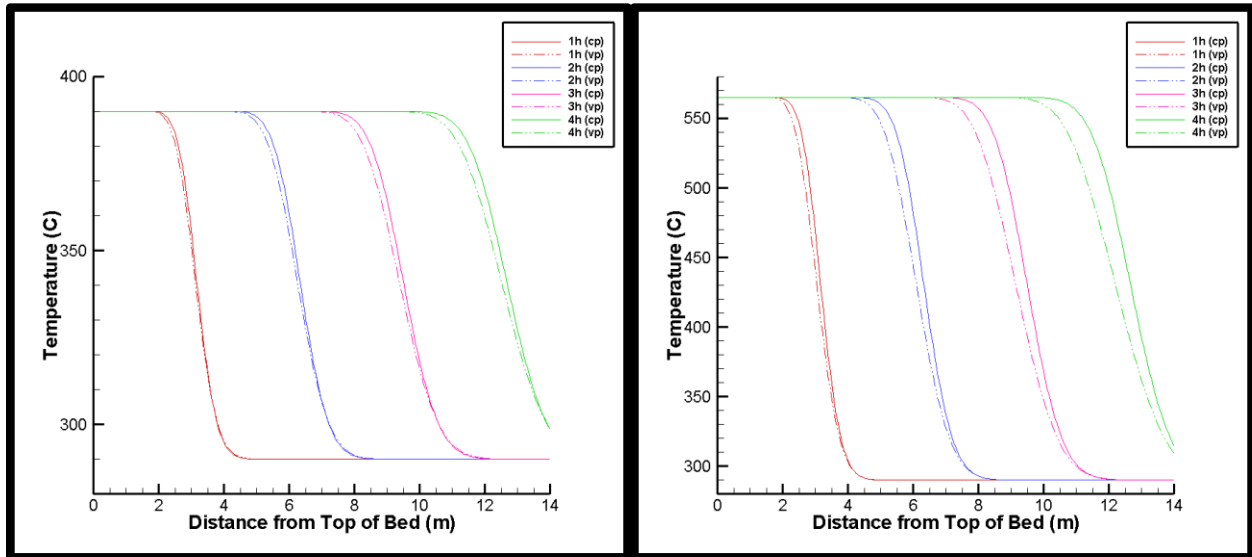
Figure 30: Temperature Profiles Generated Using Constant (Solid Line) and Variable (Dashed Line) Fluid Properties during Four-Hour Charge Cycle: 290°C-390°C (Left) and 290°C-565°C (Right)

From Figure 30, it can be seen that, as in Case I, increasing the operating temperature range increases the amount of error in accrued when assuming constant liquid material properties. A comparison of Figure 29 and Figure 30 indicates that mass flow rate of the liquid and duration of the charge cycle bear little influence on the error in assuming constant material properties. At this time, it can be concluded that operating temperature range is the primary contributor to error in assuming constant liquid material properties. Though the error is small,

even in the operating range of 290°C-565°C, it should be recognized as present. For the case of molten salt the manner in which the material properties are considered is not significant; however, this may not be the case for other liquid media, the properties of which may be more sensitive to temperature.

3.1.5 PBTC Models: Limestone Bed and Quartzite Bed

Having completed the process of validating the PBTC model with works in literature and conducting the necessary parameter convergence studies, the remaining task is to simulate charge and discharge cycles for the PBTC and attain the efficiency of the TES system. In this study, two bed materials are considered: limestone and quartzite. The properties of the PBTC model considering both media cases are presented in Table 14. The resulting charge and discharge temperature profiles are presented in Figure 31 and Figure 32 respectively.

Table 14: Material Properties of Materials Considered for Bed of PBTC

PBTC Parameters	Case I Limestone Bed	Case II Quartzite Bed
System Parameter		
Bed Height (m)	14	14
Bed Void Fraction	0.33	0.33
Tank Cross Section (m^2)	1256.64	1256.64
Mass Flow (kg/s)	1500	1500
Cycle Duration (s)	14400	14400
Time Step (s)	1	1
Nodes Used	201	201
Tmin (°C)	300	300
Tmax (°C)	585	585
Material Properties		
Bed Density (kg/m^3)	2320	2640
Bed Spec. Heat (J/kg.K)	810	1105
Fluid Density (kg/m^3)	1808	1808
Fluid Spec. Heat (J/kg.K)	1365	1365
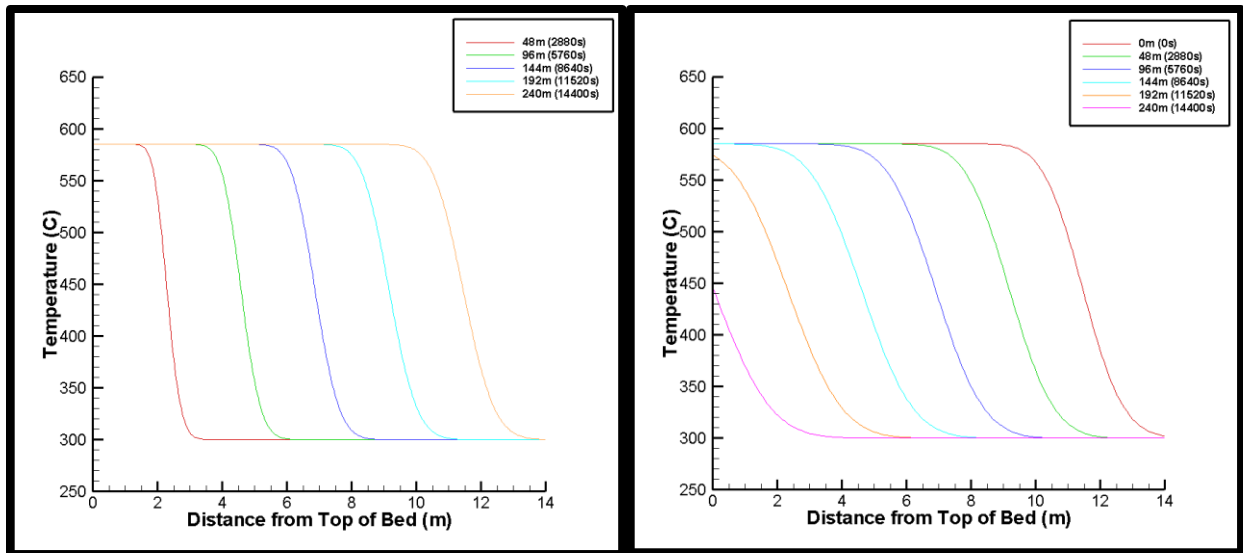
Figure 31: Charge (Right) and Discharge (Left) Temperature Profiles for PBTC Thermocline Case I, Limestone Bed
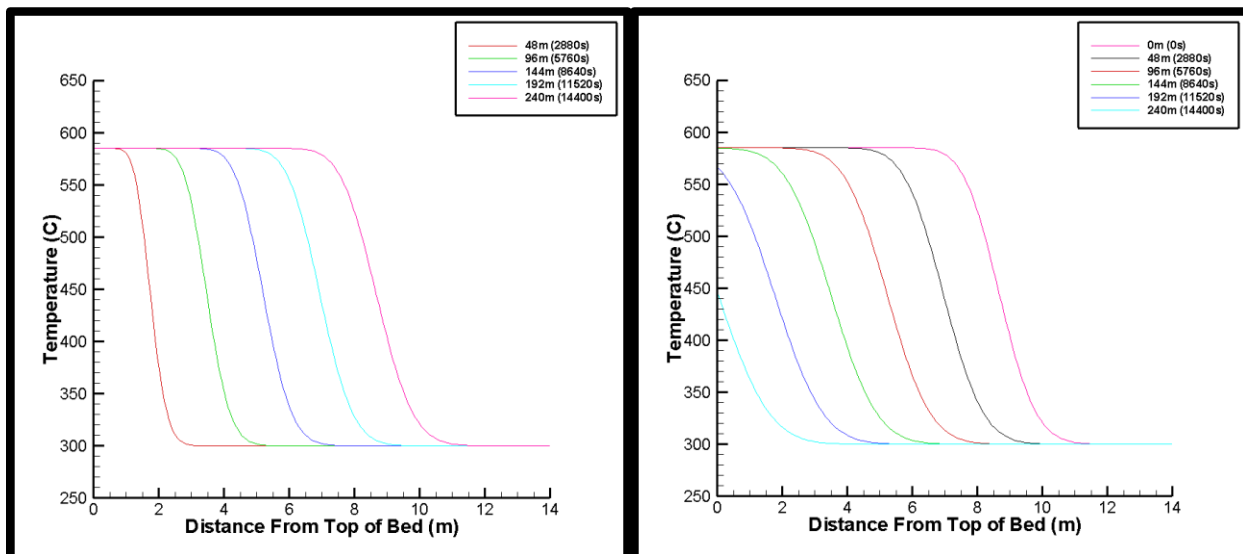
Figure 32: Charge (Right) and Discharge (Left) Temperature Profiles for PBTC Thermocline Case II, Quartzite Bed

Comparing Figure 31 and Figure 32, it can be seen that in Case I, much more of the bed is heated to its upper temperature limit. This is expected, as the density and specific heat capacity of quartzite are considerably greater than the density and specific heat of limestone. Based on a four hour charge cycle and four hour discharge cycle, the efficiencies of the thermoclines incorporating limestone and quartzite beds are 95.48% and 94.69% respectively. However, some of this energy is retrieved at temperatures approaching the lower temperature

77

limit of the system. When a thermocline is used to supply energy to a CSP plant, energy is discharged from the TES system until the temperature of the fluid pumped from the system reaches a lower limit, 500°C in this case. Applying this constraint, the efficiencies of the thermoclines with limestone and quartzite beds fall to 92.37% and 91.49% respectively.

A comparison of the system efficiencies indicates that using a bed material having lower heat capacity and density increases the efficiency of the system. However, as can be deduced from a comparison of Figure 31 and Figure 32, using a material with greater heat capacity and density increases the storage density of the TES system. When deciding on the type of bed material for a packed bed thermocline, it must be decided if a small gain in system efficiency is more valuable than a significant reduction in system size (therefore system cost) that is attained when the density and heat capacity of the bed material used is greater.

3.2 2D Structured Concrete Thermocline (SCTC) Model

The 2D structured concrete thermocline (SCTC) model, like the PBTC model, is a two-phase model that solves for solid and fluid temperatures at each point within the thermocline. This model was developed to study heat transfer in a structured concrete thermocline (Brown 2012). This model bears some significant differences to the Schumann model, namely that it considers heat transfer in the radial direction as well as conduction in both the solid and liquid material. Two variations of the 2D model were developed and optimized: a parallel-plate model considering fluid flow between rows of concrete plates and an axisymmetric model consisting of cylindrical elements with channels spanning their axial dimensions for fluid to flow through (Brown, 2012). The parallel-plate concrete arrangement was found to be optimum in the work of Brown (2012), therefore, only the parallel-plate model is considered in this work.

A thermocline tank populated with the parallel-plate structured concrete arrangement contains numerous concrete plates standing parallel to each other. Figure 33 provides the cross sectional view of a thermocline tank populated with the aforementioned parallel plate structured concrete geometry.
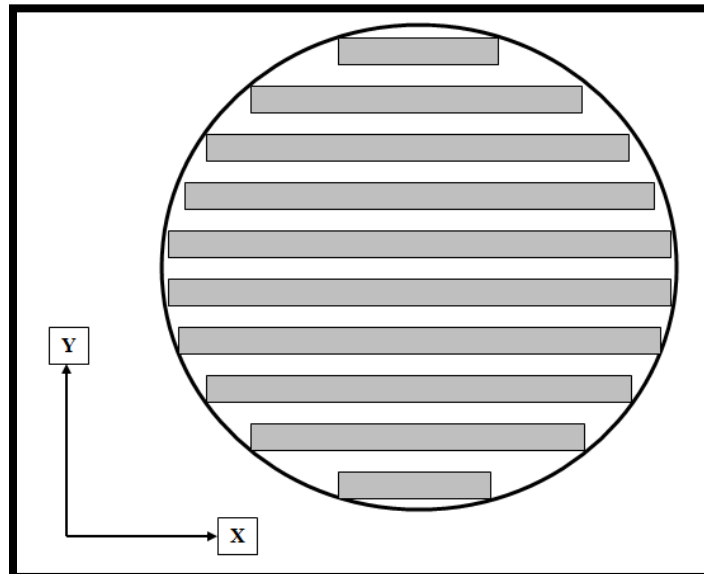
Figure 33: Cross Sectional View of Thermocline Tank Populated with Parallel Plate Structured Concrete (View from Above) (Brown et al., 2012)

It is convenient to develop the thermocline's heat transfer model in terms of the smallest repeated structural pattern. In this case, the smallest repeated pattern consists of half of the thickness of a concrete plate and half of the thickness of a fluid flow channel between two plates.

Figure 34 provides a close up view of two concrete plates with a fluid flow channel between them. The figure to the left provides a close up view of two concrete plates and a fluid flow channel, as seen in Figure 33, and the figure to the right provides an axial view of the same two plates and channel. The hatched region indicates the aforementioned smallest repeated pattern that is considered in modeling heat transfer in the thermocline. Referencing

Figure 34, 'Ti' corresponds to the thickness of half of the fluid flow channel and 'To' corresponds to the thickness of the fluid flow channel plus half the thickness of a concrete plate.

'–V' and '+V' correspond to the fluid flow velocity during discharge and charge cycles respectively. Lastly, 'L' corresponds to the axial length or height of the concrete plates being used.
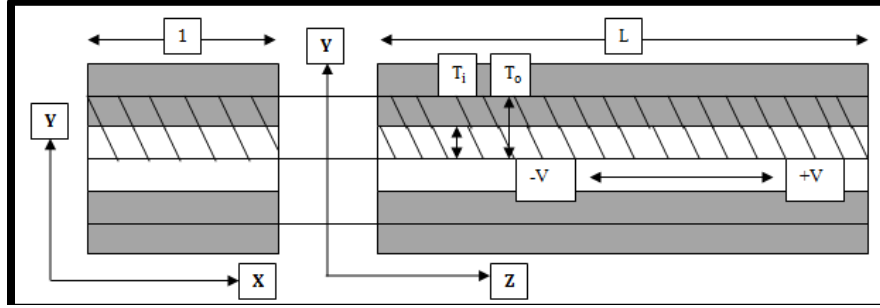
Figure 34: Two Concrete Plates and One Fluid Flow Channel (Hatched Region Indicates Computational Domain) (Brown et al., 2012)

3.2.1 SCTC Model and Assumptions

3.2.1.1 SCTC Model

EQ.3.17 and EQ.3.18 are used to describe heat transfer from liquid to the structured concrete media and heat diffusion within the concrete material respectively (Brown et al., 2012). The subscripts 'F' and 'M' correspond to fluid and material temperatures. This model assumes that fluid material properties are constant.

$$\frac{\partial T_F}{\partial t} + V\frac{\partial T_F}{\partial z} + \frac{hP}{S(C_p\rho)_f}(T_F - T_M) = 0 \qquad \text{EQ. 3.17}$$

$$\frac{1}{\propto_M}\frac{\partial T_M}{\partial t} = \frac{\partial}{\partial y}\left(\frac{\partial T_M}{\partial y}\right) + \frac{\partial^2 T_M}{\partial z^2} \qquad \text{EQ. 3.18}$$

T_F = Fluid temperature (°C)

T_M = Material temperature (°C)

t = Time (s)

V = Fluid flow velocity (m/s)

z = Axial coordinate (m)

80

h = Convection coefficient ($W/m^2 \cdot K$)

P = Perimeter of fluid flow channel (m)

S = Cross sectional area of fluid flow channel (m^2)

ρ = Density (kg/m^3)

C_p = Specific heat ($J/kg \cdot K$)

$\propto_M = \frac{k}{\rho C_p}$ = Material thermal diffusivity (m^2/s)

y = Radial coordinate (m)

The channels between parallel plates are rectangular; therefore, the convection coefficient used in the SCTC model can be calculated easily from a classical solution. The procedure for its development is made available in the work of Çengel (2007) and is not be discussed in this work. In developing the solution to the SCTC model, one additional expression is necessary to allow EQ.3.17 and EQ.3.18 to be solved, as they are functions of three variables: time, axial direction, and radial direction. This expression, EQ.3.19, states that the rates of heat transfer to the solid surface by convection and the rate of heat diffusion from the surface of the solid into the solid are equal.

$$k_M \frac{\partial T_M}{\partial y} = h(T_M - T_F) \qquad \text{EQ. 3.19}$$

k_M = Thermal conductuivity of material ($W/m \cdot K$)

Using EQ.3.17-EQ.3.19, an explicit finite-difference model is generated to solve for the solid and fluid temperature profiles. The development of this numeric model is very similar to that of the PBTC model; the only significant difference is that heat conduction is considered in the axial and radial directions in both the solid and liquid media. The SCTC model is available through private communication (Selvam, 2012); therefore, it is not necessary to construct the

model. The SCTC model is validated through in the work of Brown (2012), therefore, no further comparisons are conducted in this work.

3.2.1.2 SCTC Model Assumptions

Five primary assumptions or boundary conditions are considered in using the SCTC model (Brown et al., 2012).

- The outside boundaries of the concrete elements considered (half of plate thickness) are adiabatic. This assumption is valid because it is assumed that the fluid temperature is the same at each axial location within the thermocline tank; therefore, the rates of heating for each half plate should be uniform.

- No heat transfer occurs in the thermocline tank outside the region occupied by the concrete filler material.

- During a charge cycle, the temperature of the fluid at the top of the tank is held constant at the maximum operating temperature, and the fluid flow direction is assumed to be from the top to the bottom of the tank only.

- During a discharge cycle, the temperature of the fluid at the base of the tank is held constant at the minimum operating temperature, and the fluid flow direction is assumed to be from the bottom to the top of the tank only.

- No heat is lost to the environment.

3.2.1.3 Previous Work Using the SCTC Model

The SCTC model requires two input files, one of which contains information for the charge cycle and the other which contains information for the discharge cycle. Figure 35 provides examples of both of these inputs, corresponding to the optimized parallel plate model developed by Brown (2012).

82

Figure 35: Input Files for Charge (Left) and Discharge (Right) Cycles (Brown, 2012)

The temperature profiles predicted by Brown's optimized model, during both charging and discharging cycles, are provided in Figure 36. Additionally, the amount of energy stored during the charge cycle and the amount of energy retrieved during the discharge cycle are plotted over the cycle duration in Figure 37. The charge/discharge efficiency of the TES system is determined by dividing the quantity of energy stored by the amount of energy retrieved from storage. This optimized system provides a charge/discharge efficiency of 65.59%.

Figure 37 also records the amount of power being used to store and retrieve energy. Considering the charge cycle, it can be seen that during the initial stages of the charge cycle, the power usage is a straight line, as all energy is transferred from the fluid to the concrete as the fluid flows through and along it. However, as the charge cycle continues and more of the concrete has been heated, the amount of energy transferred from the fluid to the concrete begins to decrease, therefore the power consumed by the storage system decreases. When the storage system's power consumption decreases significantly, this means that fluid is being returned to heat source above the minimum operating temperature of the system. The result is increased

83

parasitic losses as increased heat transfer to the surroundings will occur during the fluid's return trip to the solar concentrator.

Figure 36: Temperature Profiles for Charge (Left) and Discharge (Right) Cycles Using Brown's (2012) Optimized Parallel Plate Model

Figure 37: Energy Stored (Left) During Charge Cycle and Energy Retrieved (Right) During Discharge Cycle

3.2.1.4 Further Optimization of SCTC Model

The DOE desires to develop TES systems with charge/discharge efficiencies of 93% by the year 2020. Based upon an initial review of Brown's work (2012), it was concluded that a structured concrete thermocline was not a viable TES option. However, after further

84

investigation and literature review, it was postulated that maintaining the void fraction in the bed while decreasing the thickness of the concrete plates would increase the charge/discharge efficiency of the TES system. The reason for this assumption is twofold: increased concrete surface area is exposed and the thicknesses of regions of the concrete plate occupied by thermal gradients are decreased.

A primary benefit of packed bed thermocline TES systems is that there is much solid media surface area exposed for heat transfer. Because the particles composing the packed bed are small, no significant thermal gradients are established within the particles. Due to this attribute, all of the energy stored within a vertical section of the TES system is transferred from the solid media to the liquid media as it flows through the tank.

No TES systems reported in literature have investigated structured solid media in active TES systems. However, several works have reported passive TES systems, in which imbedded heat exchangers are placed in ceramic and concrete blocks; these works are discussed in detail in the literature review (Chapter 2). The primary problem with these systems is that it is difficult to retrieve energy from the systems at the desired temperature. As the systems discharge, temperature gradients are established, and the temperature of the energy retrieved decreases steadily. Sensible heat TES systems operate by discharging energy until the outlet temperature of the fluid reaches a minimum temperature, then shutting off. All energy left in TES is wasted. One way to address this problem is to employ a very large number of heat exchangers; however, this would render the system economically not viable.

Based upon this discussion, it can be concluded that the way to increase the charge discharge efficiency of a structured concrete thermocline TES system is to design it so that it has the desirable characteristics of a packed bed thermocline TES system: much exposed solid

media surface area and very small to no thermal gradients within the solid media. Both of these two characteristics can be realized by decreasing the thickness of the concrete plates while increasing the number of plates used, so as to maintain the void fraction of the TES system.

A study was conducted to determine the parameters providing the optimum charge/discharge efficiency for the system. Parameters such as bed length, charge/discharge cycle duration, bed void fraction, fluid flow velocity, and temperature limits are considered to be the same as were used in the PBTC to allow a comparison between the PBTC and SCTC models. Case I considers limestone solid material properties and Case II considers quartzite material properties. The thermo-physical properties of concrete and solar salt used were very similar to those used by Brown. The convection coefficient calculated for this model is nearly three times greater than that used by Brown. The input files used in modeling the optimized structured concrete thermocline are provided in Figure 38.

Figure 38: Optimized Input Files for Charge (Left) and Discharge (Right) Cycles (Case I)

Temperature profiles for charge and discharge cycles of the optimized SCTC TES system are provided in Figure 39. The amount of energy stored and retrieved during the charge and discharge cycles is plotted in Figure 40, along with the power consumed by and retrieved from

86

the TES system. Based upon a four hour charge cycle and four hour discharge cycle, the efficiency of the optimized SCTC TES system is 93.9%. However, as discussed for the PBTC TES system, some of this energy is retrieved below the cut-off temperature limit of 500°C. Imposing this temperature limit, the efficiency of the optimized SCTC TES system falls to 83.97%.
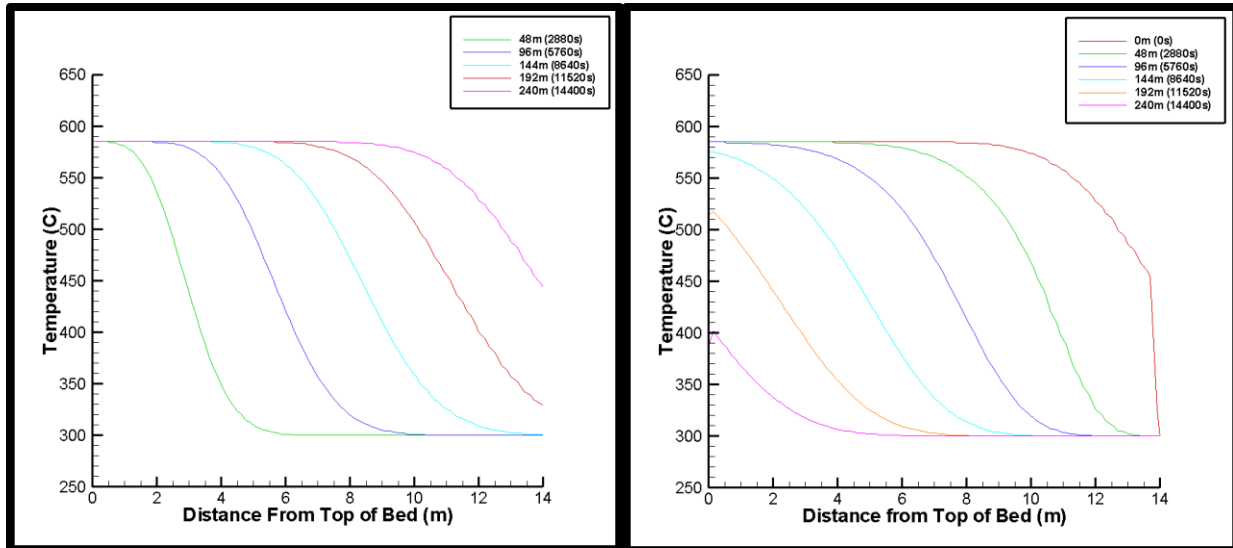
Figure 39: Temperature Profiles for Charge (Left) and Discharge (Right) Cycles Using Optimized Parallel Plate Model (Limestone Properties)
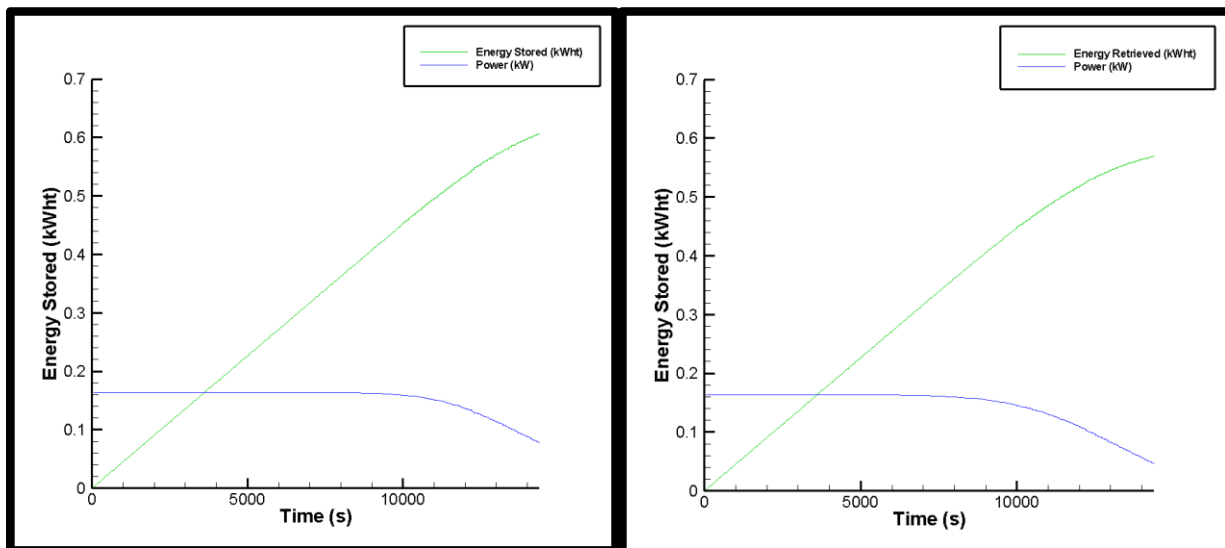
Figure 40: Energy Stored (Left) During Charge Cycle and Energy Retrieved (Right) During Discharge Cycle (Limestone Properties)

87

Comparing Case I of the PBTC model with Case I of the SCTC model (both consider limestone solid material properties), the respective efficiencies, imposing the discharge temperature limit of 500˚C, are 92.37% and 83.97% respectively. Both of these values fall below the DOE's target goal of 93% for the year 2020.

For the purpose of comparison with the PBTC Case II (considering quartzite solid material properties), a second case of the SCTC TES system is considered in which the material properties of quartzite are considered. The input files for this model are provided in Figure 41.


```
tc-i - Notepad
File  Edit  Format  View  Help
101,51,14.0,0.005581,0.016743,1,110
1808,1364,0.53,0.002,116
2640,1105,3.8,300.,585.,300.,14400

      READ(1,*)IM,JM,XLEN,RI,RO,NTUBE
      READ(1,*)DENF,CPF,TKF,VELF,HTRFS
      READ(1,*)DENM,CPM,TKM,TEMFI,TEMFM,TEMSI,TTIME

C     IM=Number of axial nodes
C     JM=Number of radial nodes
C     XLEN=Length of plate (m)
C     RI=Thickness of fluid flow channel (m)
C     RO=Thickness of fluid flow channel and plate (m)
C     NTUBE=Number of plates considered

C     DENF=Density of salt (kg/m3)
C     CPF=Specific heat of salt (J/kg.K)
C     TKF=Thermal conductivity of salt (W/m.k)
C     VELF=Velocity of salt (m/s)
C     HTRFS=Convection coeffcient (W/m2.K)

C     DENM=Density of concrete (kg/m3)
C     CPM=Specific heat of concrete (J/kg.K)
C     TKM=Thermal conductivity of concrete (W/m.k)
C     TEMFI=Initial temperatre of fluid (C)
C     TEMFM=Maximum temperatre salt (C)
C     TEMSI=Inital temperature of concrete (C)
C     TTIME=Charge cycle duration (s)
```

```
tc-id - Notepad
File  Edit  Format  View  Help
101,51,14.0,0.005581,0.016743,1,110
1808,1364,0.53,-0.002,116
2640,1105,3.8,300.,585.,300.,14400

      READ(1,*)IM,JM,XLEN,RI,RO,NTUBE
      READ(1,*)DENF,CPF,TKF,VELF,HTRFS
      READ(1,*)DENM,CPM,TKM,TEMFI,TEMFM,TEMSI,TTIME

C     IM=Number of axial nodes
C     JM=Number of radial nodes
C     XLEN=Length of plate (m)
C     RI=Thickness of fluid flow channel (m)
C     RO=Thickness of fluid flow channel and plate (m)
C     NTUBE=Number of plates considered

C     DENF=Density of salt (kg/m3)
C     CPF=Specific heat of salt (J/kg.K)
C     TKF=Thermal conductivity of salt (W/m.k)
C     VELF=Velocity of salt (m/s)
C     HTRFS=Convection coeffcient (W/m2.K)

C     DENM=Density of concrete (kg/m3)
C     CPM=Specific heat of concrete (J/kg.K)
C     TKM=Thermal conductivity of concrete (W/m.k)
C     TEMFI=Initial temperatre of fluid (C)
C     TEMFM=Maximum temperatre salt (C)
C     TEMSI=Inital temperature of concrete (C)
C     TTIME=Discharge cycle duration (s)
```

Figure 41: Optimized Input Files for Charge (Left) and Discharge (Right) Cycles (Quartzite Properties)

Charge and discharge temperature profiles are provided in Figure 42. Figure 43 tracks the amount of energy stored in the system during charging and retrieved from the system during discharging. Additionally, Figure 43 records the amount of power used on the SCTC during charging and taken from the SCTC during discharging. Based upon a four hour charge cycle and four hour discharge cycle, the efficiency of the second case of the SCTC TES system is 87.38%. However, imposing the cut-off temperature limit of 500˚C reduces the efficiency of the system to 76.40%.
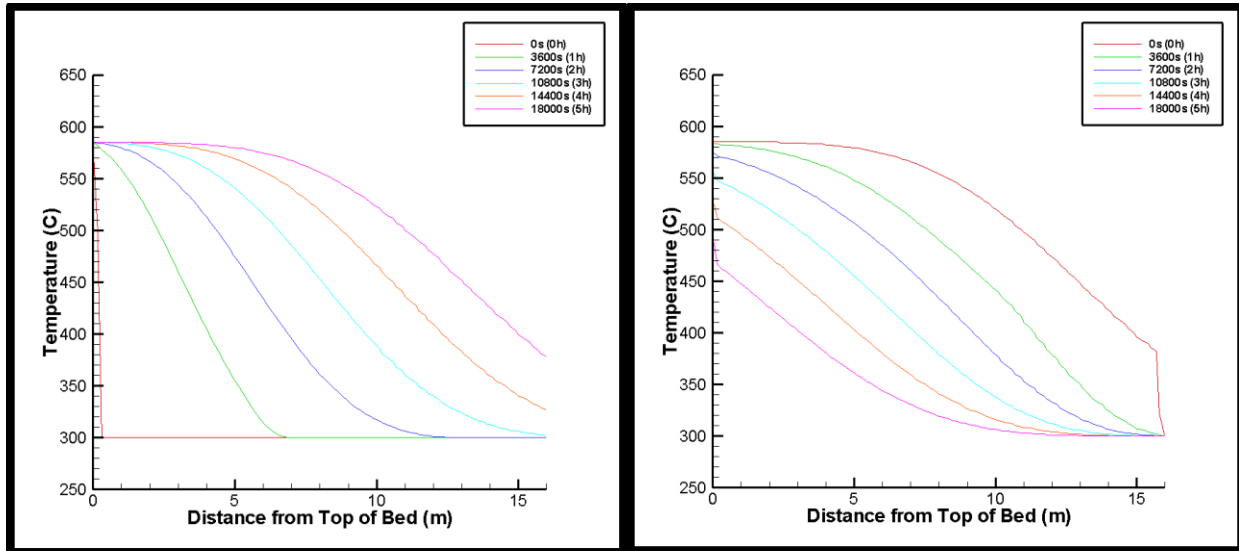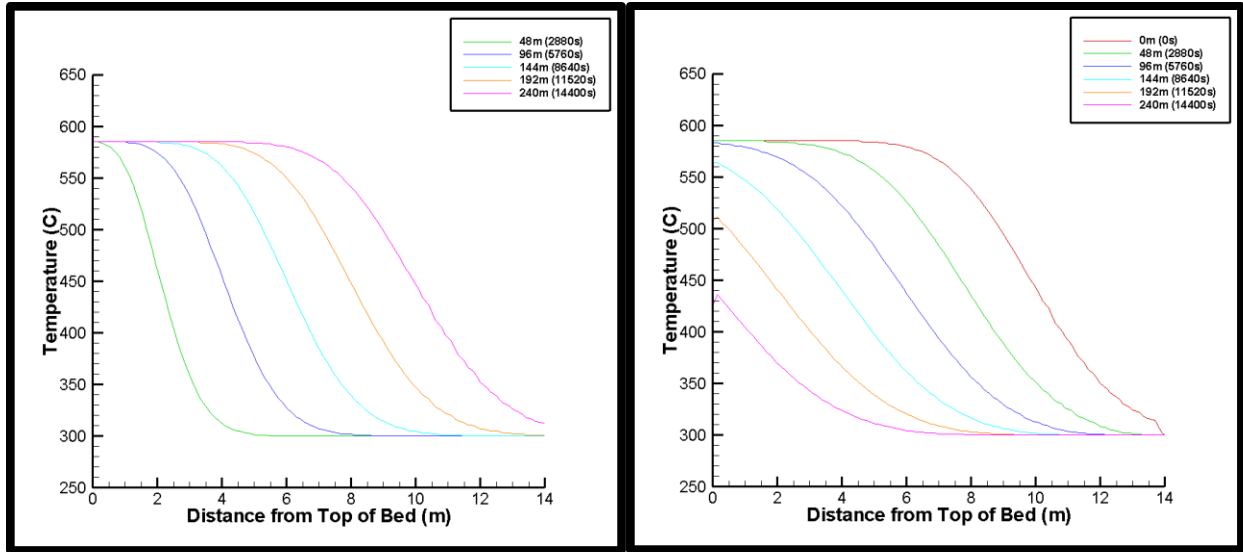
Figure 42: Temperature Profiles for Charge (Left) and Discharge (Right) Cycles Using Optimized Parallel Plate Model (Quartzite Properties)

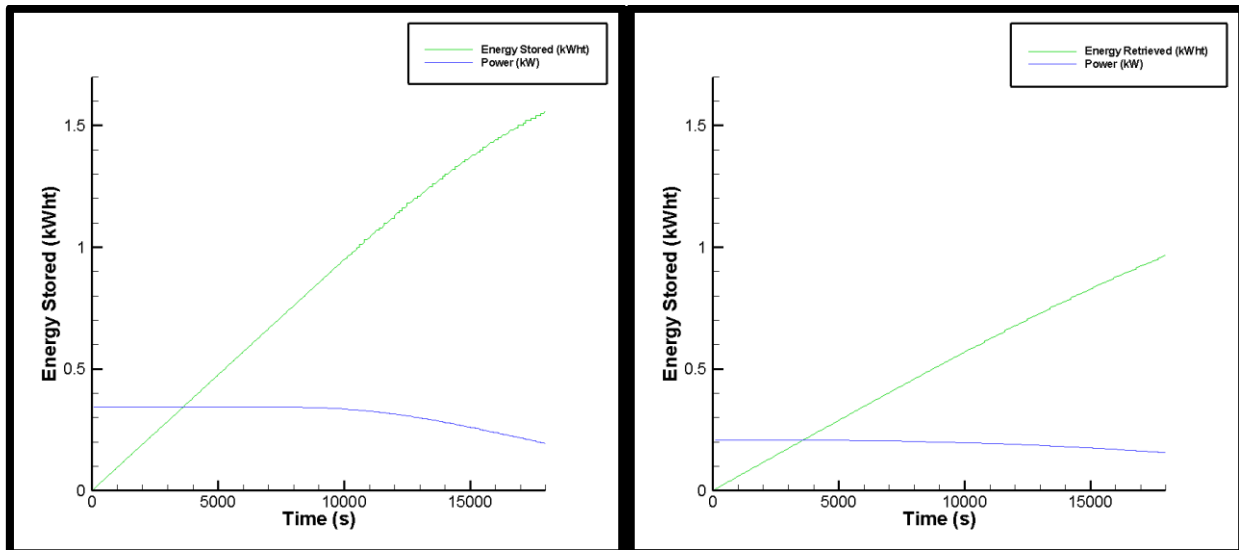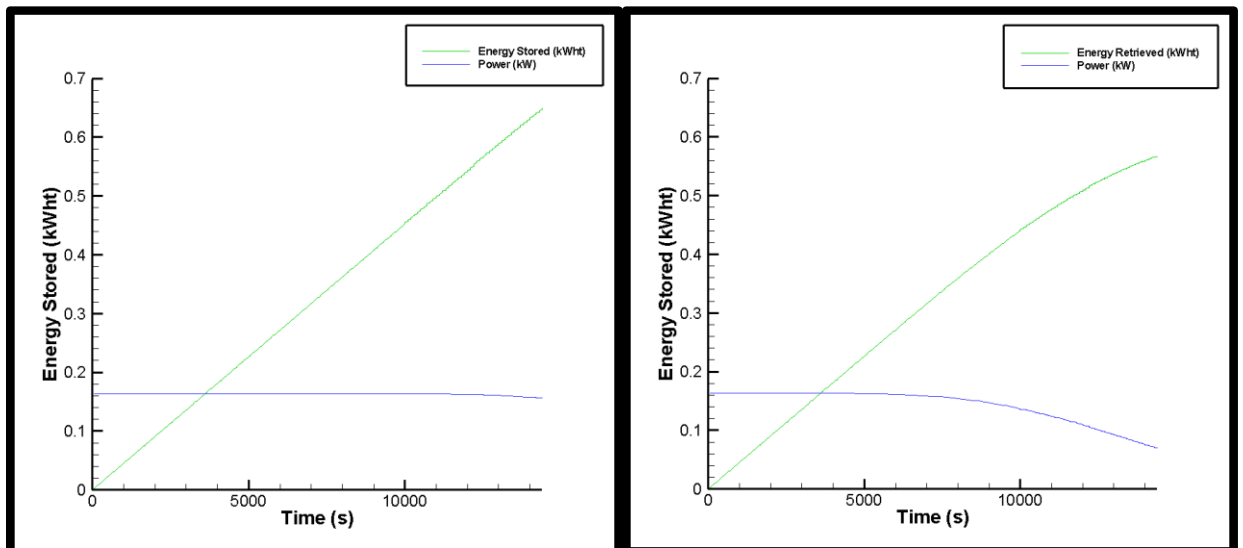**Figure 43: Energy Stored (Left) During Charge Cycle and Energy Retrieved (Right) During Discharge Cycle (Quartzite Properties)**

Comparing Case II of the PBTC model with Case II of the SCTC model, the TES system efficiencies are 91.49% and 76.40% respectively. The efficiencies of both TES systems fall short of the DOE's 2020 goal of 93%. From this point, Case II of the SCTC is no longer considered, as the properties of the concrete used in this work are very similar to those of limestone.

89

3.3 Overview of System Advisory Model

System Advisory Model (SAM) is a program developed by the National Renewable Energy Lab (NREL) to allow life cycle cost and performance studies of renewable energy systems. A major objective in this work is to compare the performance a structured concrete thermocline TES system with the performance of other TES systems to determine if it is a viable TES option.

The thermocline simulation software is a subroutine from TRNSYS; this subroutine is designed to simulate a packed bed thermocline just as the PBTC model is. However, it can be seen by comparing the modeling results from the PBTC and SCTC models that the temperature profiles and system efficiencies predicted by the two models are not always similar. If SAM is to be used to simulate the performance of as structured concrete thermocline TES system, the structured thermocline must be modeled as a packed-bed thermocline. Before the structured thermocline can be treated as a packed-bed thermocline, it is necessary to first model the thermocline with the PBTC and SCTC models and verify that the models predict similar performances.

As can be seen by comparing Case I of both thermocline models, the performance predicted by the two models, for a given system, may be similar enough that it is acceptable to simulate the structured thermocline as a packed-bed thermocline. However, taking Case II of both models as an example, the models will not always predict similar results for a given system. In this case, it is still possible to simulate the performance of a CSP plant using the given structured concrete thermocline TES system. To perform this simulation, it is necessary to modify the operating parameters in SAM so as to attain comparable thermocline performance to

the SCTC model. The process by which these modifications can be approached is discussed in Chapter 5.

3.3.1 Studies to be conducted with SAM

SAM is a valuable tool for application in conducting preliminary study to determine the optimum operating parameters for a CSP power plant. It has a large, user-updatable location library which records the solar irradiance throughout the year at numerous locations around the world. The user specifies a location and power plant capacity, and SAM updates plant components, such as the solar collection field, to meet the plant's solar energy needs to sustain power production. SAM allows four types of CSP collection to be studied: parabolic trough, linear Fresnel, central receiver, and dish. The interest in this work is to study TES at temperatures of up to 565°C, therefore the central receiver collection type is considered in this discussion.

SAM allows the user to vary the operational parameters of the power plant, such as the conversion efficiency of the power cycle, startup and standby times for the plant, and the operation of the plant's cooling system. Additional system parameters that can be varied include various sources of parasitic losses including energy required to move heliostats, energy required to pump the fluid, and heat lost from the fluid as it circulates. Though these are all important concerns in the process of optimizing the power plant's performance, they will be ignored in this work, as this study strictly concerns the impact of the TES system on plant cost and efficiency.

In this work, an optimized CSP plant is simulated with four TES configurations for comparison: none, two-tank molten salt TES, packed-bed thermocline TES, and structured thermocline TES. Based upon the life-cycle performance of the systems, conclusions are drawn as to which TES storage system provides the most viable option.

3.3.2 Works in Literature Validating the Performance of SAM

SAM allows the performance and economic analysis of CSP plants; numerous works have been conducted to evaluate the accuracy of SAM's results. Two comparative studies are referenced below; in the first study, the accuracy with which SAM models solar energy collection in a CSP plant's collector field. In the second study, the accuracy with which SAM predicts a CSP plant's monthly power production is assessed.

Wagner et al carried out a study to determine if the solar collection field employed in a parabolic trough CSP plant was valid (Wagner, Kearney, Mehos, & McMahan, 2011). In his work, Wagner compared thermal output from the trough collector field at SEGS II with modeled results from an equivalent model constructed in SAM. Figure 44 depicts plots generated in this comparison.
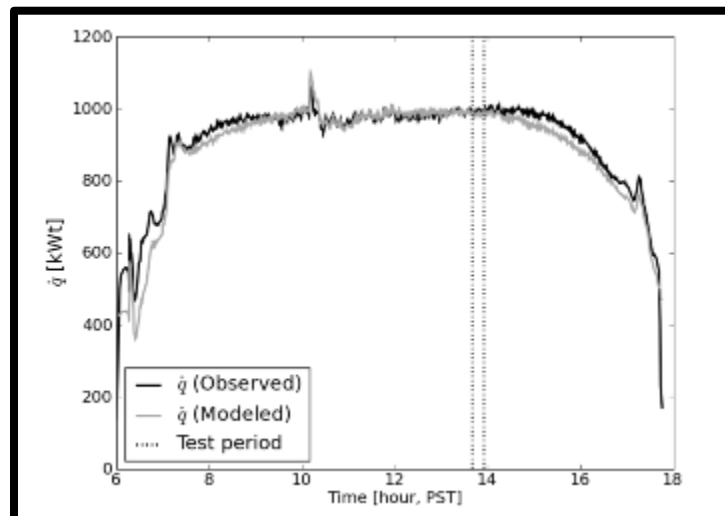
Figure 44: Comparison of Measured and Modeled Heat from Trough Collector Field (Wagner et al., 2011)

From Figure 44, it can easily be inferred that SAM accurately models the output energy from the trough collector field very well. In Wagner's work, a statistical analysis was employed

92

to determine the validity of the SAM model. The statistical model found that SAM's modeled output heat agreed with the measured trough field's output heat within a 95% confidence interval (Wagner et al., 2011). This demonstrates that SAM accurately predicts the collection of solar radiation using parabolic trough receivers.

In this work, the goal is to model the performance of a CSP power plant that collects solar radiation using a central receiver. Unfortunately, very little data are currently available from central receiver CSP plants. To date, no studies have been conducted to validate the performance of the central receiver collection method used in the SAM model. However, because the parabolic trough model used in SAM predicted actual collection performance accurately, it will be assumed that the central receiver model is accurate, and the validation process will move forward to the CSP power plant's performance.

Price conducted a study in which the power produced by the SEGS VI power plant was modeled for comparison with recorded output power (Price, 2003). Table 15 summarizes the results of this comparison.

Table 15: Comparison of Recorded and Simulated Performance of SEGS VI CSP Power Plant (Price, 2003)

Month	All Days				Removing Excluded Days			Removing Boiler Operation Days			
	Actual MWh	Model MWh	Model / Actual	No. of Excluded Days	Actual MWh	Model MWh	Model / Actual	No. of Solation Days	Actual MWh	Model MWh	Model / Actual
Jan	1,853	1,649	89.0%	3	1,781	1,564	87.8%	0	0	0	
Feb	3,080	2,950	95.8%	0	3,080	2,950	95.8%	0	0	0	
Mar	4,968	4,813	96.9%	1	4,919	4,779	97.1%	31	4,968	4,813	96.9%
Apr	5,874	6,248	106.4%	4	5,499	5,418	98.5%	30	5,874	6,248	106.4%
May	9,209	9,264	100.6%	3	8,636	8,471	98.1%	30	8,827	8,869	100.5%
Jun	10,291	10,434	101.4%	1	10,151	10,182	100.3%	18	6,904	6,985	101.2%
Jul	9,311	9,592	103.0%	1	9,137	9,401	102.9%	18	6,309	6,505	103.1%
Aug	9,517	9,762	102.6%	0	9,517	9,762	102.6%	9	2,987	3,080	103.1%
Sep	7,218	7,488	103.7%	1	6,926	7,172	103.6%	9	2,304	2,358	102.3%
Oct	5,388	5,628	104.4%	2	5,055	5,242	103.7%	31	5,388	5,628	104.4%
Nov	2,538	2,500	98.5%	1	2,446	2,397	98.0%	30	2,538	2,500	98.5%
Dec	1,798	1,818	101.1%	0	1,798	1,818	101.1%	20	1,265	1,301	102.9%
Total	**71,045**	**72,145**	**101.5%**	**17**	**68,945**	**69,155**	**100.3%**	**226**	**47,364**	**48,287**	**101.9%**

93

In the comparison presented in Table 15, the first Model/Actual column considers every day of the year; it is indicated that SAM's prediction of the plant's performance only varies by 1.5% from the plant's performance. In the second comparison, days when wind or unavailability of radiance effect power production are neglected, resulting in the difference between reported and predicted power generation falling to only 0.3%. The final column comparison omits days when backup fossil fuel is used at SEGS VI; only days when solar power is the sole fuel for power generation are considered. Once again, the results of SAM correlate well with recorded data, with modeled power generation only differing from reported power generation by 1.9%.

Based upon the works of Wagner et al (2011) and Price (2003), it can be concluded that SAM accurately models the harvesting of solar energy using a parabolic trough field and the conversion of the solar energy into electrical energy using a power plant. Though this work focuses on the use of a CSP power plant incorporating a central receiver, the model of which cannot be validated at this time because no experimental data is available, the accuracy of the model in predicting the performance of a parabolic trough CSP power plant provides sufficient confidence to move forward in this study to investigate SAM's modeling of TES systems.

3.3.3 Using SAM to Study Impact of Different Sensible Heat TES Systems

When SAM is downloaded, a built in case study considering an optimized central receiver CSP plant is pre-loaded. The purpose of this work is to study the impact of four TES configurations on the cost and performance of a CSP power plant; therefore, it is convenient to take a pre-existing optimized CSP plant and modify it with different TES systems. This saves a significant amount of time that would have to be spent optimizing parameters of the CSP plant, such as the receiver tower, heliostat field size and orientation, etc. Using this base case as a control, the impact of the TES unit can be observed as different TES scenarios are simulated.

The goal of this work is to study TES in the elevated temperature range of approximately 290$^{\text{o}}$C-565$^{\text{o}}$C; therefore, it is necessary to concentrate irradiance using a central receiver system, as linear receivers have maximum temperature potentials of approximately 390$^{\text{o}}$C. The plant's location is Dagget, CA, and its capacity is 100 MW$_{\text{e}}$ (Specified in the optimized SAM case). Parameters of the optimized power plant, collection field, and receiver of this plant are presented in Table 16. The information concerning the CSP power plant, as provided in Table 16, remains constant through all TES scenarios.

Table 16: SAM Base Case Plant, Field, and Receiver Parameters

Power Cycle		Collector Field		Receiver	
Efficiency (%)	43	Heliostats	7021	Tower Height (m)	183
High Temperature ($^{\text{o}}$C)	565	Total Area (m^2)	2,013,655	Receiver Height (m)	19
Low Temperature ($^{\text{o}}$C)	290	Field Area (ha)	610	Receiver Diameter (m)	15

All costs are based upon an assumed 30-year operating period, which is assumed in the built-in optimized study. The power plants are evaluated in terms of the nominal levelized cost of electricity (LCOE) that they achieve. The LCOE is the average price of the electricity produced by a power plant through its lifecycle. Transportation costs for the energy are considered in the LCOE. The nominal LCOE takes factors such as inflation into account and is the popular measure used by project developers (Owens, 2002); therefore, it is the metric considered when evaluating the performance of the CSP plants in this work.

3.3.3.2 Input Data for SAM

Using a built-in base case means that little modification of the input data is necessary to run SAM. The first modification is to select the desired number of hours of TES (8 hours in this case). After this, the configuration (two-tank or thermocline) is selected and in the case of thermocline TES, the solid media is selected. Additionally, the void fraction of the

thermocline's bed and the number of nodes along the axial length of the thermocline must be specified. SAM automatically calculates the necessary tank sizes and volume of liquid media based upon the provided information. Finally, it is necessary to input a unit capacity cost for the TES system ($/kWh$_t$). Attaining this value is somewhat complicated, as the cost of a TES system is contingent on numerous factors. The development of the unit capacity cost for each TES system considered in this work is discussed below.

3.3.3.2.1 Two-Tank and Thermocline TES System Cost Estimation from EPRI

The values provided in EPRI's report provide an invaluable summary of the contributors to the cost of both two-tank (Table 9) and thermocline (Table 10) TES systems. Values from this report can be used in combination with tank dimensions, salt inventory, and required TES capacity values (provided by SAM) to develop the required TES capacity cost for a given system. The procedure for developing TES capacity costs is bulleted below, then used in the upcoming Section 3.3.3.2.2 to estimate the costs of the TES systems considered in this work.

- **In SAM**

  - <u>Specify</u> the efficiency, capacity, and desired hours of operation off stored energy for the CSP plant. Specify solar salt as liquid media to be used as well as the system configuration: single-tank or two-tank. In the case of the single-tank TES system, specify the solid filler material to be used.

  - **<u>Retrieve</u>** the necessary TES system capacity (MWh$_t$), the dimensions of the tanks, and the volume of liquid salt media.

- **In Excel**

  - <u>Calculate</u> the tank volume and interpolate between values provided by EPRI (2010) to determine the tank cost.

96

o Calculate the media cost, for solid and liquid media, using values provided by John (2012) and Herrman & Kearny (2002).

o Calculate the remaining TES system cost contributions by interpolating between values in EPRI's (2010) report.

o **Retrieve** the capacity cost of the TES system ($/kWh$_t$).

- **In SAM**

o Specify the capacity cost of the TES system ($/kWh$_t$).

o Run simulation.

o **Retrieve** the LCOE, capacity factor, and yearly electricity production.

3.3.3.2.2 Using SAM and EPRI Values to Develop Capacity Cost

For this work, the CSP plant is designed for a capacity of 100 MW$_e$ and the TES system is designed to provide eight hours of operation considering 43% power cycle efficiency. To fulfill both specifications, SAM calculates that the required TES system capacity is 2164.71 MWh$_t$. If the TES configuration is selected as two-tank, SAM provides the tank dimensions and salt volume to be used (Salt volume is equivalent to volume of one tank). If the TES configuration is selected as thermocline, the filler material type must be specified; based upon the filler material, SAM calculates the necessary tank size. By knowing the tank sizes, it is possible to calculate the combined cost of the tank and storage media for each system. A summary of the tank and media cost calculations for a two-tank fluid, a packed-bed quartzite thermocline, and a structured concrete thermocline TES system is provided in Table 17. The process by which the values in the table are attained is discussed below.

Table 17: Tank and Media Costs for Two-Tank and Thermocline TES Systems

Tank and Media Cost Calculations			
TES Configuration	**Two-Tank**	**Packed Bed Thermocline**	**Structured Thermocline**
TES (MWh$_t$)	2,164.71	2,164.71	2,164.71
Tank Height (m)	20	20	20.00
Tank Diameter (m)	25.33	24.68	28.91
Tank Volume (m^3)	20,150.37	9,564.04	13,125.62
Cost/Volume ($/m^3)	$1,097.90	$1,127.20	$1,127.20
Base Tank Cost ($)	$2,000,000.00	$3,000,000.00	$3,000,000.00
Tank Cost ($)	**$24,123,093.91**	**$13,780,582.32**	**$17,795,201.78**
Filler Material Region	-	80.00%	80.00%
Filler Material Volume (m^3)	-	7,651.23	10,500.50
Filler Material Cost ($)	**$0.00**	**$282,789.44**	**$2,415,114.56**
Salt Inventory (m^3)	10,070.90	4,304.82	5,250.25
Salt Inventory Cost ($)	**$21,334,138.32**	**$9,117,181.00**	**$11,122,098.24**

TES system storage capacity and tank dimension values are obtained directly from SAM; from these values, the tank volume can be calculated. To price the tanks considered in each case, it is necessary to develop an expression for the tank cost as a function of volume. To get this expression, the tank costs attained by EPRI were plotted against tank storage capacity (Figure 45) for the two-tank and thermocline storage configurations. The reason for the difference in tank cost is not known; however, possible reasons are considerations for stresses due to extreme thermal gradients or thermal ratcheting in the thermocline tank. Applying a linear curve fit to the plots of tank cost, expressions are obtained to calculate the tank costs for any given volume. It should be noted that this approximation is only considered valid between the capacities of 100 MWh$_t$ and 3000 MWh$_t$, as it is not known how the cost of tanks outside this capacity range will vary with size.
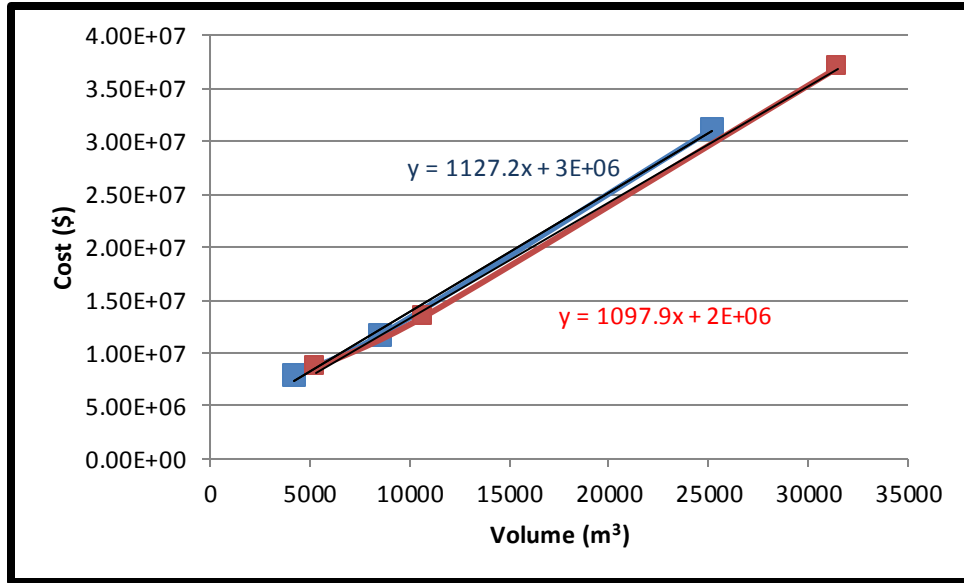
Figure 45: Tank Cost for Thermocline Tank (Blue) and Two-Tank (Red) TES Systems

After determining the cost of the tanks used in the TES system, the next step is to determine the cost of the storage media. Unit prices for liquid salt and all solid storage media considered in this work are provided in Table 18. For the two tank case, this simply consists of multiplying the volume of liquid media provided by SAM by the liquid media cost provided in. For the thermocline case, both solid and liquid media must be considered. Knowing that the solid media is typically contained in the middle 80% of the tank's volume, the solid media weight is obtained by multiplying 80% of the tank's volume by the density of the solid media. This value is then multiplied by the unit price of solid media. The quantity of liquid media found is taken to be 20% of the tank's volume plus 80% of the tank's volume multiplied by the void fraction of the bed. The cost of the liquid media is then attained by multiplying its volume by its unit cost.

Table 18: Average Thermo-Physical Properties and Costs of Liquid and Solid Media

	ρ (kg/m³)	Cp (J/kg.K)	Cost ($/kg)	Cost ($/m³)	TES (kWh_t/m³)	Cost ($/kWh_t)
TES Media Properties and Costs						
Energy Storage Media	**Property**					
Properties based on T_avg						
Solar Salt (Na60K40)	1,815.25	1,365.70	$1.17	$2,118.39	195.57	**$10.83**
Properties from SAM						
Limestone (3/4")	2,320.00	810	$0.01	$32.48	148.25	**$0.22**
Quartzite (3/4")	2,640.00	1,105.00	$0.01	$36.96	230.13	**$0.16**
UHPC Mix Designs						
Mix 2	2,082.40	950.4	$0.11	$228.51	156.13	**$1.46**
Mix 11	2,202.53	889.7	$0.10	$230.00	154.59	**$1.49**
Mix 15	2,106.43	803.87	$0.06	$122.07	133.58	**$0.91**
Mix 26	2,322.68	904.35	$0.22	$501.14	165.71	**$3.02**

Having determined the costs of the tanks and media of the TES systems, the costs of the remaining items under the direct cost category are determined by linear interpolation between values in the EPRI approximation. A summary of direct cost values and the total direct cost, including the price of the tanks and storage media calculated in Table 17, is provided in Table 19.

Table 19: Direct Cost Contributions, Excluding Tank and Media, and Direct Cost Subtotal

Remaining Direct Cost Contributors and Direct Cost Subtotal			
TES Configuration	Two-Tank	Packed Bed Thermocline	Structured Thermocline
Foundation	$7,936,310.00	$4,772,480.00	$4,772,480.00
Platform and Steel	$1,837,130.00	$1,449,300.00	$1,449,300.00
Insulation	$347,700.00	$1,062,800.00	$1,062,800.00
Filler Preheating Equip.	$0.00	$1,833,770.00	$1,833,770.00
Surge Tanks	$0.00	$366,471.00	$366,471.00
Pumps and PCE	$7,278,250.00	$6,673,660.00	$6,673,660.00
Salt Melting System	$3,096,000.00	$2,764,530.00	$2,764,530.00
Piping and Valves	$2,179,080.00	$2,177,830.00	$2,177,830.00
Electrical	$550,742.00	$550,742.00	$550,742.00
Instrumentation/Controls	$322,118.00	$322,118.00	$322,118.00
Energy Cost Melting Salt	$103,294.00	$347,076.00	$347,076.00
Direct Cost Subtotal ($)	**$69,107,856.23**	**$45,501,329.76**	**$53,653,191.58**

After determining the direct cost of the TES systems, the next task is to calculate the indirect costs of the system. Indirect costs include such things as taxes, project management, and contingency put in place to cover unexpected expenses. The values for project management and indirect construction costs are interpolated from values in EPRI's report (2010). Contingency for the TES system is taken as 15% of the direct cost, and engineering costs are assumed to be 3% of the direct cost. Finally, tax on materials is taken to be 8.75%. Values for the indirect costs and the indirect cost subtotal are provided in Table 20.

Table 20: Indirect Cost Contributions and Indirect Cost Subtotal

Indirect Cost Contributors and Indirect Cost Subtotal			
TES Configuration	Two-Tank	Packed Bed Thermocline	Structured Thermocline
Contingency	$10,366,178.43	$6,825,199.46	$6,825,199.46
Material Sales Tax	$6,046,937.42	$3,981,366.35	$3,981,366.35
Engineering	$2,073,235.69	$1,365,039.89	$1,365,039.89
Construction Indirect Costs	$10,726,600.00	$5,847,630.00	$5,847,630.00
Construction Management	$1,500,000.00	$1,500,000.00	$1,500,000.00
Indirect Cost Subtotal ($)	**$30,712,951.54**	**$19,519,235.71**	**$19,519,235.71**

101

Having determined the direct and indirect cost contributions of the TES system, adding these two quantities provides the total cost of the TES system. Dividing the total cost of the system by its storage capacity in kilowatt-hours yields the unit capacity cost value needed as input for SAM. Table 21 provides the total TES system costs and their respective unit storage capacity costs.

Table 21: TES System Costs and Unit Capacity Cost Values for Input in SAM

Total TES System and Unit Capacity Costs			
TES Configuration	**Two-Tank**	**Packed Bed Thermocline**	**Structured Thermocline**
Total Cost ($)	$99,820,807.77	$65,020,565.47	$73,172,427.27
Unit Capacity Cost ($/kWh$_t$)	**$46.11**	**$30.04**	**$33.80**

CHAPTER 4: EVALUATION OF CONCRETE FOR A STRUCTURED CONCRETE THERMOCLINE

Concrete has been identified as a promising sensible heat storage media option in thermocline applications because of the low energy storage media cost it provides and because it eliminates the issue of thermal ratcheting of the storage tank's walls. The amount of energy stored in a sensible heat TES is directly proportional to the temperature range in which energy can be stored; therefore, the greater the temperature that energy can be stored at, the greater the energy storage density the TES system will have. Molten salts have gained increased interest as HTF because they can operate up to temperatures of $585^{o}C$. Concrete is under evaluation for application in a dual media thermocline TES system incorporating molten salt as HTF. Details concerning the development and testing of concrete as TES media are discussed in this chapter.

The molten salt selected for testing in this work is a binary mix of 40% potassium nitrate and 60% sodium nitrate. This salt was selected because of its low cost, relative to other salts, and its thermal stability at temperatures of up to $593^{o}C$ (Skinner, 2011). Thermo-physical properties of the binary salt are listed in Chapter 2.

4.1 Considerations for Concrete for High Temperature Applications

As stated previously, benefits of concrete in sensible heat TES applications include its low cost and the fact that it eliminates the issue of thermal ratcheting of the storage tank's walls. Two major concerns must be addressed before a concrete and salt thermocline can be incorporated in a TES application. The first consideration is the physical of concrete at high temperatures, namely at the elevated temperature of $585^{o}C$. The concrete must retain sufficient strength to maintain its structural integrity at high temperatures. The second consideration is the chemical compatibility of the concrete and molten salt combination; the salt must not attack and cause significant deterioration of the concrete.

103

4.1.1 Structural Compatibility of Concrete with High Temperatures

Typical structural concrete loses strength at elevated temperatures: Reportedly 10-20% at 300°C and 40-60% at 600°C (Phan & Carino, 2000). However, testing reported by John (2011) indicates that structural concrete spalls and explodes violently around the temperature of 300°C. Figure 46 depicts a testing oven and a cylinder cage damaged during heating of concrete cylinder specimens. It should be noted that the oven was damaged during testing in which the concrete specimens were not contained in cages.
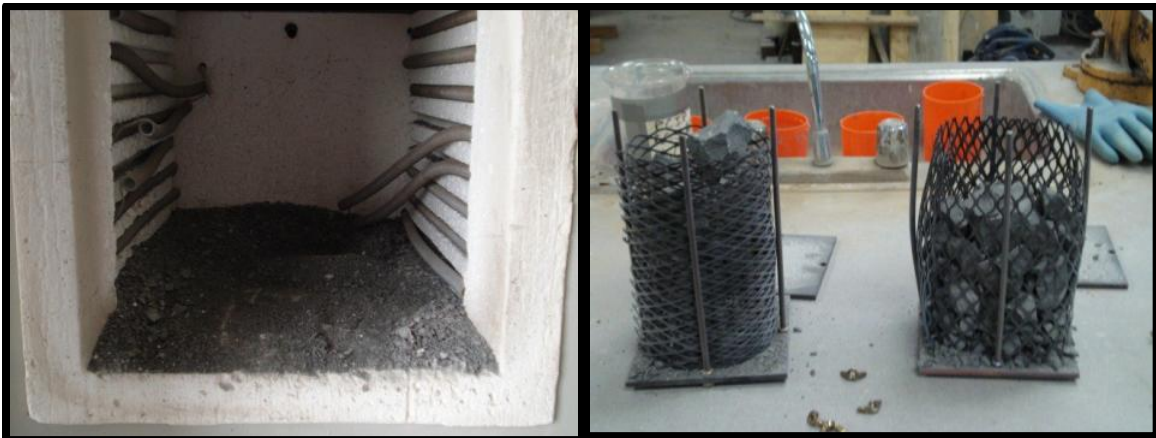
Figure 46: Oven Damaged While Heating Concrete Specimen (Left) and Cylinder Cage Damaged While Heating Specimen (Right) (John, 2012)

One possible cause of the concrete's violent spalling and explosion is postulated to be superheated steam entrapped in the concrete. Concrete specimens retain a certain amount of entrapped water throughout their life. When superheated, this trapped water vaporizes; if there is no means for the vapor to escape the specimens, pressure will build as temperature increases until the internal forces in the specimens result in rupture. To mitigate this problem, polypropylene fibers are mixed in with the concrete (John, 2012). When the concrete is heated, the fibers melt, leaving tiny channels through which the steam can exit the specimens. This, along with variations in concrete mix designs, allows specimens to maintain structural integrity at temperatures exceeding 600°C.

4.1.2 Chemical Compatibility of Concrete with Molten Salt

In addition to being able to maintain its structural integrity at high temperatures, it is necessary that the concrete being used in a dual media thermocline be chemically compatible with the molten salt being used. If the concrete is not chemically compatible with the nitrate salts, it can degrade over time and contaminate the salt, possibly leading to blockages within the system.

When developing the concrete mix designs, it is desirable to use considerable quantities of course aggregate because it is the cheapest component of concrete. Pacheco et al. (2002) conducted thermal cycling experimentation to test various aggregates for compatibility with molten nitrate salts. His testing consisted of cycling the aggregates between $290^{o}C$ and $400^{o}C$ in molten nitrate salt; he concluded that taconite, marble, NM limestone, and quartzite are viable aggregate for application in a molten salt thermocline. Further testing is reported by Brosseau et al (2005), in which quartzite aggregate and sand were subjected to thermal cycling between $285^{o}C$ and $500^{o}C$. Brosseau's work also concludes that quartzite is compatible with molten nitrate salt. Finally, Brown (2012) conducted testing with AR sandstone and limestone in the temperature range of $300^{o}C$ to $550^{o}C$. Brown reported that both course aggregates perform well under testing and that they are compatible with molten nitrate salt.

The cementitious paste is the most expensive component of concrete; cements considered include ordinary portland cement (OPC), calcium aluminate cement (CAC), and fly ash (FA). OPC is the most commonly used cementitious material, used widely in structural applications. However, it spalls and loses strength at high temperatures. CAC is a much less temperature-sensitive cementitious material that has been demonstrated to maintain its strength up to temperatures of $600^{o}C$ (Brown, 2012). However, this is also the most expensive of the three

mentioned cementitious pastes. FA is a byproduct of coal combustion; it is the least costly of the three cementitious materials. The negative attribute of concrete containing FA is that it gains strength slower after set; however, this is not a significant problem for TES applications. The concrete specimens evaluated and tested in the upcoming portions of this chapter contain course and fine aggregate along with varying proportions of the three aforementioned cementitious materials.

4.2 Evaluation of Mix Designs

Twenty-six unique concrete mix designs were created and tested for compatibility with molten salt and are discussed in detail in the work of John (2012). The goal in developing mix designs is threefold: to find concrete capable of surviving the molten salt environment, to optimize the thermal properties of the concrete, and to minimize the cost of the concrete.

4.2.1 Testing of Concrete Specimens at Elevated Temperatures

In the work of John (2012), cubes are cast from each of the mix designs and subjected to three regiments of testing. Prior to testing, specimens are massed and control specimens are crushed so that the thermal tests' effects on the specimens' compressive strength and mass can be evaluated. Figure 47 depicts specimens in the molten salt environment; the specimen in the second row and the fourth column disintegrated and failed during thermal cycling.

- Thermal cycling in the presence of air between 300°C and 600°C.

- Sustained isothermal bath in the presence of molten salt at 550°C.

- Thermal cycling between 300°C and 565°C.

Figure 47: Concrete Specimens in Molten Salt Bath (John, 2012)

Details concerning changes and mass and compressive strength for each mix design can be found in the works of John (2012) and Brown (2012). General observed trends are presented below. Hale performed a statistical analysis to find what combination of cementitious materials and quantity of water used in mixing the concrete would produce the optimum resistance to deterioration under thermal cycling. The results indicated that a combination of OPC and FA with a 0.30 water weight to cement weight mixing ratio provides the best thermal fatigue resistance (Hale, 2012).

- Specimens undergoing thermal cycling in the presence of air or molten salt decrease in compressive strength.

- Specimens subjected to an isothermal bath in molten salt increase in compressive strength.

- Specimens subjected to an isothermal bath or thermal cycling in molten salt gain mass.

- Specimens subjected to an isothermal bath in air or thermal cycling in air lose mass.

4.2.2 4 Concrete Mix Designs for Lab-Scale Testing

Based upon thermal cycling and cost analysis four mix John (2012) recommends four mix designs for further testing. Average material properties (considering properties pre and post thermal cycling tests) of these four mix designs are presented in Table 22 along with the TES capacity cost. It can be seen that three of the four mix designs are comparable with the $1/kWh_t value reported by Herrmann et al. (2002). The outlying mix design, number twenty-six, is a proprietary mix design known as TC1000, selected for testing because of its superior strength and thermal properties (John, 2012). In this work, mix designs 11 and 26 are tested.

Table 22: Average Properties of Concrete Mix Designs Selected for Testing (John, 2012)

Property	Concrete Mix Design (# of 26)			
	Mix 2	Mix 11	Mix 15	Mix 26
ρ (kg/m^3)	2,082.40	2,202.53	2,106.43	2,322.68
Cp (J/kg.K)	950.40	889.70	803.87	904.35
Cost ($/m^3)	$228.51	$230.00	$122.07	$501.14
TES Cost ($/kWh$_t$)	$1.46	$1.49	$0.91	$3.02

The thermocline test system designed to perform this testing is reported in the work of Brown (2012). Due to complications in regulating fluid flow rate and budget constraints, it was realized that the test system is not capable of establishing a thermocline. Having acknowledged that it is not possible to establish a thermocline in the test system, the goal of testing is shifted to evaluating the performance of concrete beams when subjected to extreme thermal gradients and circulating molten salt. The goal of this testing is to determine if the beams can survive thermal stresses introduced when they are heated non-uniformly and to determine if circulating molten salt around the concrete specimens causes deterioration that the thermal cycling reported by John (2012) did not cause.

4.3 Testing of Concrete Beam Specimens

4.3.1 Lab-Scale Test System

A dimensioned schematic of the lab-scale test apparatus used in this work is provided in Figure 48. The test unit consists of three primary units: the thermocline tank, the salt storage tank, and the salt pumping unit. Solar salt's corrosive properties require that the tanks, pump, and exhaust pipes all be constructed from stainless steel. The thermocline tank component (Right side of Figure 48) consists of a rectangular tank, a frame which elevates it above the salt storage tank and an adaptor pipe through which molten salt is pumped. The salt storage tank component of the test system (Left side of Figure 48) consists of a rectangular tank and the burners used to heat and melt the nitrate salt. The salt pumping unit (Right side of salt storage tank in Figure 48) consists of the pump, the motor used to drive the pump, and a regulating valve system; it transports molten salt from the reservoir to the thermocline tank. Details of each of the major system components are discussed in detail in upcoming sections.
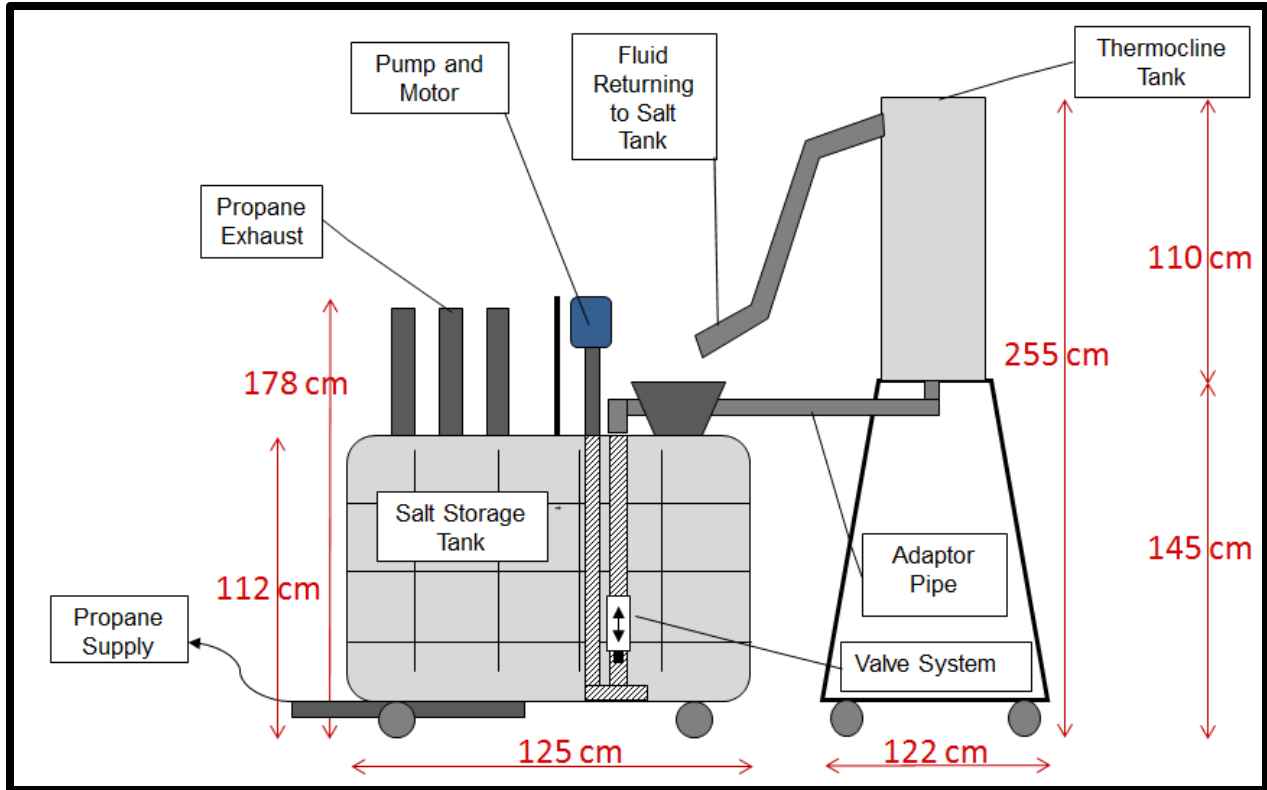
Figure 48: Dimensioned Schematic of Lab-Scale Thermocline Test System

4.3.1.1 Thermocline Tank

The thermocline tank component of the test system houses the concrete specimens being evaluated for application in TES.   The thermocline tank gained its name because it was initially designed for as part of a thermocline test system.   It should be understood that the purpose of this work is to evaluate the performance of the concrete beams as molten salt is circulated around them and that the purpose of this testing is not to develop a thermocline.   The tank's dimensions are as follows: cross section of 41cm by 41 cm (16in by 16 in) and length of 110cm (44 in). Though the tank has a height of 110cm (44in), only 92cm (36in) is available to hold concrete.   Its base is located at a higher elevation than is the top of the salt storage tank so that it gravity drains when the pump is shut off.   The tank and adaptor pipe are wrapped in two layers of 5cm (2in) ceramic insulation having thermal conductivity of 0.13 W/m-K (Skinner, 2011).   An intermediate layer of aluminum foil applied between the layers of insulation reduces radiation

110

losses. Figure 49 depicts the thermocline tank in three levels of insulation: un-insulated, with one layer of insulation and aluminum foil, and completely insulated.

Figure 49: Thermocline Tank: Un-insulated (Left), One Layer of Insulation and Aluminum Foil (Middle), and Two Layers of Insulation (Right)

4.3.1.2 Salt Storage Tank

The salt storage tank component of the test system is used to house and heat the nitrate salt inventory. Its dimensions are as follows: length of 122cm (48in), width of 61cm (24in), and height of 92 cm (36in). The tank is insulated with ceramic insulation and aluminum foil in the same manner as the thermocline tank is. The salt reservoir is heated by six propane burners located under the tank; each burner has an output of 117 kW (400,000 BTU/h) (Skinner, 2011). The salt storage tank is depicted in Figure 50.

Figure 50: Insulated Salt Storage Tank

111

www.manaraa.com

4.3.1.3 Salt Pumping Unit

The pumping unit component of the test system is used to transport molten salt from the salt reservoir component of the test system to the thermocline component of the test system. The pump is a stainless steel sump pump and is powered by a 373 W (0.5 hp), single-speed electric motor. Because the motor is single-speed, a valve system is used to regulate the fluid flow rate. This system consists of a collar and a slit cut in the pipe running from the pump's impeller; the flow rate is increased by sliding the collar to cover more of the slit or decreased by sliding the collar to expose more of the slit. Figure 51 depicts the salt pumping system and a close up view of the collar and slit used to regulate the salt's flow rate.

Figure 51: Salt Pumping System (Left) and Close Up of Collar and Slit (Right)

4.3.2 Selection and Construction of Concrete Specimens for Lab-Scale Testing

Two models are considered for the filler concrete geometry in the work of Brown (Brown, 2012): a parallel-plate model and an axisymmetric model. The parallel-plate model, discussed in Chapter 3, consists of rows of rectangular concrete prisms with gaps separating

them through which the molten salt circulates during charging and discharging. The axisymmetric model consists of rectangular concrete prisms with square cross sections. A fluid flow channel spans the longitudinal axis of each prism, and fluid is passed through it to charge and discharge the system. Because the axisymmetric filler concrete arrangement is more convenient to construct and arrange, it is the model selected for evaluating the concrete's performance in this work.

The dimensions of the concrete specimens tested in this work are limited to the following by the size of the thermocline tank: cross section of 41cm by 41 cm (16in by 16 in) and length of 92cm (36 in). Because of the size restrictions, the concrete filler used in each round of testing consists of nine concrete beams, each having the following dimensions: cross section of 10cm by 10cm (4in by 4in) and length of 92cm (36 in). Brown's (2012) work found that the optimum fluid flow channel diameter for the given prism size is 4cm (1.5in), therefore, the prisms tested in this work are cast with a 4cm (1.5in) diameter fluid flow channel.

For testing purposes, sets of nine prisms are cast from concrete mix designs 11 and 26, discussed in the previous section. The fluid flow channels are constructed by casting the concrete around plastic tubing which is removed after the concrete sets. A lubricant is applied to the tube prior to casting the concrete to allow the tube's removal from the prism after the concrete sets. After the specimens set, they are removed from the molds and placed in a curing room for at least twenty-eight days, the assumed length of time for concrete to reach its design strength (Nilson et al., 2010). The curing room provides constant temperature and humidity, preventing premature drying of the specimens, which can reduce their strength by up to 30% (Nilson et al., 2010).

4.3.3 Testing Procedure

Testing of the concrete beams specimens is very time consuming; the test procedure is bulleted below with an approximation of the time required to complete each step. Throughout the testing process, the temperature of the salt in the salt reservoir tank is monitored to make sure that the salt temperature does not drop below 400°C. If the salt temperature falls below this limit, the pump is turned off and the salt reservoir is heated until it reaches a minimum temperature of 500°C. The assembled test system is depicted during testing in Figure 52.

- Attach hose between propane tank and burners on salt storage tank (10 min).

- Position fan to circulate air over pump to prevent overheating (5 min).

- Install 'type K' thermocouple in salt storage tank to monitor salt temperature (10 min).

- Fire burners and allow entire tank to heat to 550°C (5-6 hr).

- Connect salt storage tank and thermocline tank using the adaptor pipe. Apply anti-seize to threads to prevent seizing of joints (20 min).

- Turn on pump, circulating molten salt through system (3 hr).

- Turn off pump and allow salt to drain back to salt storage tank before removing adaptor pipe (5 min).

114

Figure 52: Assembled Test System during Testing

CHAPTER 5: RESULTS AND DISCUSSION

5.1 Equivalent Parameters between PBTC and SCTC Models

The thermocline function in SAM simulates a thermocline using a two-phase 1D model similar to the PBTC model described in Chapter 3. The Schumann model is designed to approximate heat transfer for fluid flow through a porous media; therefore, it is applicable for modeling a packed bed thermocline TES system. Unfortunately, the structured concrete thermocline considered in this work cannot be considered a simple porous media. Theoretically, as the thickness of the plates becomes very small, the approximation becomes accurate, as more solid media surface area is exposed and the thickness of the concrete plates over which a thermal gradient can exist approaches zero. However, incorporating concrete plates of this small thickness in a structured concrete thermocline is not feasible at this time.

To effectively simulate the performance of a structured concrete thermocline in SAM, it is necessary to develop a system of equivalent parameters, which will cause the PBTC model to behave as the SCTC model. Both the PBTC and SCTC model are described and optimized in Chapter 3. SAM is primarily to be used as "black box" software, allowing life-cycle CSP plant performance and analysis considering numerous factors such as parasitic losses and harvesting of solar energy without extensive software development. SAM is constructed such that many variables are dependent on each other. Therefore, the first step in developing equivalent parameters between the two models is to identify the parameters that can be changed without influencing other aspects of the model.

5.1.1 Sensitivity Analysis

Table 23 provides a list of the input parameters for simulating a structured concrete thermocline using SAM. The parameters in the upper region of the table are fixed; the two

116

parameters in the lower portion of the table are variables investigated in the search for equivalent parameters. A final parameter that is held constant through all cases is that the TES system must store 2,164.71 MWht, the necessary amount of energy to allow 8 hours of full capacity power production off of stored energy. A study of the individual impacts of each of the variable parameters follows.

Table 23: Fixed and Variable Parameters Considered in Equivalent Parameter Search

Fixed Parameters	
T_L (C)	585
T_H (C)	300
Mass Flow (kg/s)	1500
ρ_f (kg/m^3)	1804
Cp_f (J/kg.K)	1390.98
Tk_f (W/m.K)	0.5
ρ_s (kg/m^3)	2320
Cp_s (J/kg.K)	810
Tk_s (W/m.K)	1.89
Cycle Duration (s)	8640
Variable Parameters	
Bed Void Fraction	
Bed Height	

5.1.1.1 Effect of Bed Void Fraction on Temperature Profile

The first parameter to be considered in this equivalent parameter search is the effect of the void fraction of the filler material on the performance of the thermocline. Recalling that the void fraction is the ratio of the fluid volume to the combined fluid and solid volume, it can be seen that the possible void fraction values range from 1, a completely fluid bed, to 0, a completely solid bed. The specific heat and density of concrete and solar salt are different; therefore, changing the void fraction of the storage region requires that the tank volume be changed as well to maintain the specified energy storage capacity. In this portion of the study, the diameter of the storage tank is held constant, and the height of the tank is adjusted to

117

maintain the specified energy storage capacity. Table 24 summarized the tank dimensions and other properties in the 1D model that are affected by increasing the void fraction of the bed.

Table 24: Parameters in 1D Model Affected by Void Fraction of Bed

Parameter	Bed Void Fraction					
	0.01	0.2	0.4	0.6	0.8	0.99
D_{tank} (m)	41.574	40.618	39.679	38.803	37.982	37.248
Ac_{tank} (m^2)	1357.48	1295.74	1236.55	1182.53	1133.02	1089.69
h (W/m^2.K)	997.14	272.82	218.11	194.83	181.38	179.92
V_{fluid} (m/s)	0.061	0.0032	0.00168	0.00117	0.000915	0.000771

Temperature profiles resulting from a 144 minute charge cycle in a thermocline having each of the void fractions considered above are displayed in Figure 53. After reviewing the impact of the bed's void fraction on its performance during charging, it is clear that the void fraction of the bed has little impact and the charge/discharge performance of the bed.
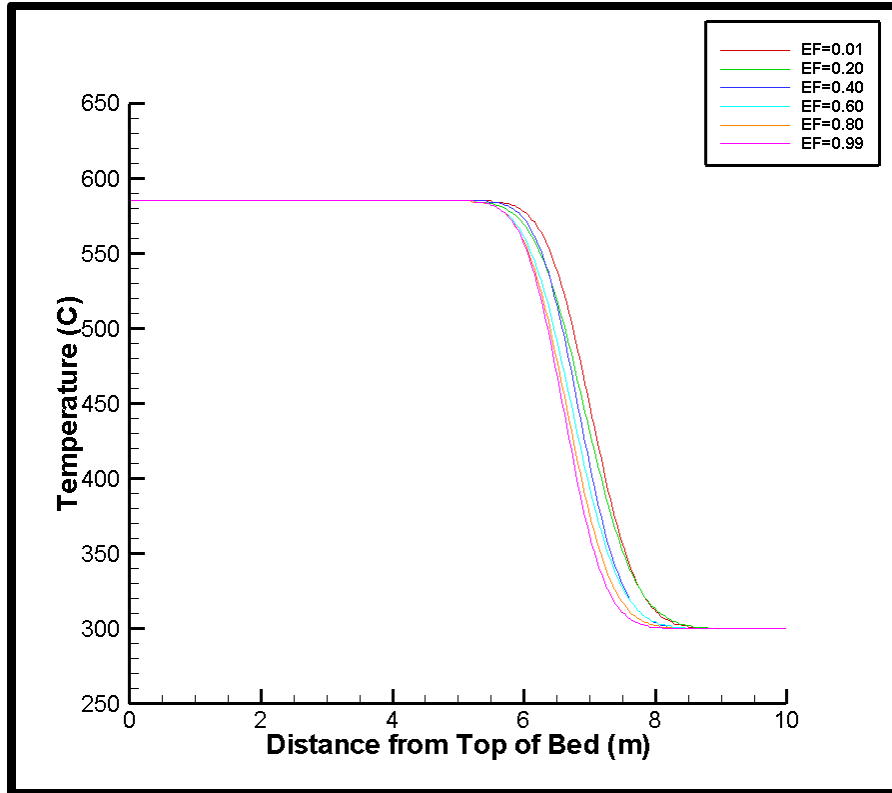
Figure 53: Effect of Void Fraction on Charge Cycle Temperature Profile

118

5.1.1.2 Effect of Bed Height on Temperature Profile

The second parameter considered in the search for equivalent parameters is the height of the bed; in this section, the void fraction of the bed is held constant and the diameter of the tank is adjusted to maintain the required tank volume. Table 25 summarizes the tank heights considered, along with other system parameters influenced by changing the height of the bed.

Table 25: Parameters in 1D Model Affected by Height of Bed

Parameter	Bed Height (m)				
	10	15	20	25	30
D (m)	47.32864	38.64367	33.4664	29.93326	27.3252
A_c (m²)	1759.292	1172.861	879.6459	703.7168	586.4306
V (m³)	17592.92	17592.92	17592.92	17592.92	17592.92
h (W/m².K)	207.22	236.69	261.81	284.13	304.52
V_f (m/s)	0.00143	0.00214	0.00286	0.00357	0.00429

Temperature profiles resulting from a 144 minute charge cycle in a thermocline having each of the bed heights considered above is provided in Figure 54. For all five bed heights, the amount of energy stored in the TES system during the charge cycle is within a fraction of a percent of the same value. Investigating Figure 54, it can be seen that as the height of the bed increases, the thermocline region begins to become slightly less pronounced. However, this change is very small. A fixed number of nodes is used for all heights of the bed; therefore, as the height of the bed is increased, the size of the differential elements considered increases. With this increase in differential element size, it must be assumed that some degree of error in the numerical model is present. This means that the decrease in sharpness of the thermocline zone may be attributed to numeric error; therefore, it can be concluded that the height of the bed used has little impact on the performance of the thermocline TES system.

119
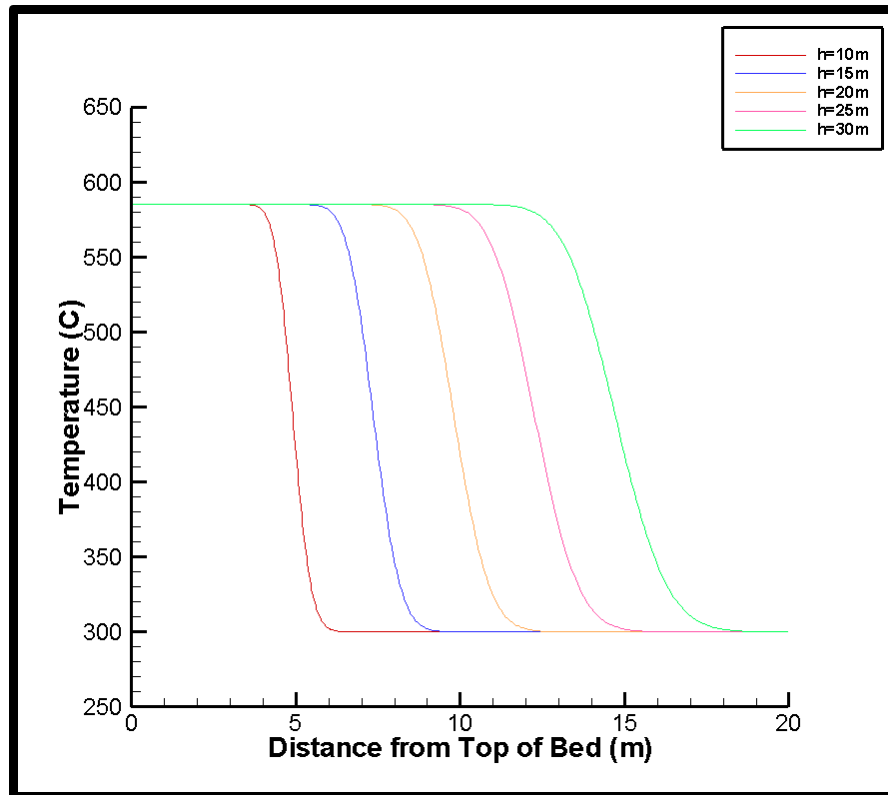
Figure 54: Effect of Tank Height on Charge Cycle Temperature Profile

5.1.2 Impact of Number of Nodes Used on Performance of PBTC Model

Neither of the two parameters investigated above significantly influence the performance of the PBTC model. Reviewing the PBTC convergence studies conducted in Chapter 3 reveals a possible way of reaching equivalence between the models: by varying the number of nodes used in SAM for simulating the PBTC. In Chapter 3, two cases of the PBTC and SCTC model are presented; in these cases, the solid filler material is assumed to have the properties of limestone and quartzite respectively. Comparing the results predicted by both models for each solid media case, it can be seen that the PBTC model predicts sharper temperature profiles, corresponding to higher efficiency for each case. In the convergence study to determine the number of nodes needed for the PBTC model, it can be seen that as the number of nodes used is decreased, the temperature profiles in the tank become less sharp. It is postulated that reducing the number of nodes used in the PBTC model may cause this model to perform like the SCTC model.

Before this discussion moves further, the significance of varying the number of nodes must be understood. The PBTC model converges well when 201 nodes are used; convergence means that the equations, as they are expressed numerically, are being solved correctly. Using a decreased number of nodes corresponds to adding error to the solution of the PBTC model. In this work, software developed to model a PBTC is to be used to analyze a SCTC; reviewing the description of each model (Chapter 3), it can be concluded that the results predicted by the two models, for equivalent systems, are not the same. Decreasing the number of nodes used in the PBTC model means increasing the amount of error in the packed bed thermoclines that it is simulating. However, having a converged case of the SCTC model in hand, error can be added to the PBTC model to make it predict results similar to those of the SCTC model.

To gain a qualitative measure of the impact of the number of nodes used on the performance of the PBTC model, the optimized PBTC Case I presented in Chapter 3 is considered. Considering a 96 minute charge cycle, the number of nodes used in varied between 21 and 100; the variation in the temperature profile is presented in Figure 55. Based upon the degree of variation in the temperature profile, it can be concluded that the number of nodes used in the PBTC model significantly affects the predicted results. Moving forward, the applicability of node spacing as an equivalent parameter is investigated further.
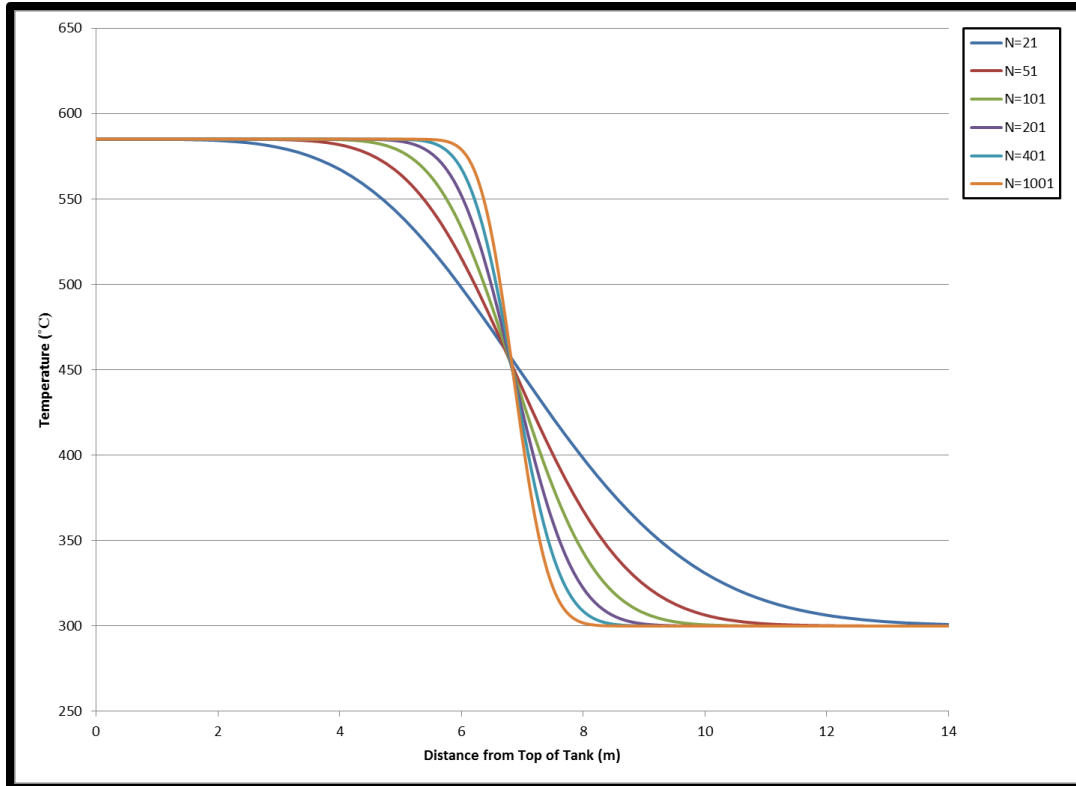
Figure 55: Effect of Changing the Number of Nodes on Charge Temperature Profile

5.1.2 Equivalence between PBTC Model and Brown's SCTC Model

Figure 56 depicts the charge cycle temperature profiles calculated by the optimized PBTC model (Left) and Brown's optimized SCTC model (Right). A qualitative comparison of the two cases indicates that the PBTC model predicts a much sharper thermocline region than does Brown's SCTC model.

122
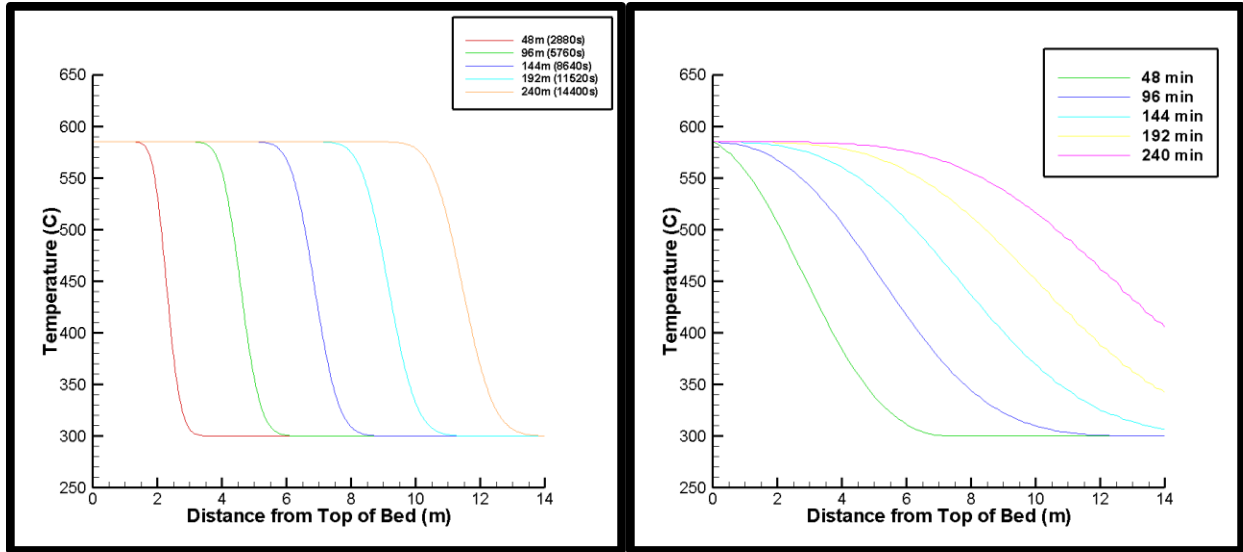
Figure 56: Charge Cycle Temperature Profile from PBTC Case I (Left) and Brown's SCTC Model (Right)

From Figure 55, it can be seen that decreasing the number of nodes used in the PBTC model significantly decreases the sharpness of the thermocline region. Comparing the temperature profiles with the temperature profile corresponding to 96 minutes for Brown's SCTC model, it can be seen that the curve for corresponding to 21 nodes is sharper than that predicted by the SCTC model. Therefore, 17 nodes are used in the PBTC model for this preliminary comparison. In Figure 57, charge cycle temperature profiles generated by Brown's SCTC and the PBTC Case I are plotted, along with the charge cycle temperature profile attained using the PBTC Case I with 17 nodes.

www.manaraa.com
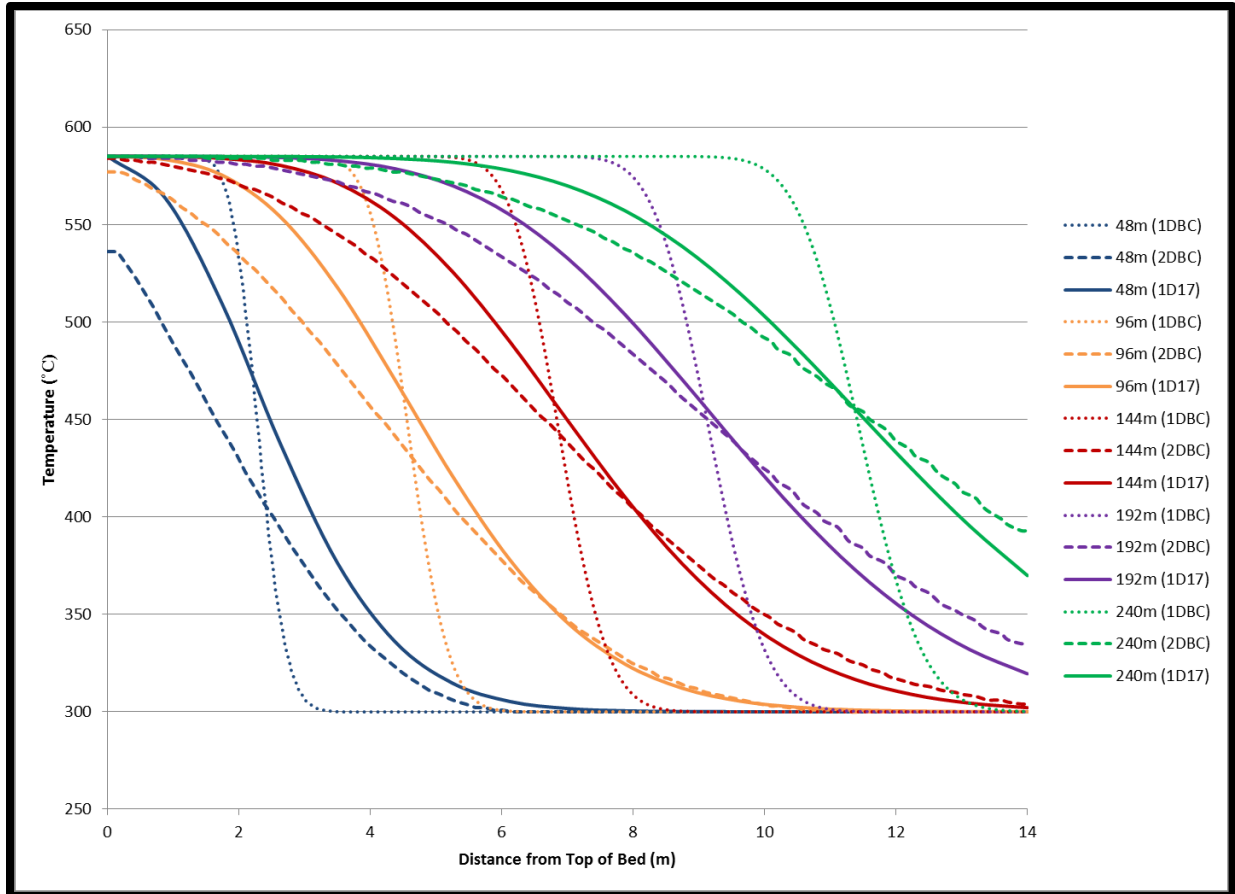
Figure 57: Comparison of PBTC Case I (Dotted Line), Brown's SCTC Model (Dashed Line), and PBTC Model Using 17 Nodes (Solid Line)

Qualitatively comparing the three charge cycle temperature profiles, it can be concluded that the results of the PBTC model using 17 nodes are much more similar to those predicted by Brown's SCTC model then are those predicted by the fully converged PBTC model. The similarity of the temperature profiles predicted by Brown's SCTC model and the PBTC model using 17 nodes indicates that the PBTC model will behave like a SCTC model when a decreased number of nodes is used. However, a qualitative comparison of temperature profiles will not suffice for this procedure to be accepted.

In Chapter 3, two efficiencies are provided for each model case considered: an efficiency corresponding to fixed four-hour charge and discharge cycles and an efficiency considering a minimum fluid discharge temperature of 500˚C. Because the latter of the two efficiencies is the

124

metric used in CSP plant operation, it is considered the metric for performance in this work. In the next section, a procedure is discussed by which TES system efficiency is used to determine the number of nodes needed to be used in the PBTC model to simulate a SCTC.

5.1.3 Equivalence between PBTC Case I and SCTC Case I

In Chapter 3, the optimized packed bed case is found by PBTC Case I to have an efficiency of 92.37% accounting for a discharge shut-off temperature of 500°C. For the same shut-off temperature, the optimized SCTC model predicts an efficiency of 83.97%. This means the efficiency of the PBTC model must be reduced by nearly 10% to allow an equivalent simulation of the SCTC model.

In Section 5.1.2, the idea of using a decreased number of nodes in the PBTC model to simulate a SCTC is introduced. In the study, the number of nodes used in this PBTC model is determined qualitatively by looking at temperature profiles and selecting the closest fit. An alternative approach to this method is to select the number of nodes based upon the efficiency of the SCTC model that is to be modeled. The efficiencies of the two models is presented in the preceding chapter; a study conducted to study the impact of decreasing the number of nodes on the efficiency of the PBTC model is summarized in Table 26.

Table 26: Decrease in Efficiency of PBTC Model with Decrease in Number of Nodes

Nodes Used	E Stored	Difference	E Retrieved	Difference	Efficiency
301	4,103,916	---	3,811,366	---	92.87%
201	4,103,525	0.01%	3,764,615	1.23%	92.37%
101	4,099,236	0.11%	3,658,358	4.01%	89.24%
51	4,079,851	0.59%	3,512,126	7.85%	86.08%
41	4,067,451	0.89%	3,454,604	9.36%	84.93%
35	4,055,856	1.17%	3,408,790	10.56%	84.05%
31	4,045,273	1.43%	3,371,203	11.55%	83.34%
21	3,999,682	2.54%	3,233,775	15.15%	80.85%

125

From Table 26, it can be seen that decreasing the number of nodes from 301 to 21 decreases the model's efficiency by 12%. The reason for this can be understood upon investigating the temperature profiles provided in Figure 55. As the sharpness of the temperature profile decreases, the significance is that more energy is stored at lower temperatures. Imposing the discharge temperature limit makes much of this energy stored at low temperatures unusable, thereby decreasing the system's efficiency. The case of 301 nodes is considered as the most accurate case, and the percent difference in terms of energy stored and retrieved is computed for each variation in the number of nodes used. The amount of energy stored and retrieved is expressed in terms of the difference in inlet and outlet temperatures during charge and discharge cycles respectively.

Based upon results from the efficiency study, using 35 nodes in the PBTC model provides an efficiency of 84.05%, only 0.08% different from the results predicted by the optimized SCTC case. A comparison of the four-hour charge cycle temperature profiles as determined by the PBTC Case I, SCTC Case I, and the PBTC with 35 nodes is provided in Figure 58.

Comparing the temperature profiles, it can be seen that the temperature profiles predicted by the PBTC model considering 35 nodes are very similar to those predicted by the SCTC model. It can be seen that the PBTC model considering 35 nodes predicts somewhat more energy storage than does the SCTC model. However, most of this energy is stored at temperatures below the discharge temperature limit, explaining why Case I of the SCTC and the PBTC model considering 35 nodes predict such similar efficiencies. The similarity of the temperature profiles and modeled system efficiencies provide sufficient confidence to conclude that the SCTC model can accurately be modeled using the PBTC model with 35 nodes.
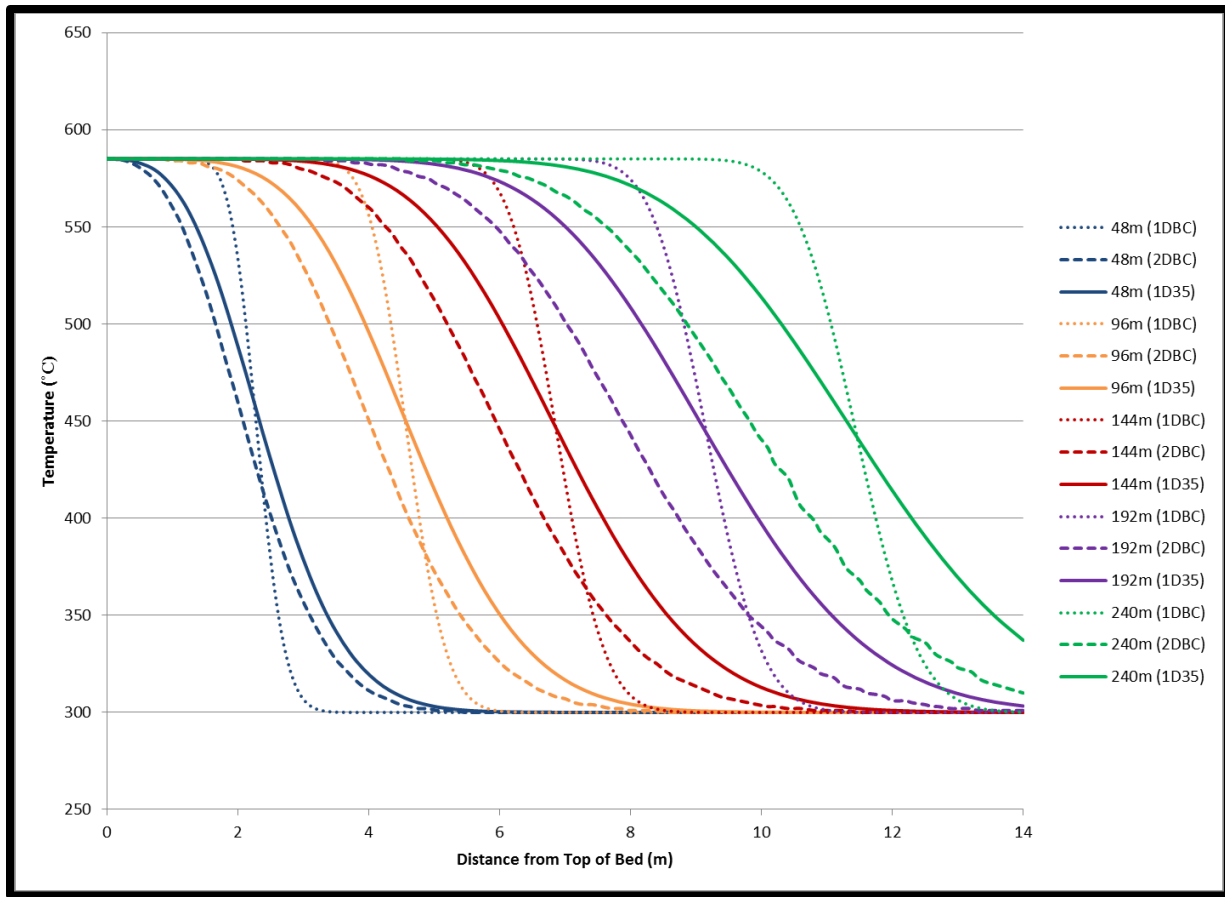
Figure 58: Comparison of SCTC Case I (Dotted Line), SCTC Case I (Dashed Line), and PBTC Model Using 35 Nodes

127

5.2 SAM Modeling Results

As stated in Chapter 3, an optimized central receiver CSP plant having a capacity of 100 MW_e was used as the base case for this study. In this study, four TES configurations are modeled and compared to demonstrate the advantages gained by adding TES, in terms of both performance and cost reduction of the electrical power produced by the plant. The first scenario considers the CSP plant with no TES system. The second and third cases consider a two-tank molten salt TES system and a quartzite packed-bed thermocline TES system respectively. The final scenario simulates TES in a structured concrete thermocline.

5.2.1 Scenario One: No TES

The first scenario considered is a 100 MW_e central receiver power plant incorporating no form of TES. Figure 59 depicts a breakdown of the cost nominal LCOE produced by the CSP plant with no TES. The contribution of each major cost contributor to the LCOE of power produced by the plant is indicated. Figure 60 provides the monthly electrical output from the plant.
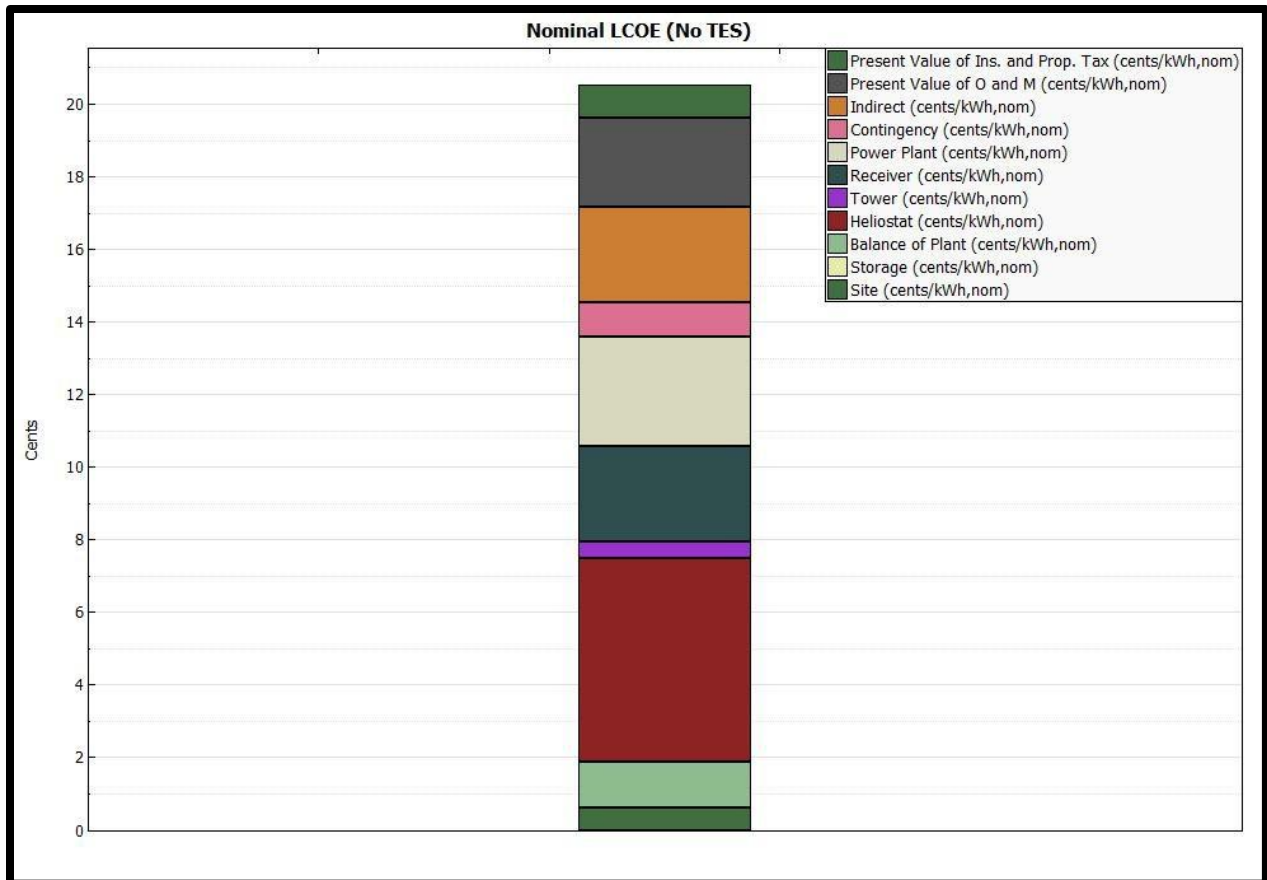
Figure 59: Nominal LCOE of CSP Plant with No TES
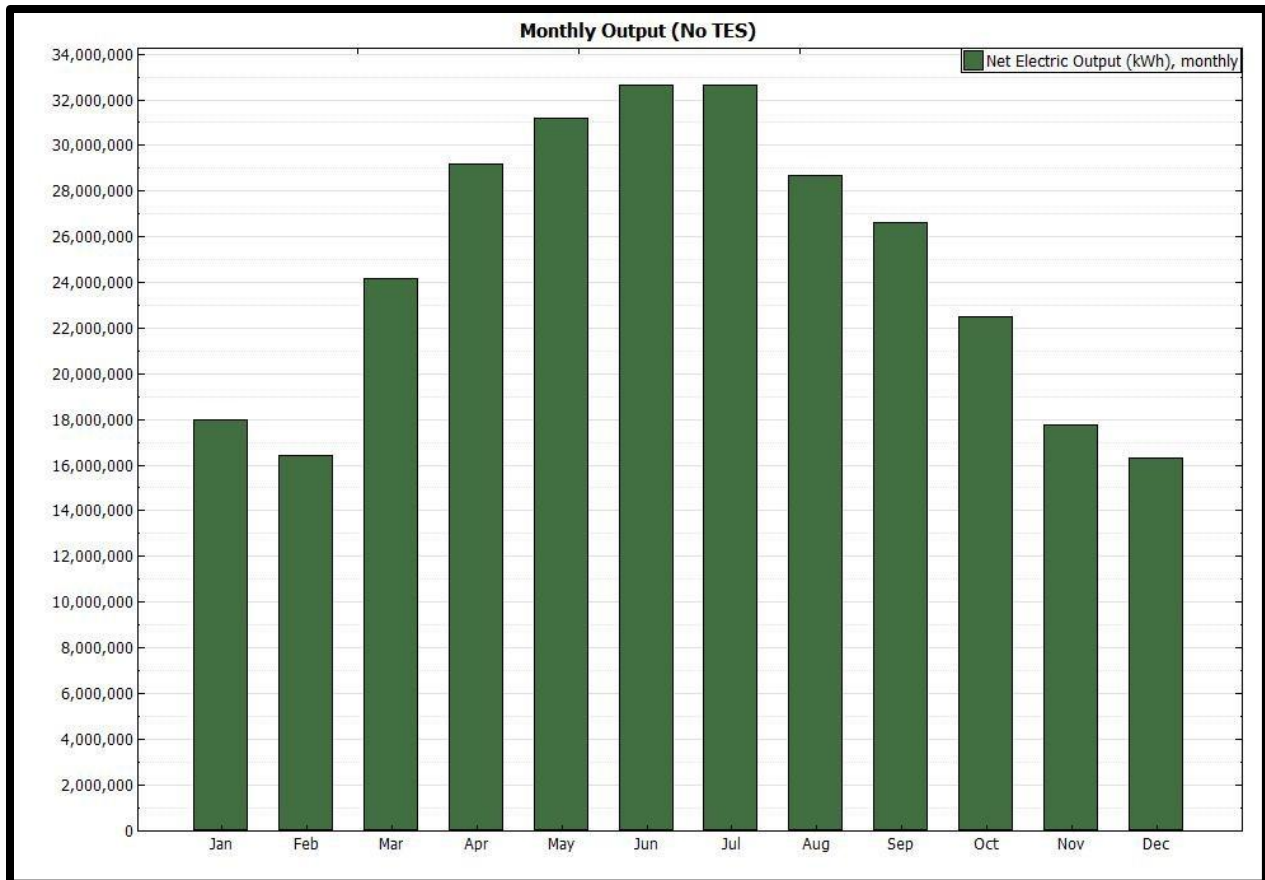
Figure 60: Monthly Electrical Output for CSP Plant with No TES

Table 27 provides a summary of the total yearly electrical power output from the plant,
the plant's capacity factor, and the nominal LCOE of the power produced by the plant.

Table 27: Performance Summary for CSP Plant with No TES

Performance Summary	
Net Annual Energy Production (kWh$_e$)	284,316,678
Capacity Factor (%)	32.40%
Nominal LCOE (¢/kWh$_e$)	20.53

5.2.2 Scenario Two: Two-Tank Molten Salt TES

The second scenario considered is a 100 MW$_e$ central receiver power plant incorporating
two-tank molten salt TES. Figure 61 depicts a breakdown of the cost nominal LCOE produced
by the CSP plant with no TES. The contribution of each major cost contributor to the LCOE of

130

power produced by the plant is indicated. Figure 62 provides the monthly electrical output from the plant.
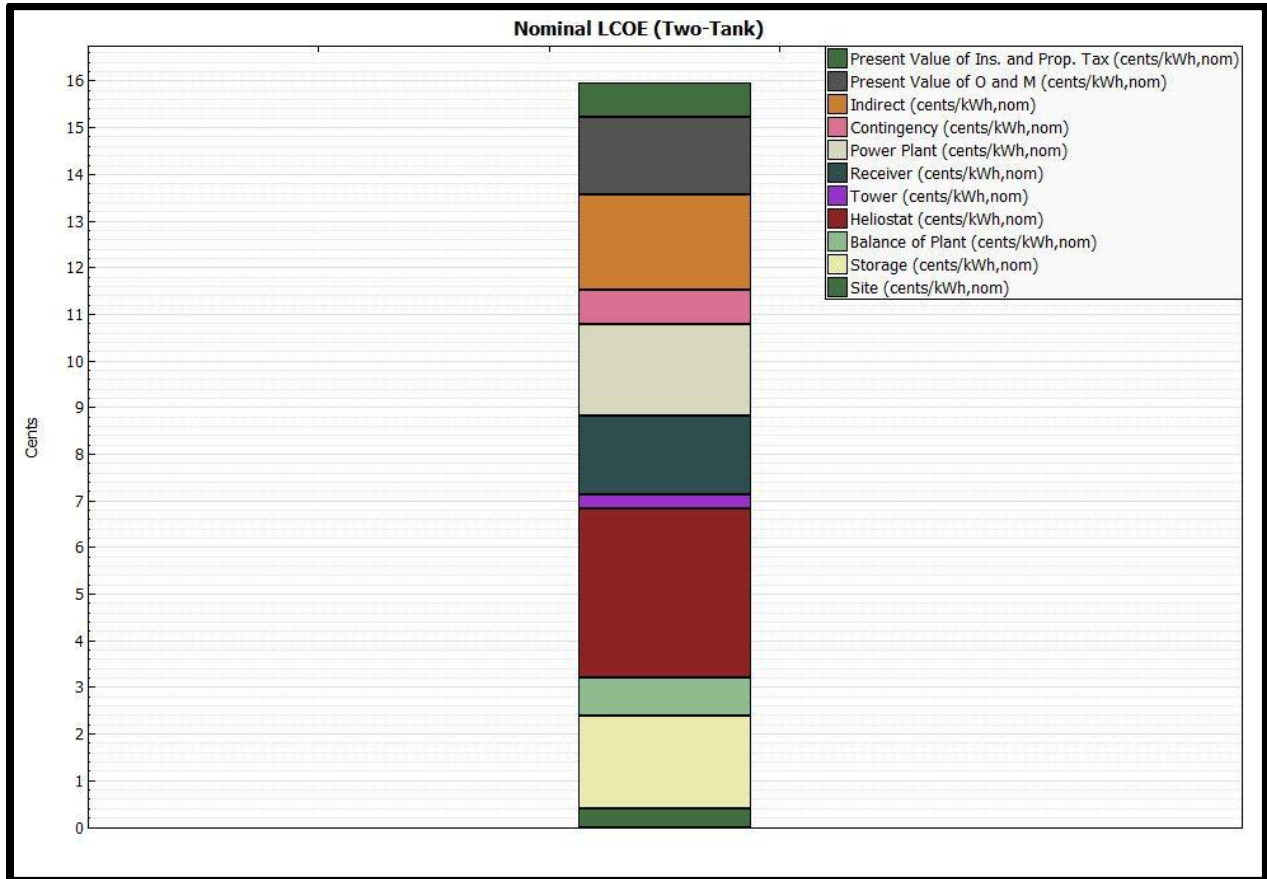
Figure 61: Nominal LCOE of CSP Plant with Two-Tank TES
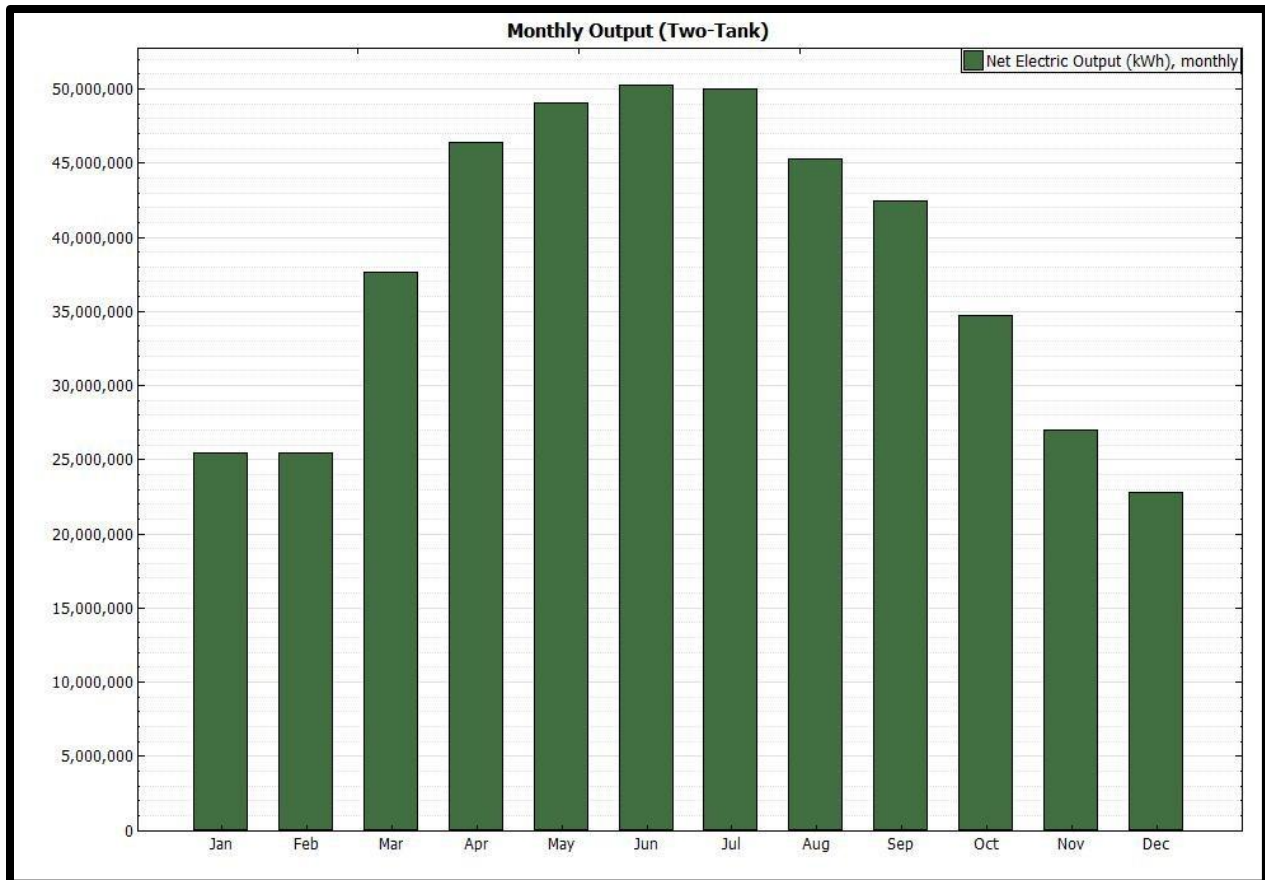
Figure 62: Monthly Electrical Output for CSP Plant with Two-Tank TES

Table 28 provides a summary of the total yearly electrical power output from the plant, the plant's capacity factor, and the nominal LCOE of the power produced by the plant.

Table 28: Performance Summary for CSP Plant with Two-Tank TES

Performance Summary	
Net Annual Energy Production (kWh$_e$)	438,335,374
Capacity Factor (%)	50.00%
Nominal LCOE (¢/kWh$_e$)	15.96

5.2.3 Scenario Three: Quartzite Packed-Bed Thermocline TES

The third scenario considered is a 100 MW$_e$ central receiver power plant incorporating a quartzite packed-bed thermocline TES system. Figure 63 depicts a breakdown of the cost nominal LCOE produced by the CSP plant with no TES. The contribution of each major cost

contributor to the LCOE of power produced by the plant is indicated. Figure 64 provides the monthly electrical output from the plant.
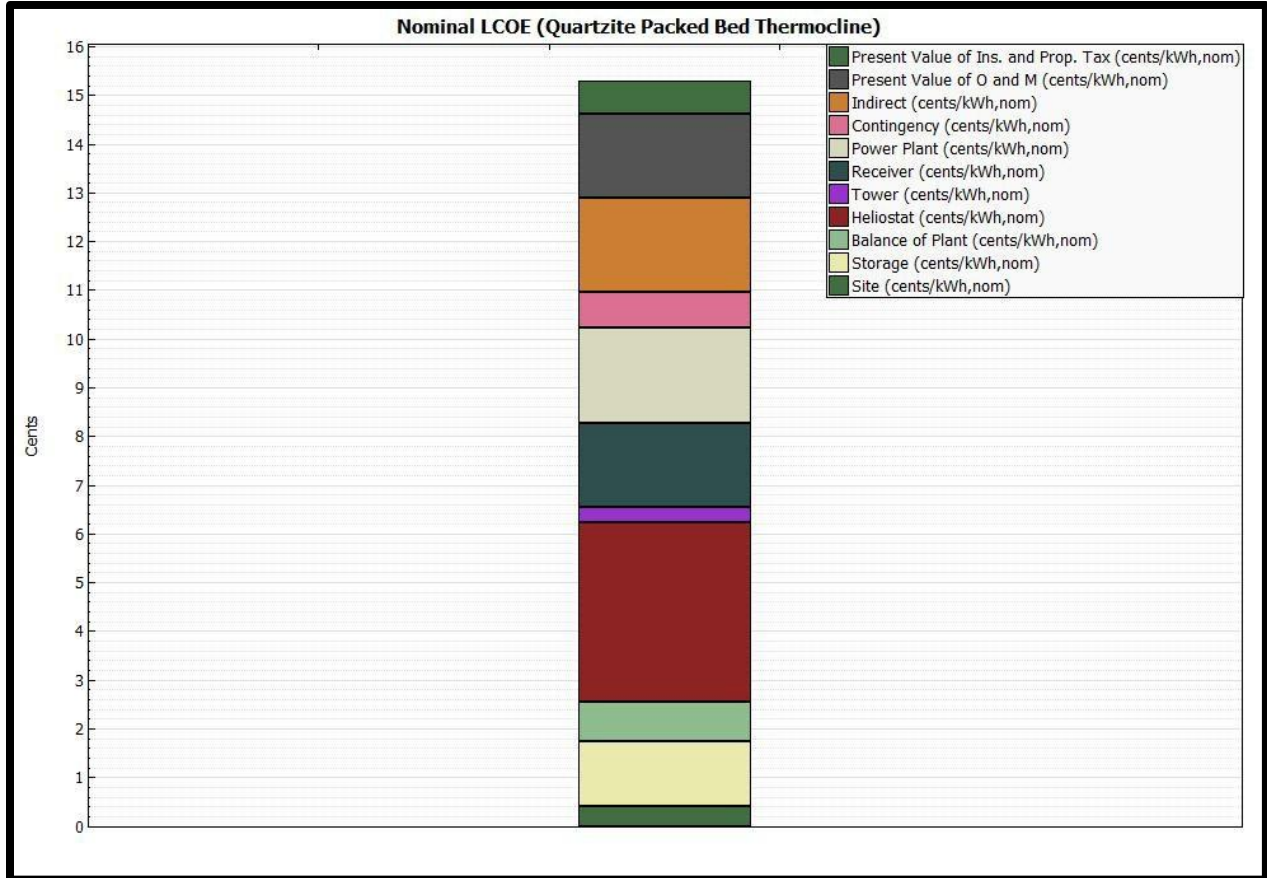
Figure 63: Nominal LCOE of CSP Plant with Packed-Bed Thermocline TES
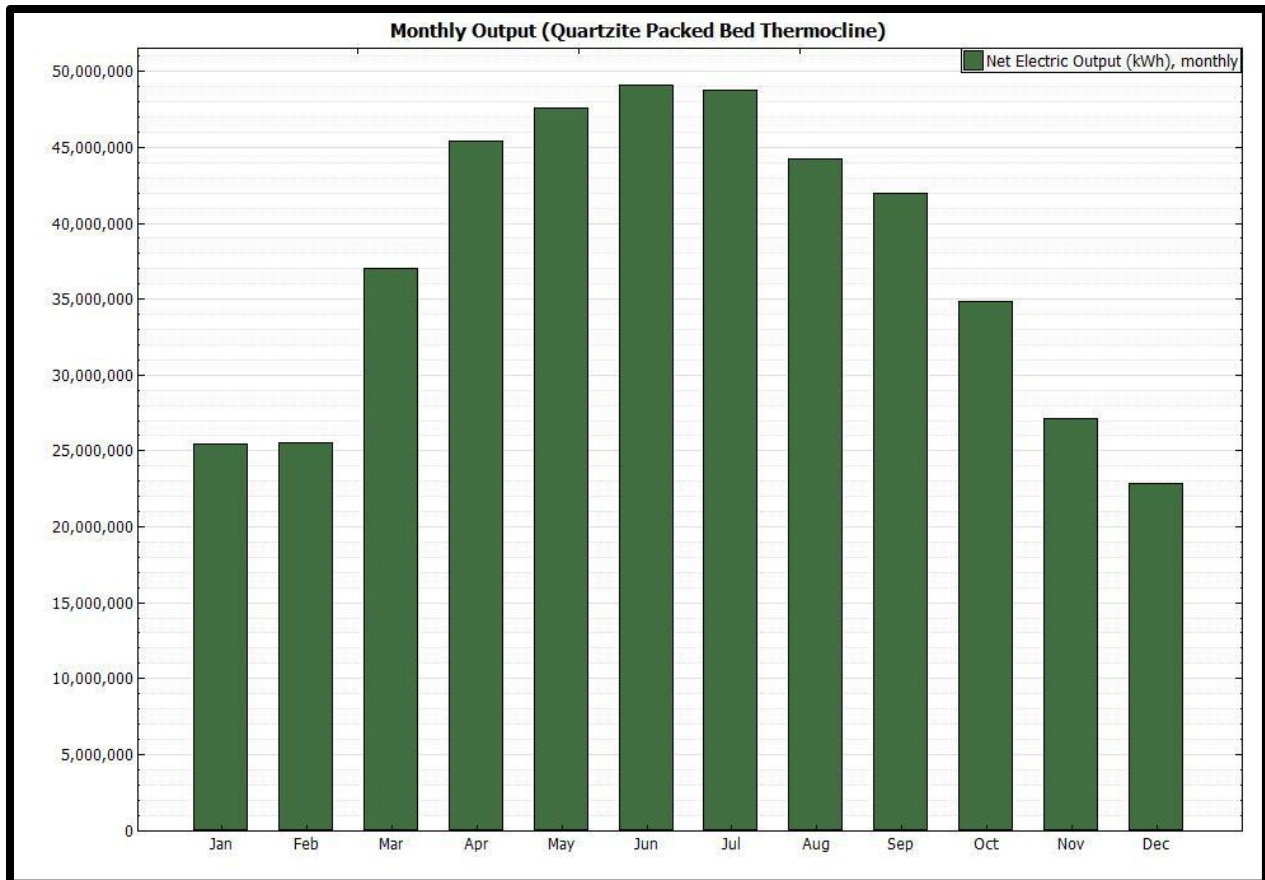
Figure 64: Monthly Electrical Output for CSP Plant with Packed-Bed Thermocline TES

Table 29 provides a summary of the total yearly electrical power output from the plant, the plant's capacity factor, and the nominal LCOE of the power produced by the plant.

Table 29: Performance Summary for CSP Plant with Packed-Bed Thermocline TES

Performance Summary	
Net Annual Energy Production (kWh$_e$)	435,577,612.00
Capacity Factor (%)	49.70%
Nominal LCOE (¢/kWh$_e$)	15.18

5.2.4 Scenario Four: Structured Concrete Thermocline

The final scenario considered is a 100 MW$_e$ central receiver power plant incorporating a quartzite packed-bed thermocline TES system. Figure 65 depicts a breakdown of the cost nominal LCOE produced by the CSP plant with no TES. The contribution of each major cost

134

contributor to the LCOE of power produced by the plant is indicated. Figure 66 provides the monthly electrical output from the plant.
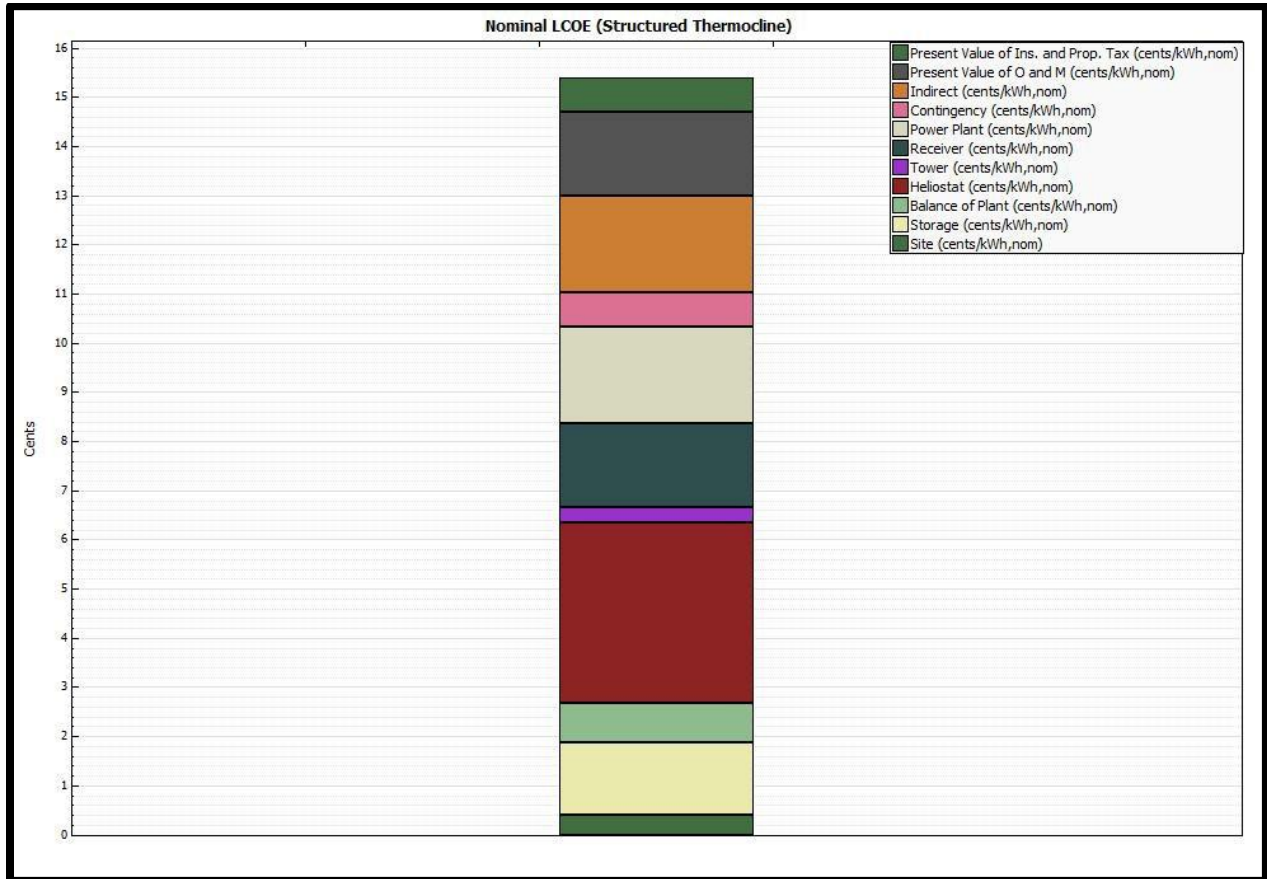
Figure 65: Nominal LCOE of CSP Plant with Structured Thermocline TES
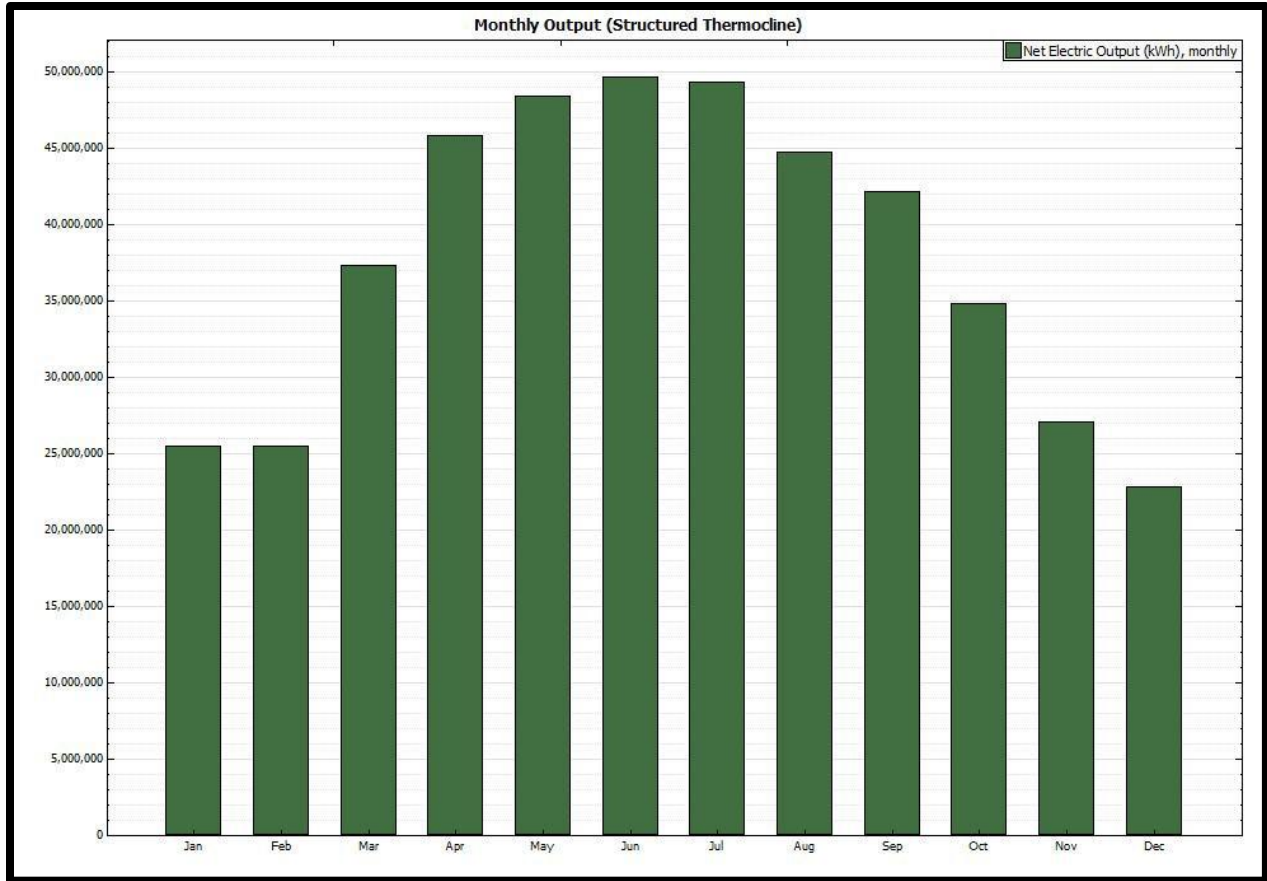
Figure 66: Monthly Electrical Output for CSP Plant with Structured Thermocline TES

Table 30 provides a summary of the total yearly electrical power output from the plant, the plant's capacity factor, and the nominal LCOE of the power produced by the plant.

Table 30: Performance Summary for CSP Plant with Structured Thermocline TES

Performance Summary	
Net Annual Energy Production (kWh$_e$)	428,362,389
Capacity Factor (%)	48.90%
Nominal LCOE (¢/kWh$_e$)	15.64

5.2.5 Summary and Comparison of TES Scenarios

Results obtained from simulating each of the aforementioned TES scenarios are provided in Table 31. Additionally, the installed cost of each plant and TES scenario are provided. The individual and direct cost breakdowns are determined by SAM.

136

Table 31: Cost and Performance of 100 $_{MWe}$ CSP Plant with Different TES Configurations

Components	TES Configuration			
	None	**Two-Tank**	**Packed Bed Thermocline**	**Structured Thermocline**
Direct Cost Contributors				
Site Improvements	$20,273,109.42	$20,273,109.42	$20,273,109.42	$20,273,109.42
Heliostat Field	$182,457,984.74	$182,457,984.74	$182,457,984.74	$182,457,984.74
Balance of Plant	$40,250,000.00	$40,250,000.00	$40,250,000.00	$40,250,000.00
Power Block	$97,750,000.00	$97,750,000.00	$97,750,000.00	$97,750,000.00
Storage	$0.00	$99,814,588.24	$65,092,705.88	$73,167,058.82
Tower	$14,736,146.03	$14,736,146.03	$14,736,146.03	$14,736,146.03
Receiver	$84,944,751.58	$84,944,751.58	$84,944,751.58	$84,944,751.58
Contingency	$30,828,839.42	$37,815,860.60	$35,385,328.84	$35,385,328.84
Direct Cost Subtotal	**$471,240,831.19**	**$578,042,440.61**	**$540,890,026.49**	**$548,964,379.43**
Indirect Cost Contributors				
EPC and Ower Costs	$51,836,491.43	$63,584,668.47	$59,497,902.91	$60,448,254.26
Total Land Costs	$15,080,213.28	$15,080,213.28	$15,080,213.28	$15,080,213.28
Sales Tax	$18,849,633.25	$23,121,697.62	$21,635,601.06	$21,958,575.18
Indirect Cost Subtotal	**$85,766,337.96**	**$101,786,579.37**	**$96,213,717.25**	**$97,509,650.90**
Summary Of 100 MW$_e$ Central Receiver CSP Plant Cost				
Total Installed Cost	**$557,007,169.15**	**$679,829,019.99**	**$637,103,743.73**	**$647,039,235.04**
Capacity Cost ($/kWh$_e$)	**$5,570.07**	**$6,798.29**	**$6,371.04**	**$6,467.16**

From Table 36, it can be seen that the CSP plant without TES is the cheapest to construct; however, its capacity factor is only 32.40%. Because of this low capacity factor, the electricity produced by this plant has the highest LCOE. When a two-tank TES system is added, the capacity factor increases by 17.60%; though adding the two-tank TES system increases the direct cost of installing the plant, it leads to a significant reduction in the LCOE of electricity produced by the plant. A PBTC TES system can be installed in place of the two-tank TES system, resulting in a cost reduction of about 35% in the TES system. The capacity factor of the plants incorporating the PBTC TES system is only a tenth of a percent less than that of the plant incorporating two-tank TES. Consequently, the LCOE of the plant incorporating a PBTC is nearly three quarters of a cent lower than the LCOE of the plant with two-tank TES. Finally,

137

replacing the PBTC TES system with a SCTC TES system leads to a 12.5% increase in TES system cost. The SCTC TES system is less efficient, resulting in a drop in capacity factor of about 1.5%. The result of the decrease in capacity factor and increase in TES system cost is that the LCOE of the plant incorporating the SCTC TES system is about one-half of a cent more than that of the plant incorporating PBTC TES.

5.3 Testing of Concrete Mix Designs

Testing of the concrete specimens in the presence of circulating molten salt has proven to be a challenging process, which has been plagued with numerous equipment failures. A brief summary of the most significant problems encountered during testing is presented. Preventative measures taken to prevent these problems from occurring in future tests are reported as well. Unfortunately, no complete tests, as specified in Chapter 4, were completed. Observations of the concrete mix designs' response to the limited testing that was able to be performed are reported.

5.3.1 Problems Encountered During Testing of Concrete Specimens

- **Problem 1:** *Seizing of Adapter Pipe* – During preliminary testing, the adapting pipe which is used to connect the salt storage tank and thermocline test chamber (Figure 48) was installed without applying any lubricant to the threads of the male connections. Following the second day of preliminary testing, the connection between the adaptor pipe and thermocline test chamber seized. A costly repair and loss of time resulted, as the connection had to be cut off and replaced.

- ✓ **Solution 1:** *Before all testing, anti-seize is applied to the threads of the male connectors. When the connection is heated during testing, the liquid portion of the interface dissolves, leaving an interface of silver between the stainless steel components being connected. This solved the issue of seizing.*

138

- **Problem 2:** *Leaking at Joints* – Prior to each test, the test system must be assembled; three connections must be made: the adaptor pipe must be connected to the salt storage tank, the adaptor pipe must be connected to the thermocline test chamber, and the two pieces of the adaptor pipe must be connected. Because of the floating joints used at each connection, it is necessary to check and re-tighten each of the connections after the preliminary assembly. During testing, it was observed that these connections, even though they had been tightened very well, were leaking. These leaks create a dangerous working environment as molten salt at temperatures exceeding 550˚C was being expelled from the test system.

- ✓ **Solution 2:** *Because the salt being pumped through the test system is at a very high temperature, significant thermal expansion occurs at the joints. This problem was addressed by heating the connections with a hand torch prior to performing the second round of tightening of the joints. This addressed the issue of leaking at the joints.*

- **Problem 3:** *Salt Freezing in Lines* – During testing, it is crucial to monitor the temperature of the molten salt being used, as the salt freezes at the high temperature of 222˚C. For the test system used in this work, critical points tended to be the connection joints. This is due to the fact that they were not insulated very well during the initial months of testing. Freezing of salt in the lines can lead to significant problems; after salt solidifies and blocks a small section of the pipe, it can trap a significant volume of salt which will also solidify. Figure 67 depicts some of the instances when salt freezing in the lines was encountered during testing.

Figure 67: Salt Frozen in Lines during Testing

✓ **Solution 3:** *After identifying this issue of salt freezing in the lines, much more care was taken when insulating the connection joints. This addressed the issue of salt freezing in the lines.*

• **Problem 4:** *Salt Freezing in Thermocline Test Chamber* – A potentially fatal problem for a molten salt TES system is the solidification of molten salt within the storage tank. In molten salt TES systems used today, heaters are placed in the tanks to ensure that the temperature doesn't fall below 300˚C; however, no such precautionary measures are taken for the system used in this work. During thermal cycling tests of the second group of beams, the pump's motor lost much of its head, only maintaining enough head to pump the thermocline test chamber about three-quarters full of molten salt and to hold the salt in place. As heat passed from the salt to the concrete in the test chamber, the

www.manaraa.com

temperature of the salt dropped below its melting point. The end result was a completely solidified concrete and salt mass in the thermocline test chamber.

✓ **Solution 4:** *Solar salt is an expensive material; therefore, it was desired to retrieve as much as possible for reuse. A propane burner, capable of supplying about 70,000 Btu, was placed under the thermocline test chamber for about 30 hours, resulting in the removal of about 50% of the frozen salt. After this, the tank was stripped of insulation, inverted, and suspended. A rose-bud-tipped acetylene torch, capable of supplying about 1,000,000 Btu, was then used to beat the sides of the test chamber for about 4 hours until the concrete/salt mass fell free from the test chamber (This process and the freed mass are depicted in Figure 68). This procedure was very time and labor intensive; fortunately, the small size of the thermocline test chamber made this simple of a procedure a possible solution. The motor on the pump was replaced, and for future tests, the pump was shut off when the temperature of the salt in the reservoir fell below 450 ℃.*

Figure 68: Heating Frozen Thermocline Test Chamber (Left) and Cleared Thermocline Chamber with Concrete/Salt Blockage on the Ground (Right)

- ✓ **Problem 5:** *Failure of Motor on Pumping Unit* – The plaguing issue throughout the testing procedure was failure of the motor driving the pumping unit. The motor is positioned about two feet above the salt storage tank. Therefore, it is working in a very high temperature environment. The motor used in this test system is designed for operation at 1750 RPM; following short-term operation, this rate was observed to fall to an approximated 400 RPM. This means that the motor could not drive the pump at anywhere the necessary capacity to establish salt circulation through the system.

- ✓ **Solution 5:** *The issue of motor failure due to overheating was not successfully addressed. The first approach taken to reduce the heating of the pump was to position a fan to maintain air circulation over the pump; this did not lead to significant reduction in the surface temperature of the pump. The alternative approach taken was to significantly increase the amount of insulation on top of the salt storage tank. All exposed metal surfaces were covered with two layers of ceramic insulation. However, this did not significantly reduce the amount of heat transmitted to the motor. The motor sits atop a stainless steel shaft, through which the pump's output passes. This is the source of most of the heat transported to the motor, and no measures were developed to allow the reduction of the heat input to the motor from this source. Through the course of attempted tests, three motors were used. Figure 69 depicts the first motor used in testing being cooled by a fan during testing; it also depicts the removal of the pumping unit to allow the replacement of the motor after it failed.*

Figure 69: Motor Driving Pumping Unit During Testing (Left) and Pumping Unit Being Removed to Allow Replacement of First Motor (Right)

5.3.2 Testing of Mix 26 (TC1000)

The first concrete prisms tested in the thermocline test system are cast using the proprietary TC1000 mix. Due to problems with the pump's motor, molten salt was only circulated through the beams for approximately one hour. One observation made during this testing was that the specimens need to be predicted from thermal shock. The first round of testing was conducted with the top left off the thermocline tank; when salt was first circulated through the specimens then allowed to drain off, significant spalling and cracking of the specimens occurred. Damage from spalling is depicted in Figure 70. It should be noted that the second and third beams from the left cracked when dropped after testing. The beam farthest to the left, however, cracked during testing.

Figure 70: Spalling Damage to TC1000 Concrete Specimens

5.3.3 Testing of Mix 11 (40FA-60CA)

The second mix to be tested employs a mixture of 40% fly ash and 60% calcium aluminate as cementitious material. After a short period of salt circulation, problems with the pump's motor resulted in salt becoming trapped in the thermocline tank and freezing. The salt and specimens were frozen in the thermocline tank for almost a month before being removed. The removal process involved heating the walls of the thermocline tank with an acetylene torch; therefore, some of the concrete was likely exposed to temperatures well above 600°C. After removing the concrete and salt from the tank, it was noticed that the concrete was degrading over time. This is unexpected, as the concrete cube specimens cast from mix 11, thermally cycled, and crushed in the work of John (2012) have exhibited no deterioration even though they are stored in the same environment as the beams have been after their removal from the thermocline test chamber. Figure 71 depicts the observed deterioration of the beams, and Figure 72 depicts the crushed cube specimen exhibiting no deterioration.

144

Figure 71: Progressive Deterioration of Mix 11 Specimens: 1 Month After Testing (Left) and 3 Months After Testing (Right)

Figure 72: Crushed Mix 11 Specimen Exhibiting no Deterioration more than 1 Year After Thermal Cycling

CHAPTER 6: CONCLUSIONS

6.1 Conclusions

✓ *Central receivers (solar towers) currently offer the most viable means of collecting irradiance for conversion in a CSP plant.*

  o Central receivers collect energy at very high temperatures (theoretically up to 1300˚C but in proven application up to 565˚C); higher operating temperatures lead to higher CSP plant efficiencies. The low solar-to-electrical efficiency attained by parabolic trough CSP plants, reportedly around 15%, is attributed to their low operating temperature range of 290˚C-390˚C. Solar-to-electric conversion efficiencies for central receiver CSP plants have not been released at this time.

✓ *Finite-difference-based numeric modeling was used to improve the efficiency of a structured concrete thermocline by 18.38% (from 65.57% to 83.97%).*

  o It was found that if the void fraction of the structured concrete bed is maintained at 0.33 while the thickness of the individual plates is decreased, the efficiency of the TES system improves significantly. This increase in efficiency is attributed to the increase in exposed material surface area and the reduction in thermal gradients within the concrete plates.

✓ *A structured concrete thermocline TES system is competitive, in terms of cost and performance, compared with two-tank and packed-bed thermocline TES systems.*

  o Unit capacity storage costs for two-tank fluid, packed-bed thermocline, and structured concrete thermocline are, respectively, $46.11, $30.04, and $33.80 per kWh_t storage.

  o System Advisory Model was used to simulate the performance of a 100 MWh_e central receiver plant with each form of TES.

- A 1D packed-bed thermocline model, similar to that used by SAM, was developed; it accurately describes a packed-bed thermocline when 301 nodes are used. When 35 nodes are used, the packed-bed thermocline model describes the structured concrete thermocline optimized in this work. This allows the simulation of a SCTC using SAM.

o The LCOE produced by the central receiver plant considering no TES, two-tank TES, packed-bed TES, and structured concrete TES is as follows: 20.53¢/kWh, 15.93¢/kWh, 15.18¢/kWh, and 15.64¢/kWh.

✓ *Assuming constant, non-temperature-dependent fluid properties does not have significant impact on the accuracy of a thermocline model in the temperature ranges of 290˚C-390˚C or 290˚C-565˚C.*

o Graphical representations provided in this work demonstrate that using constant versus temperature-dependent fluid properties have little impact on the model accuracy in the 290˚C-390˚C. More error is present when the temperature range considered is increased to 290˚C-565˚C; however, it is still not very significant.

✓ *Concrete has been tested as a structured filler material at temperatures exceeding 565˚C and seems to be chemically and physically compatible with a molten salt environment.*

o No complete thermal cycling tests, as defined in Chapter 4, were completed. However, from the limited testing that was completed, conclusions are drawn regarding each of the mix designs.

- Beams cast from mixture #26, TC1000, exhibit no significant deterioration 1 year after exposure to the molten salt environment, indicating that mixture #26 is chemically compatible with molten salt. Significant spalling of the beams'

147

surface is believed to be due to extreme thermal shock that occurred when the beams were subjected to thermal cycling with the top removed from the system. Further testing is needed to determine if similar spalling will occur under normal cycling conditions. At this time, TC 1000 is considered a promising candidate based upon the limited testing that has been completed. Unfortunately, it costs nearly three times more than do the three other mix designs suggested by John (2012).

▪ Beams cast from mixture #11, FA60-CA40, exhibit significant deterioration four months after testing in the molten salt environment. However, these beams were in the thermocline test chamber when salt solidified in it, and were subjected to extreme heat from an acetylene torch during the clearing of the solidified mass from the tank. Cube specimens subjected to the molten salt environment, then crushed, do not show any sign of deterioration more than one year after the testing. No observable spalling or cracking of the beams has been observed. Due to the extreme, unstable conditions of this testing, no conclusions may be drawn without further testing of beams cast from mixture #11.

6.2 Suggestions for Future Work

• Elevating the temperatures at which CSP plants operate can lead to increased power cycle efficiency and increased energy storage density in TES systems. It has been suggested that concentrating irradiance using central receivers can lead to temperatures in excess of 800°C. However, at this time, the operating temperatures of CSP plants are limited by the properties of solid and liquid media.

148

- Solar salt is a relatively inexpensive liquid media that has a relatively high specific heat capacity and operating temperature limit. However, solar salt freezes at the relatively high temperature of 222˚C and is chemically unstable at temperatures exceeding 585˚C unless shielded by an inert gas. New liquid media are needed, having lower freezing points and higher maximum operating temperatures.

- Typical structural concrete explodes violently at temperatures exceeding 300˚C. Concrete mix designs have been tested in ovens and deemed usable as structured filler material in a thermocline TES system at temperatures up to 600˚C. Incorporating structured filler material avoids the issue of thermal ratcheting experienced in packed-bed thermocline TES systems. New concrete mix designs are needed for operation at higher temperatures in the 800˚C range, the suggested capability of central receiver CSP plants.

- Though concrete specimens from two of the four proposed mix designs have been tested in an oven, and at some level in the presence of circulating salt, they have yet to be subjected to a testing regimen like they would be exposed to in a thermocline TES system. Further testing is needed so that the effects of circulating molten salt on the integrity of the concrete can be investigated. Additionally, the long-term stability of concrete under the conditions of circulating salt needs to be evaluated.

- A small scale thermocline TES system incorporating structured concrete filler material needs to be constructed and tested. This will allow conclusions to be drawn regarding the validity of the modeling results presented in this thesis.

149

WORKS CITED

Abengoa. (2012). *PS20, the Largest Solar Power Tower Worldwide*. Retrieved 2012, from www.abengoasolar.com:
www.abengoasolar.com/corp/web/en/nuestras_plantas/plants_en_operacion/espana/PS20_la_mayor_torre_comercial_del_mundo

Abengoa. (2012). *Solana, the Largest Solar Power Plant in the World*. Retrieved 2012, from www.abengoasolar.com:
www.abengoasolar.com/corp/web/en/nuestras_plantas/pantas_en_construccion/estados_unidos

Adeyanj, A. (2009). Performance characterization of Packed Bed Storage System. *Engineering and Applied Sciences*, 96-99.

Adinberg, R., Zvegilsky, D., & Epstein, M. (2010). Heat Transfer Efficient thermal Energy Storage for Steam Generation. *Energy Conversion and Management*, 9-15.

Aggenim, F., Hewitt, N., Eames, P., & Smyth, M. (2010). A Review of Material, Heat Transfer and Phase Change Problem Formulation for Latent Heat Thermal Energy Storage Systems (LHTESS). *Renewable and Sustainable Energy Reviews*, 615-628.

Agyenim, F., Hewitt, N., Eames, P., & Smyth, M. (2010). A Review of Materials, Heat Transfer and Phase Change Problem Formulation for Latent Heat Thermal Energy Storage Systems (LHTESS). *Renewable and Sustainable Energy Reviews*, 615-28.

Brosseau, D., Kelton, J., Ray, D., Edgar, M., Chisman, K., & Emms, B. (2005). Testing of Thermocline Filler Materials and Molten-Salt Heat Transfer Fluids for Thermal Energy Storage Systems in Parabolic Trough Power Plants. *Solar Energy Engineering*, 109-116.

Brown, B. (2012). *Development of a Structured Concrete Thermocline Thermal Energy Storage System (Master's Thesis)*. Fayetteville: University of Arkansas Civil Engineering Department.

Brown, B., Strasser, M., & Selvam, R. (2012). Development of a Structured Concrete Thermocline Thermal Energy Storage System. *World Renewable Energy Forum*, (p. 0074). Denver.

Çengel, Y. (2007). *Heat and Mass Transfer: A Practical Approach (3rd ed.)*. New York: McGraw-Hill.

CleanEnergy. (2012). *Concentrating Solar Power Case Studies: Linear Fresnel Reflector Solar CSP: Puerto Errado 2 Thermosolar Power Plant*. Retrieved 2012, from www.cleanenergyactionproject.com:
www.cleanenergyactionproject.com/CleanEnergyActionProject/Solar_CSP_Concentratin

_Solar_Power_Case_Studies_files/Puerto%20Errado%202%20Thermosolar%20Power%20Plant

Craig, L. (2011, October 18). *Andasol Now Europe's Biggest Solar Plant*. Retrieved September 26, 2012, from Earth Techling: http://www.earthtechling.com/2011/10/andasol-1-3-now-europes-biggest-solar-plant/

DOE. (2008). *United States Department of Energy, Solar Energy Technologies Program 2008-2012*. Retrieved 2012, from www1.eere.energy.gov: www1.eere.energy.gov/solar/pdfs/solar_program_mypp_2008-2012

EIA. (2009). *Average Energy Efficiency of Photovoltaic Cells and Modules Shipped Between 2007 and 2009*. Retrieved 2012, from www.eia.gov: www.eia.gov/cneaf/solar.renewables/page/solarphotv/table3_8

EIA. (2009). *Energy Perspectives*. Retrieved 2012, from www.eia.gov: www.eia.gov/totalenergy/data/annual/pdf/perspectives

EIA. (2012). *Annual Energy Outlook*. Washington DC: Department of Energy.

EPRI. (2010). *Solar Thermocline Storage Systems: Preliminary Design Study*. Palo Alto.

Flueckiger, S., Yang, Z., & Garimella, S. (2011). An Integrated Thermal and Mechanical Investigation of Molten-Salt Thermocline Energy Storage. *Applied energy*, 1-8.

Fraser, J. (2005, August 16). *About Dish/Engine Concentrating Solar Power*. Retrieved September 26, 2012, from The Energy Blog: http://thefraserdomain.typepad.com/energy/2005/08/about_dishengin.html

Gil, A., Medrano, M., Martorell, I., Lazaro, A., Dolado, P., Zalba, B., et al. (2010). State of the Art on High Temperature Thermal Energy Storage for Power Generation Part 1-Concepts, Materials, and Modellization. *Renewable and Sustainable Energy Reviews*, 31-55.

Goswami, Y., Kreith, F., & Kreider, J. (2000). *Principles of Solar Energineering 2nd Edition.* New York: Taylor & Francis Group.

Hale, M. (2012). *Statistical Analysis of Effects of Cementitious Material Combination and Water content on Concrete Resistance to Strength Deterioration under Thermal Cycling*. University of Arkansas Civil Engineering Department: Private Communication.

Hammerschlag, R., Pratt, R., Schaber, C., & Widergren, S. (2006). Chapter 18: Energy Storage, Transmission, and Distribution. In *Handbook of Energy Efficiency and Renewable Energy* (pp. 18.1-18.33). Taylor & Francis Group.

Harrington, K. (2012, March 2). *Spain's Gemasolar: The World's First Baseload Solar Power Plant*. Retrieved September 26, 2012, from Chenected.AICHE: http://chenected.aiche.org/energy/spains-gemasolar-the-worlds-first-baseload-solar-power-plant/attachment/2012-03-02_1251-gemasolar5/

Herrmann, U., & Kearney, D. (2002). Survey of Thermal Energy Storage for Parabolic Trough Power Plants. *Solar Energy Engineering*, 145-152.

IEA. (2010). *Technology Roadmap: Concentrating Solar Power.* Paris Cedex, France.

John, E. (2012). *The Development of a High Performance Concrete to Store Thermal Energy for Concentrating Solar Power Plants (Doctoral Dissertation).* Fayetteville, AR: University of Arkansas Civil Engineering Department.

John, E., Hale, M., & Selvam, R. (2011). Development of a High-Performance Concrete to Store Thermal Energy for Concentrating Solar Power Plants. *5th International Conference on Energy Sustainability*, (p. 54177). Washington DC.

Kearney, D., Kelly, B., Cable, R., Potrovitza, N., Herrmann, U., Nava, P., et al. (2002). Assessment of a Molten Salt Heat Transfer Fluid in a Parabolic Trough Solar Field. *Solar Energy Engineering*, (Submitted for Review).

Laing, D., Lehmann, D., FiB, M., & Bahl, C. (2009). Test Results of Concrete Thermal Energy Storage for Parabolic Trough Power Plants. *Solar Energy Engineering*, 1-6.

Laing, D., Steinmann, W.-D., Tamme, R., & Richter, C. (2006). solid Media Thermal Storage for Parabolic Trough Power Plants. *Solar Energy*, 1283-9.

Mawire, A., McPherson, M., van den Heetkamp, R., & Mlatho, S. (2009). Simulated Performance of Storage Materials for Pebble Bed Thermal Energy Storage (TES) Systems. *Applied Energy*, 1246-52.

McMahan, A. (2006). *Design & Optimization of Organic Rankine Cycle Solar-Thermal Powerplants (Master's Thesis).* University of Wisconsin-Madison Department of Mechanical Engineering.

Medrano, M., Gil, A., Martorell, I., Potau, X., & Cabeza, L. (2010). State of the Art on High Temperature Thermal Energy Storage for Power Generation Part 2-Case Studies. *Renewable and Sustainable Energy Reviews*, 56-72.

Molina, P. M. (2009, November 26). *Abener Receices ASICA Award for the PS20 Construction*. Retrieved September 26, 2012, from Abengoa: http://www.abengoa.es/corp/web/en/noticias_y_publicaciones/noticias/historico/2009/11_noviembre/abe_20091126_1.html

Morris, B. (2011, December 27). *Sonoran Solar Energy Project Approved*. Retrieved September 26, 2012, from IVN: http://ivn.us/2011/12/27/sonoran-solar-energy-project-approved/

NASS. (2012, March 8). *Concentrated Solar Power*. Retrieved September 26, 2012, from North American Solar Stores: http://www.northamericansolarstores.com/SolarNews/solar-power/concentrated-solar-power/

Nilson, H., Darwin, D., & Dolan, C. (2010). *Design of Concrete Structures (14th ed.).* New York: McGraw-Hill.

NovatecSolar. (2012). *Introduction of the World's Largest CSP Power Station Based on Fresnel Technology*. Retrieved 2012, from www.estelasolar.eu: www.estelasolar.eu/fileadmin/ESTELAdocs/documents/powerplants/Puerto_Errado/120615_Presentation-Puerto_Errado_2

NREL. (2010). *Concentating Solar Power Projects*. Retrieved 2012, from www.nrel.gov: www.nrel.gov/csp/solarpaces/project_detail.cfm/projectID=53

NREL. (2010, January 28). *Parabolic Trough Power Plant System Techology*. Retrieved September 26, 2012, from NREL: http://www.nrel.gov/csp/troughnet/power_plant_systems.html

NREL. (2011). *Concentrating Solar Power Projects (159)*. Retrieved 2012, from www.nrel.gov: www.nrel.gov/csp/solarpaces/project_detail.cfm/projectID=159

NREL. (2011). *Concentrating Solar Power Projects: Andasol-1*. Retrieved 2012, from www.nrel.gor: www.nrel.gov/csp/solarpaces/project_detail.cfm/projectID=3

NREL. (2011). *Concentrating Solar Power Projects: Gemasolar Thermosolar Plant*. Retrieved 2012, from www.nrel.gov: www.nrel.gov/csp/solarpaces/project_detail.cfm/projectID=40

NREL. (2011). *U.S. Parabolic Trough Power Plant Data*. Retrieved 2012, from www.nrel.gov: www.nrel.gov/csp/troughnet/power_plant_data

NREL. (2012). *Concentrating Solar Power Milestone Report: Incorporating Existing 1-D TRNSYS Thermocline Model into SAM.*

Owens, B. (2002). *An Economic Valuation of a Geothermal Production Tax Credit.* Golden: NREL.

Pacheco, J., Showalter, S., & Kolb, W. (2002). Development of a Molten-Salt Thermocline Thermal Storage System for Parabolic Trough Plants. *Solar Energy Engineering*, 153-159.

PE2, T. (2010). *Puerto Errado 2*. Retrieved September 26, 2012, from Tubosol PE2: http://www.puertoerrado2.com/home/

153

Phan, T., & Carino, N. (2000). Fire Performance of High Strength Concrete: Research Needs. *ASCE/SEI Structures Concress*. Philidelphia,PA.

Price, H. (2003). A parabolic Trough Plant Simulation Model. *ISES*. Hawaii Island,Hawaii.

Romero, M., Buck, R., & Pacheco, J. (2002). An Update on Solar Central Receiver Systems, Projects, and Technologies. *Solar Energy Engineering*, 98-108.

Schmidt, F., & Willmott, A. (1981). *Thermal Energy Storage and Regeneration*. Washington: McGraw-Hill.

Schoenung, S. (2011). *Energy Storage Systems Cost Update*. Albuquerque: Sandia National Labs.

Schumann, T. (1929). Heat Transfer: A Liquid Flowing Through a Porous Prism. *Franklin Institute*, 405-16.

Selvam, R. (2011). *Thermal Finite Difference Model*. Private Communication.

Selvam, R., & Castro, M. (2010). 3D FEM Model to Improve the Heat Transfer in Concrete for Thermal Energy Storage in Solar Power Generation. *Energy and Sustainability Conference*, (pp. 699-707). Phoenix,AZ.

Sharma, A., Tyagi, V., Chen, C., & Buddhi, D. (2009). Review on Thermal Energy Storage with Phase Change Materials and Applications. *Renewable & Sustainable Energy Reviews*, 318-45.

Siemens. (2009, October 15). *Siemens to Decisively Strengthen its Position in the Growth Market Concentrating Solar Thermal Power; Acquisition of Solel Solar Systems for $412 Million*. Retrieved September 26, 2012, from Solar Server: http://www.solarserver.com/solar-magazine/solar-news/current/siemens-to-decisively-strengthen-its-position-in-the-growth-market-solar-thermal-power-acquisition-of-solel-solar-systems-for-about-418-million.html

Singh, R., Saini, R., & Saini, J. (2009). Models for Predicting Thermal Performance of Packed Bed Energy Storage Systems for Solar Air Heaters-A Review. *Open Fuels & Energy Science*, 47-53.

Skinner, J. (2011). *Testing of Ultra-High Performance concrete as a Thermal Energy Storage Medium at High Temperatures (Master's Thesis)*. Fayetteville,AR: University of Arkansas Civil Engineering Department.

Skinner, J., Brown, B., & Selvam, R. (2011). Testing of High Performance Concrete as a Thermal Energy Storage Medium at High Temperatures. *9th Fuel Cell Science, Engineering, and Technology Conference*, (p. 54463). Washington DC.

SNL. (2011). *Energy, Climate, and Infrastructure Security Executive Summary*. Retrieved 2012, from www.sandia.gov: energy.sandia.gov/wp/wp-colntent/gallery/uploads/ECIS_SMU_Exective_Summary

Tahat, M., Babus'Haq, R., & O'Callaghan, P. (1993). Thermal Energy Storage. *Building Service Engineering Research Technology*, 1-11.

Tamme, R., Laing, D., & Steinmann, W.-D. (2004). Advanced Thermal Energy Storage Technology for Parabolic Trough. *Journal of Solar Energy Engineering*, 794-800.

Wagner, M., Kearney, D., Mehos, M., & McMahan, A. (2011). Modeling of a Parabolic Trough Field for Acceptance Testing: A Case Study. *ASME ES Fuel Cell*, (p. 54245). Washington DC.

Wesoff, E. (2011). *Update: Solar Junction Breaking CPV Efficiency Records, Raising $30 Million*. Retrieved 2012, from Greentech Media: www.greentechmedia.com/articles/red/solarjunction-setting-new-cpv-efficiency-records

Xu, C., Wang, C., He, Y., Li, X., & Bai, F. (2012). Sensitivity Analysis of the Numerical Study on the Thermal Performance of a Packed-Bed Molten Salt Thermocline Thermal Storage System. *Applied Energy*, 65-75.

Zalba, B., Marin, J., Cabeza, L., & Mehling, H. (2003). Review on Thermal Energy with Phase Change: Materials, Heat Transfer Analysis and Applications. *Applied Thermal Engineering*, 251-83.

155

COURSEWORK AND PUBLICATIONS

Course Name	Course Number	Semester	Hours
Structural Analysis	CVEG 3304	Fall 2011	4[*]
Steel Design	CVEG 4313	Fall 2011	3
Computational Methods in Engineering	CVEG 563-V	Fall 2011	3
Reinforced Concrete Design	CVEG 4303	Spring 2012	3
Matrix Analysis of Framed Structures	CVEG 5313	Spring 2012	3
Design of a Thermoacoustic Cooler	CVEG 563-V	Spring 2012	3
Master's Thesis	CVEG 600-V	Summer 2012	6
Advanced Thermodynamics	CHEG 5333	Fall 2012	3
Finite Element in Civil Engineering	CVEG 5383	Fall 2012	3
Advanced Steel Design	CVEG 5373	Fall 2012	3
Civil Engineering Seminar	CVEG 5100	Fall 2012	0

*No graduate credit awarded for this class
MS Requirements: 24 hr. Coursework + 6 hr. Thesis

Conference Proceedings

Brown, B., Strasser, M., and Selvam, R.P. Development of a Structured Concrete Thermocline
Thermal Energy Storage System. Proceedings of 2012 World Renewable Energy Forum,
0074, May 13-17, Denver, CO.

Journal Publications

Skinner, J., Strasser, M., Brown, B., and Selvam, R. P. (2012). Testing of High-Performance
Concrete as a Thermal Energy Storage Medium at High Temperatures. Journal of Solar
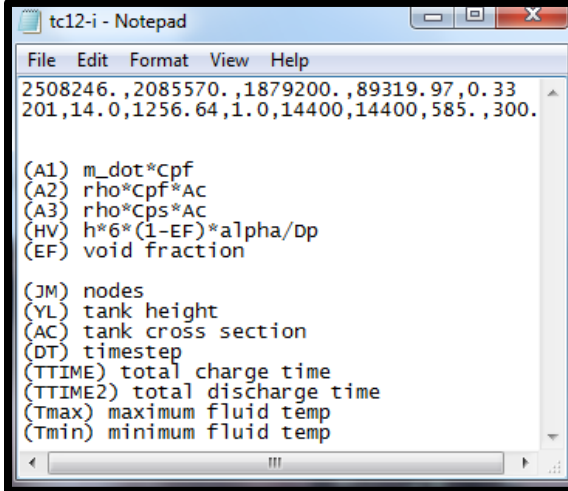Energy Engineering. (Accepted for Review).

APPENDIX A: PACKED BED THERMOCLINE MODEL

User's Manual

Input File

This program requires that the user construct an input file following the format provided below. This file must be saved as a .txt file and in the same directory as the program is stored.

- o Expressions for A1, A2, and A3 can be found in Chapter 3.
- o Expressions for HV and EF can be found in Chapter 3.
- o The number of nodes needed to attain convergence is dependent on the height of the bed. In this work, 201 nodes provided good convergence for a bed height of 14m. If the bed height is to be changed, a convergence study should be completed.
- o When specifying the time step and mass flow rate, ensure that the fluid velocity is small enough so as to not travel more than the spacing between two nodes in a single time step.
- o The user must specify the charge and discharge cycle durations. This allows the user to obtain temperature profiles at the different stages of each cycle.

Input File "tc12-i.txt"

Output Files

- *"charge.txt"* records the node height, fluid temperature, and bed temperature at each node at the end of the charge cycle.
- *"chginfo.txt"* records the time, fluid outlet temperature, quantity of energy stored at the current time in the cycle, and power used storing energy during the time step.
  - o The values reported for energy and power are attained by tracking the difference in the inlet and outlet fluid temperatures. Actual values can be attained by multiplying by mass flow rate and specific heat.
- *"discharge.txt"* records the node height, fluid temperature, and bed temperature at each node at the end of the charge cycle.

157

- *"dchginfo.txt"* records the time, fluid outlet temperature, quantity of energy retrieved at the current time in the cycle, and power retrieved from storage during the time step.
  - The values reported for energy and power are attained by tracking the difference in the inlet and outlet fluid temperatures. Actual values can be attained by multiplying by mass flow rate and specific heat.

Source Code

```
C     %%%%%%%%%%%%%%%%%%%%%%%%%%%%%%%%%%%%%%%%%%%%%%%%%%%%%%%%%%%%%
C     %  This program was developed to simulate thermal energy storage %
C     %  in a packed-bed thermocline thermal energy storage system.    %
C     %%%%%%%%%%%%%%%%%%%%%%%%%%%%%%%%%%%%%%%%%%%%%%%%%%%%%%%%%%%%%
C     %  Program Developed by: Matt Strasser                          %
C     %  Candidate for MS in Civil Engineering, University of Arkansas %
C     %  October 23, 2012                                             %
C     %%%%%%%%%%%%%%%%%%%%%%%%%%%%%%%%%%%%%%%%%%%%%%%%%%%%%%%%%%%%%
      PARAMETER(NY=20000)
      IMPLICIT REAL *8 (a-h,o-z)
      DIMENSION TF(NY,2),TB(NY,2),TOUT(NY),PWR(NY),E(NY)
      ! Input Data File
      OPEN(2,FILE='tc12-i.txt')
      ! Charge Cycle Fluid and Bed Temperature Profiles
      OPEN(3,FILE='charge.plt')
      ! Discharge Fluid Temperature and Bed Temperature Profiles
      OPEN(4,FILE='discharge.plt')
      ! Records the outlet fluid temperature, power, and energy stored
      OPEN(5,FILE='chginfo.plt')
      ! Records the outlet fluid temperature, power, and energy
      OPEN(7,FILE='dchginfo.plt')
C.....READ DATA FROM INPUT FILE
      READ(2,*)A1,A2,A3,HV,EF
      READ(2,*)JM,YL,AC,DT,TTIME,TTIME2,Tmax,Tmin
      C1=A1*EF
      C2=A2/AC
      C3=A3*(1.-EF)
      DY=YL/(JM-1)     ! Node Spacing
      NIT=1200         ! Maximum Iterations Per Time step
      TOL=1.E-5        ! Allowable Average Error in Calculation
C.....INITALIZE FLUID & BED TEMPERATURES
      DO J=1,JM
         TF(J,1)=Tmin
         TB(J,1)=Tmin
         IF(J.EQ.1)THEN
            TF(J,1)=Tmax
            TB(J,1)=Tmax
         END IF
         TF(J,2)=TF(J,1)
         TB(J,2)=TB(J,1)
      END DO
C............................................................C
C.............................CHARGE CYCLE...................C
C............................................................C
      ECHG=0.0
      EDCHG=0.0
C.....START TIME LOOOP
      ITERT=0
      TIME=0.0
1000  TIME=TIME+DT
      ITERT=ITERT+1
      DO ISUB=1,5
```

158

```
C.....START SOR LOOP
C.....SOLVE FOR FLUID TEMPERATURE
          ITER=0
1100      ITER=ITER+1
          RNORM=0.0
          DO J=2,JM
             AP=C1/DT+C2/DY+HV
             AW=-C2/DY
             SC=-C1/DT*TF(J,2)-HV*TB(J,1)
             RES=AP*TF(J,1)+AW*TF(J-1,1)+SC
             RNORM=RNORM+ABS(RES)
             TF(J,1)=TF(J,1)-RES/AP
          END DO
          ERR=RNORM/JM
          IF(ERR.GT.TOL.AND.ITER.LT.NIT)GO TO 1100
          PRINT*,'t=',time,'RES=',RES,'T=',TF(J,1)
C.....SOLVE FOR BED TEMPERATURE
          DO J=2,JM
             AP=C3/DT+HV
             SC=-C3/DT*TB(J,2)-HV*TF(J,1)
             TB(J,1)=-SC/AP
          END DO
C.....END ISUB
      END DO
C.....REPLACE PREVIOUS FLUID AND BED TEMPERATURES WITH CURRENT
      DO J=1,JM
         TF(J,2)=TF(J,1)
         TB(J,2)=TB(J,1)
      END DO
C.....END TIME LOOP
      PWRINC=abs(TF(1,1)-TF(JM,1))  ! Power Used During Time Step
      ECHG=ECHG+PWRINC              ! Total Energy Stored
      NTS=TIME/DT                   ! Total Time Steps
      TOUT(NTS)=TF(JM,1)
      PWR(NTS)=PWRINC
      E(NTS)=ECHG
      IF(TIME.LT.TTIME)GO TO 1000
C.....WRITE CHARGE CYCLE FILES
      DO J=1,JM
        y1=(j-1)*dy
        WRITE(3,*)y1,TF(J,1),TB(J,1)      ! Write "charge.txt"
      END DO
      DO J=1,NTS
        WRITE(5,*)J,TOUT(J),PWR(J),E(J)   ! Write "chrginfo.txt"
      END DO
      DO J=1,NTS                          ! Reset arrays for reuse
        TOUT(J)=0.0
        PWR(J)=0.0
        E(J)=0.0
      END DO
C.................................................................C
C.........................DISCHARGE CYCLE.........................C
C.................................................................C
      TF(JM,1)=Tmin
      TF(JM,2)=Tmin
      TB(JM,1)=Tmin
      TB(JM,2)=Tmin
C.....START TIME LOOOP
      ITERT=0
      TIME=0.0
1200  TIME=TIME+DT
      ITERT=ITERT+1
      DO ISUB=1,5
```

159

```fortran
C.....START SOR LOOP
C.....SOLVE FOR TF
            ITER=0
1300        ITER=ITER+1
            RNORM=0.0
            DO J=1,JM-1
                AP=C1/DT+C2/DY+HV
                AW=-C2/DY
                SC=-C1/DT*TF(JM-J,2)-HV*TB(JM-J,1)
                RES=AP*TF(JM-J,1)+AW*TF(JM+1-J,1)+SC
                RNORM=RNORM+ABS(RES)
                TF(JM-J,1)=TF(JM-J,1)-RES/AP
            END DO
            ERR=RNORM/JM
            IF(ERR.GT.TOL.AND.ITER.LT.NIT)GO TO 1300
            PRINT*,'t=',time,TF(JM,1),TF(50,2)
C.....SOLVE FOR TB
            DO J=1,JM-1
                AP=C3/DT+HV
                SC=-C3/DT*TB(JM-J,2)-HV*TF(JM-J,1)
                TB(JM-J,1)=-SC/AP
            END DO
C.....END ISUB
        END DO
C.....REPLACE NEW TO OLD
        DO J=1,JM
            TF(J,2)=TF(J,1)
            TB(J,2)=TB(J,1)
        END DO
C.....CHECK IF FLUID OUTLET TEMP IS BELOW LIMIT FOR DISCHARGE
        IF (TF(1,1).GE.500.)THEN
            PWRINC=abs(TF(1,1)-TF(JM,1))
        ELSE IF (TF(1,1).LT.500.)THEN
            PWRINC=0.0
        END IF
C.....END TIME
        EDCHG=EDCHG+PWRINC
        NTS=TIME/DT
        TOUT(NTS)=TF(1,1)
        PWR(NTS)=PWRINC
        E(NTS)=EDCHG
        IF(TIME.LT.TTIME2)GO TO 1200
C.....WRITE DISCHARGE CYCLE FILES
        DO J=1,JM
          y1=(j-1)*dy
          WRITE(4,*)y1,TF(J,1),TB(J,1)         ! Write "dcharge.txt"
        END DO
        DO J=1,NTS
          WRITE(7,*)J,TOUT(J),PWR(J),E(J)      ! Write "dchargeinfo.txt"
        END DO
C.....PRINT CHARGE/DISCHARGE EFFICIENCY
        PRINT*,'Stored Energy / (Mdot*Cp)=',ECHG
        PRINT*,'Discharged Energy / (Mdot*Cp)=',EDCHG
        CDEFF=100.0*EDCHG/ECHG
        PRINT*,'Charge/Discharge Efficiency (%)=',CDEFF
        STOP
        END
```

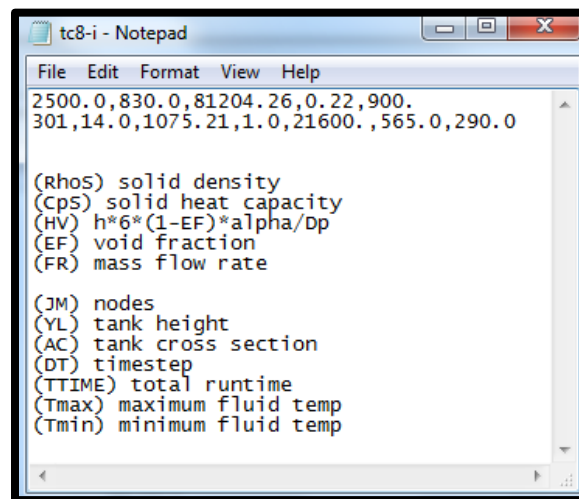## APPENDIX B: PACKED BED THERMOCLINE MODEL (VARRIABLE PROPERTIES)

User's Manual

Input File

This program requires that the user construct an input file following the format provided below. This file must be saved as a .txt file and in the same directory as the program is stored.

This program is very similar to the program discussed in Appendix A except for the fact that it considers the thermal conductivity, specific heat, and density of the liquid media (solar salt) to be temperature-dependent. Initial values for A1, A2, and A3 do no matter, as they are calculated by the program following the initialization of the initial temperatures. HV should be calculated considering average thermo physical properties.

- The process for constructing the input file for this program is that there is no input value for the discharge cycle duration.

```
tc8-i - Notepad

File  Edit  Format  View  Help
2500.0,830.0,81204.26,0.22,900.
301,14.0,1075.21,1.0,21600.,565.0,290.0


(RhoS) solid density
(CpS) solid heat capacity
(HV) h*6*(1-EF)*alpha/Dp
(EF) void fraction
(FR) mass flow rate

(JM) nodes
(YL) tank height
(AC) tank cross section
(DT) timestep
(TTIME) total runtime
(Tmax) maximum fluid temp
(Tmin) minimum fluid temp
```

Input File "tc9-i.txt"

Output File

- *"tco8.txt"* records the final fluid and bed temperature profiles after the specified charge cycle.

```
C      %%%%%%%%%%%%%%%%%%%%%%%%%%%%%%%%%%%%%%%%%%%%%%%%%%%%%%%%%%%%
C      %  This program was developed to simulate thermal energy storage %
C      %  in a packed-bed thermocline thermal energy storage system.   %
C      %  Fluid thermal conductivity, specific heat, and density are   %
C      %  considered.                                                   %
C      %%%%%%%%%%%%%%%%%%%%%%%%%%%%%%%%%%%%%%%%%%%%%%%%%%%%%%%%%%%%
C      %  Program Developed by: Matt Strasser                          %
C      %  Candidate for MS in Civil Engineering, University of Arkansas %
C      %  October 23, 2012                                             %
C      %%%%%%%%%%%%%%%%%%%%%%%%%%%%%%%%%%%%%%%%%%%%%%%%%%%%%%%%%%%%
       PARAMETER(NY=10001)
       IMPLICIT REAL *8 (a-h,o-z)
       DIMENSION TF(NY,2),TB(NY,2)
C.....OPEN I/O FILES
       OPEN(2,FILE='tc8-i.txt')
       ! Records the Final Fluid and Bed Temperature Profiles
       OPEN(3,FILE='tc8-o.txt')
C.....READ DATA FROM INPUT FILE
       READ(2,*)RhoS,CpS,HV,EF,FR
       READ(2,*)JM,YL,AC,DT,TTIME,Tmax,Tmin
       A3=RhoS*CpS
       C3=A3*(1.-EF)
       DY=YL/(JM-1)       ! Node Spacing
       NIT=1200           ! Maximum Iterations Per Time step
       TOL=1.E-5          ! Allowable Average Error in Calculation
C.....INITALIZE FLUID & BED TEMPERATURES
       DO J=1,JM
          TF(J,1)=Tmin
          TB(J,1)=Tmin
          IF(J.EQ.1)THEN
             TF(J,1)=Tmax
             TB(J,1)=Tmax
          END IF
          TF(J,2)=TF(J,1)
          TB(J,2)=TB(J,1)
       END DO
C.....START TIME LOOOP
       ITERT=0
       TIME=0.0
1000   TIME=TIME+DT
       ITERT=ITERT+1
       DO ISUB=1,5
C.....START SOR LOOP
C.....SOLVE FOR FLUID TEMPERATURE
          ITER=0
1100      ITER=ITER+1
          RNORM=0.0
          DO J=2,JM
             RhoF=2090.-0.636*TF(J,2)     ! T Dependent Density
             CpF=1443.-0.172*TF(J,2)      ! T Dependent Specific Heat
             A1=RhoF*CpF
             A2=FR*CpF
             C1=A1*EF
             C2=A2/AC
             AP=C1/DT+C2/DY+HV
             AW=-C2/DY
             SC=-C1/DT*TF(J,2)-HV*TB(J,1)
             RES=AP*TF(J,1)+AW*TF(J-1,1)+SC
             RNORM=RNORM+ABS(RES)
             TF(J,1)=TF(J,1)-RES/AP
```

162

```fortran
         END DO
         ERR=RNORM/JM
         IF(ERR.GT.TOL.AND.ITER.LT.NIT)GO TO 1100
         PRINT*,'t=',time,'RES=',RES,'T=',TF(J,1)
C.....SOLVE FOR BED TEMPERATURE
         DO J=2,JM
            AP=C3/DT+HV
            SC=-C3/DT*TB(J,2)-HV*TF(J,1)
            TB(J,1)=-SC/AP
         END DO
C.....END ISUB
      END DO
C.....REPLACE PREVIOUS TEMPERATURE VALUES WITH NEW VALUES
      DO J=1,JM
         TF(J,2)=TF(J,1)
         TB(J,2)=TB(J,1)
      END DO
C.....END TIME LOOP
      IF(TIME.LT.TTIME)GO TO 1000
      DO J=1,JM
        y1=(j-1)*dy
        WRITE(3,*)y1,TF(J,1),TB(J,1)
      END DO
      STOP
      END
```

163